48èmes Journées des Actinides (JdA2018)

Hotel Golf Mar, Praia de Porto Novo, PORTUGAL
21 - 24 March 2018

Book of Abstracts

Instituto Superior Técnico
Universidade de Lisboa

TÉCNICO LISBOA

CENTRO DE CIÊNCIAS E TECNOLOGIAS NUCLEARES

Conference Sponsors

Welcome to JdA2018

It is our great pleasure to invite you to participate in the 48èmes Journées des Actinides (JdA2018), to be held in Hotel Golf Mar, Praia de Porto Novo, PORTUGAL, between 21 and 24 March 2018. This conference is part of a long series of annual conferences following the 47èmes Journées des Actinides, which took place in Karpacz, Poland, between 26 and 30 March 2017.

The Journées des Actinides is an informal meeting that covers all aspects (fundamental and applied) related to the physics and chemistry of the 5f elements, their alloys and compounds. It brings together experts and young researchers from the different fields involved, emphasizing exchanges and discussions on the current issues in actinide sciences.

JdA2018 always encourage open discussion on different topics, in a mixture of oral presentations and poster sessions. It encompasses, but is not limited, to Condensed matter and electronic structure, Inorganic and organometallic chemistry, Networks, large instruments and new facilities, Nuclear forensics, Reactors, nuclear fuel cycle, environment, Strongly correlated behavior, Surface science, etc.

Experts, scientists, students and young researchers from Academia and Industry all around Europe and other continents are invited and expected for attending JdA2018 and discuss the state-of-the-art of the actinide sciences.

We feel confident that you will enjoy JdA2018, which will be also a wonderful opportunity to meet old friends and make new ones, and hope that the conference will be a memorable event.

On behalf of the Local Organizing Committee

António Pereira Gonçalves

Instituto Superior Técnico, Universidade de Lisboa, PORTUGAL

Chairperson

Conference Committees

International Advisory Committee

- Jean Aupiais (Arpajon, France)
- Eric Colineau (Karlsruhe, Germany)
- Nicolas Dacheux (Montpellier, France)
- David Geeson (Reading, UK)
- Mauro Giovannini (Genova, Italy)
- Antonio Pereira Gonçalves (Sacavém, Portugal)
- Itzhak Halevy (Be'er Sheva, Israel)
- Ladislav Havela (Prague, Czech Republic)
- Dariusz Kaczorowski (Wrocław, Poland)
- Thomas Scott (Bristol, UK)

Local Organizing Committee

- António Pereira Gonçalves, Chairman (IST, Univ. Lisbon)
- José A. Paixão (Univ. Coimbra)
- Joaquim B. Branco (IST, Univ. Lisbon)
- João Paulo Leal (IST, Univ. Lisbon)
- Laura C.J. Pereira (IST, Univ. Lisbon)
- Manuel Almeida (IST, Univ. Lisbon)

Programme Schedule

	Wednesday 21st March	Thursday 22nd March	Friday 23rd March	Saturday 24th March
8:35		**Late Registration**		
8:50		***Welcome***	**O20 -** M. Pasturel	**O35 -** A. Banos
9:10		**O1 - I.** Halevy	**O21 -** G. Li	**O36 -** Y. Sun
9:30		**O2 - I.** Izosimov	**O22 -** Y. Zhang	**O37 -** F. Housaer
9:50		**O3 - A. -** L. Ronzani	**O23 -** G. Rogl	**O38 -** A. Angileri
10:10		**O4 -** Y. Huilong	**O24 -** R. Qiu	**O39 -** H. Li
10:30		***Coffee Break***	***Coffee Break***	***Coffee Break***
11:00		**O5 -** J.G. Tobin	**O25 -** L. Havela	**O40 -** J. C. Griveau
11:20		**O6 -** D. Legut	**O26 -** L. Sandratskii	**O41 -** A.V.Karavaev
11:40		**O7 -** V.V. Dremov	**O27 -** A. Hen	**O42 -** H. Song
12:00		**O8 -** B. Dorado	**O28 -** E. Colineau	**O43 -** G. Zhang
12:20		**O9 -** T. Mingfeng	**O29 -** N. Goldman	**O44 -** D. Chaney
12:40				***Summary and Closing remarks***
13:05		***Lunch***	***Lunch***	***Lunch***
14:00				
14:20		**Poster Session**	**Visit To Adega Cooperativa Lourinhã**	**Return to Lisbon**
14:40				
15:00				
15:20		**O10 -** J. Spalek		
15:40		**O11 -** A.P. Pikul		
16:00	**Registration**	**O12 -** M. FidrysiaK		
16:20		**O13 -** A. Amon		
16:40		**O14 -** V. Buturlim		
17:00		***Coffee Break***		
17:20		**O15 -** E. Svanidze	**O30 -** P. Rogl	
17:40		**O16 -** J.K. Gibson	**O31 -** S. Maskova	
18:00	***Welcome Address***	**O17 -** S. Kalmykov	**O32 -** S.Chowdhury	
18:20		**O18 -** E. Gerber	**O33 -** P. Shi	
18:40		**O19 -** L.C.J. Pereira	**O34 -** J.C. Alexandre	
19:00				
19:20				
19:40				
20:00	***Dinner***	***Dinner***		
20:20			***Conference Dinner***	
20:40				
21:00				
21:20		**Poster Session**		

Contents

Oral Communications

O1

Nuclear forensics: New frontiers with Fission Track Analysis and TOF-SIMS Techniques 2

O2

Laser Spectroscopy and Detection of Actinides/Lanthanides in Solutions 4

O3

Isotopic analysis of uranium particles by laser ablation – ICP-MS 5

O4

Microscopic behavior of hydrogen on PuO_2 (110) surface: A DFT study 6

O5

An Experimentalist's Viewpoint: The Tremendous Strengths and Occasional Weaknesses of Actinide Cluster Calculations 8

O6

Thermal expansivity and thermal conductivity of Th and Ac from first principles calculations 10

O7

Dependence of Mechanical Properties of Actinides on Nano-Grain Structure and Alloying Addition Distribution 11

O8

A unifying DFT+U approach for plutonium modeling 13

O9

The phase transitions in plutonium studied by an LDA + Gutzwiller method 14

O10

Spin-triplet superconducting phases at the border of ferromagnetic transitions: The case of UGe_2 16

O11

Anisotropic response of high-density specific heat and magnetocaloric effect of single-crystalline UGe_2 on magnetic field 18

O12

Local-correlation-driven spin-triplet superconductivity in UGe_2 in applied magnetic field 20

O13

Tracking Al impurities in UBe_{13}: impact on structure and physics 22

O14

Electronic transport of the Ti rich U hydrides 24

O15

Novel Canonical Heavy Fermion Compound 26

O16

Exploring and Expanding High Oxidation States of Actinides 27

O17

Minor actinide separation using new N-donor ligands 29

O18

Probe of plutonium oxide nanoparticles at the large-scale facility 30

O19
Single-ion magnets based on uranium compounds 31
O20
Spark Plasma Sintering of uranium carbides and silicides 33
O21
The influence of gaseous impurities on the initial kinetics of uranium-hydrogen reaction 34
O22
Study of the microstructure evolution in monoclinic U-Nb alloy during aging using in-situ X-ray diffraction 35
O23
Structure and properties of a novel boride $ThNi_{12}B_6$ 36
O24
Stability of plutonium monoxide from first-principles calculation 37
O25
UH_2– a new ferromagnetic uranium hydride analogous to ThH_2, NpH_2 and PuH_2 39
O26
Discontinuous behavior of Uranium compounds in magnetic field 41
O27
XMCD studies of UH_3-based ferromagnets: $(UH_3)_{1-x}Mo_x$ and $(UH_3)_{1-x}Zr_x$ 42
O28
Magnetic properties of the Np-Ge binary system 44
O29
Development of Rapid Semi-empirical Quantum Models for Plutonium Surface Corrosion 46
O30
Actinoid Metal-Boron-Carbon Systems: Phase Equilibria, Crystal Structures and Physical Properties in Th – B - C 48
O31
Influence of hydrogen absorption on crystal structure and magnetic properties of the UNi(Al,Ga) solid solution 49
O32
Recent developments in UC_x targets at C^2TN 51
O33
Influence of Niobium content on the hydriding behavior of binary uranium alloys 53
O34
Revisiting the Pu(V) and Pu(VI) carbonate systems by CE-ICPMS 54
O35
Oxidation of uranium in liquid water under initial vacuum contained conditions 56
O36
Chemical durability of titanite ($CaTiSiO_5$) - a host phase of nuclear waste 58
O37
Multi-scale characterization of UMo/ZrN coated particles used in Al dispersion fuel for research reactors 60

O38

Use of Digital Autoradiography to characterize the effect of acidic leaching on mobilisation of ^{238}U series radionuclides in ISR context. 62

O39

The oxidation kinetics of nitriding uranium based on ultraviolet-visible reflectance spectroscopy 64

O40

Heat capacity of $NpPt_3$ and $NpPt_5$ at low temperatures 65

O41

Atomistic Simulations of Self-Irradiation Effects on Dislocation Dynamics in fcc Actinide Alloys 67

O42

Theoretical studies of the properties of actinide hydride 69

O43

The hydriding resistance of plutonium mononitride: A view from AIMD 70

O44

Disorder effects in the electrical resistivity of γ-($U_{0.78}$-$Mo_{0.22}$) single crystal thin films 71

Poster Session

P1

Structure and electronic properties of Uranium-Vanadium alloys 74

P2

Magnetic Excitation Spectrum and Bulk Modulus Behavior of δ-phase Pu 75

P3

Ground State of Pu Metal: What We Know and What Have Not Yet 76

P4

Application of electrospinning technique to nanostructured intermetallic, borates and chalcogenides 78

P5

Thermal expansivity and thermal conductivity of UC – a density functional theory study 79

P6

Cerium Behavior in Various Media as Compared with Plutonium 80

P7

The Development of Ceramic Matrices on the Phosphate Basis with $NaZr_2(PO_4)_3$ Structure for Immobilization of Actinides 82

P8

Thermal Expansion Anisotropy in the Uranium-Niobium Alloy 85

P9

Metallographic study of U-Zr-Mo alloy shell after explosive loading 86

P10

Thermal and elastic properties of $(Th,Ce)O_2$ mixed oxides: a self-consistent thermodynamic approach 88

P11

Preliminary study of $U_{1-x}M_xC$ systems (M = Ta, Nb) for ISOLDE targets 90

P12

Nano-UCx target for CERN-MEDICIS facility 92

P13

Evaluation of the thermal stability of uranyl peroxide clusters under different atmospheres (inert, reductive and oxidative) 93

P14

The probability of actinide protection with metal coatings 95

P15

Upgrading of a U/Th laboratory for regulatory compliance in France 97

P16

Methanation of CO_2 over nickel – actinide bimetallic oxides 98

P17

"MEDICIS-Promed", a EU project to produce radioisotope beams for medicine: an actinide perspective .. 99

P18

The Platform of Instituto Superior Técnico for Nanotechnology and Materials (IST-NM) 101

P19

Novel Aminopolycarboxylate-Based Metal Complexants for Improved Differentiation of Trivalent 4*f* and 5*f*-Elements 103

P20

Comparison of Conventional and Advanced Nuclear Fuel Performance 104

P21

Contribution to the understanding of uranium natural geochemical cycles in granitic rock 105

P22

Morphological characterization of UMo/ZrN fresh powders for the EMPIrE irradiation experiment by a statistical approach 107

P23

Influence of chemical pressure on the ferromagnetism in UBeGe 109

P24

CVD growth of graphene on proton irradiation targets: the case of tantalum 110

List of Participants 111

Oral Communications

O1

Nuclear forensics: New frontiers with Fission Track Analysis and TOF-SIMS Techniques

Itzhak Halevy,[1,2] Roman Radus[2], Silvie Maskova[3], Anna Kogan[1], Shmuel Samuha[1], Dmitry Gridchin[1], Eyal Grinberg[1], Eli Boblil[1], Nitsa Haikin[1], Itzhak Orion[2] and Aryeh M. Weiss[4]

[1] Department of Physics, IAEC-NRCN, Beer-Sheva 84190, Israel halevy.itzhak.dr@gmail.com
[2] Department of Nuclear Engineering, Ben-Gurion University -Negev, Beer-Sheva 8410501 Israel
[3] Department of Condensed Matter Physics, Charles University, Prague, Czech Republic
[4]Faculty of Engineering, Bar-Ilan University, Ramat Gan 52900 Israel;

Illicit trafficking of radioactive materials is known to exist from the early days of radioactive era. The nuclear forensics deals with recognizing the materials and processes of the radioactive industry. The properties of the materials can give a hint about the source of material and its original use.
The most common radioactive material involved in illicit trafficking is uranium. Uranium is a common natural element which can be found everywhere. The cosmogenic uranium is well known and defined. The natural enrichment of uranium is varying within a small range around 0.72 % and is indicative to its source. The enrichment of the anthropogenic uranium can vary much depending on the purpose and use of the material. Different enrichments are known for individual nuclear power plants, research reactors and military uses.
Measuring the uranium properties can indicate its enrichment, presence of other elements or impurities and can help in finding its attribution, namely its origin.
To learn more about the history of found material accurate isotopic measurements are needed. The ratio between ^{230}Th and ^{234}U can give a good estimation of how much time passed from the last chemical cleaning of the material. This technique is called radio-chronometry or age dating.
We developed new Lexan detectors with much better signal to noise ratio to improve sensitivity and reduce the false alarm, in figure 1.

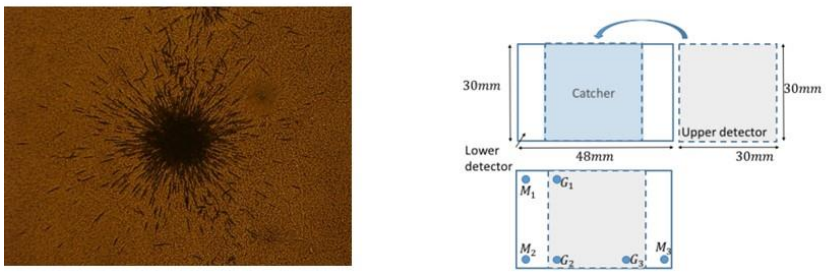

Fig. 1. FTA (Fission Track Analysis) of natural uranium mine sample.

New Automated software can recognize the fission track (FT) automatically and give the parameters of the track, like: roundness, intensity, number of tracks and color histogram. In that program we can add ROI (region of interest) or to cancel a false positive FT identification.
Analytical equipment like TOF-SIMS (Time Of Flight - Secondary Ion Mass Spectrometry) and ICP-MS (Inductively Coupled Plasma - Mass Spectrometer) together with new FTA software give new frontiers to the nuclear forensic research, see figure 2. The sample is a reference material IAEA-314 containing U~60ppm and Th~18ppm.
The ICP-MS is in the GSI (geophysical survey of Israel.

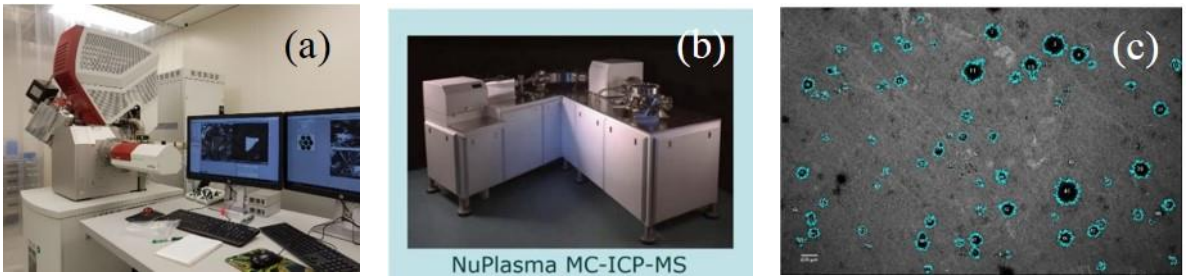

Fig. 2. TOF-SIMS (a), ICP-MS (b) and result of an automated FTA software to recognize FT (c)

A microscope equipped with TOF-SIMS gives the ability to measure quantitatively the ratio between the different isotopes and molecules. Using the scanning electron microscope, we are able to choose the desired particle (fig. 3) which can be then analyzed using the TOF-SIMS. TOF-SIMS is a technique capable to distinguish not only between elements but also different isotopes. Knowing the ratio between the isotopes is very important as it can help us to classify the material looking for its possible origin.

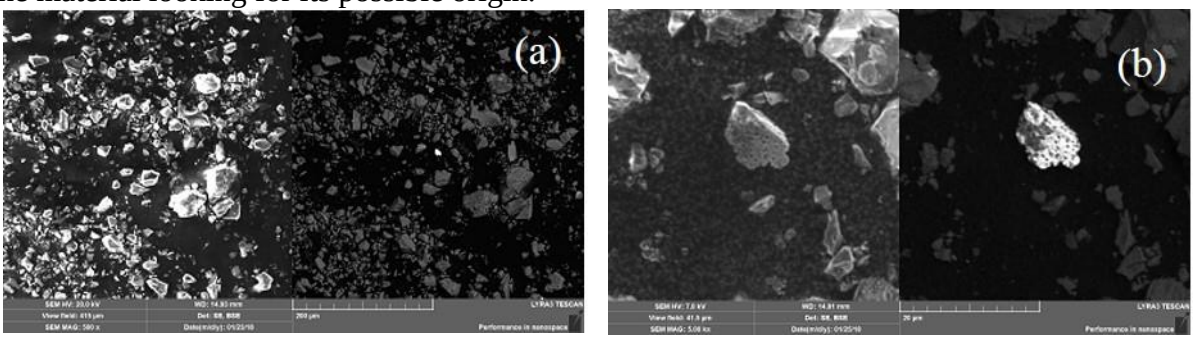

Fig. 3. The microscope image of the studied sample (a) and U particle (b) using SE detector (left) or BSE detector (right).

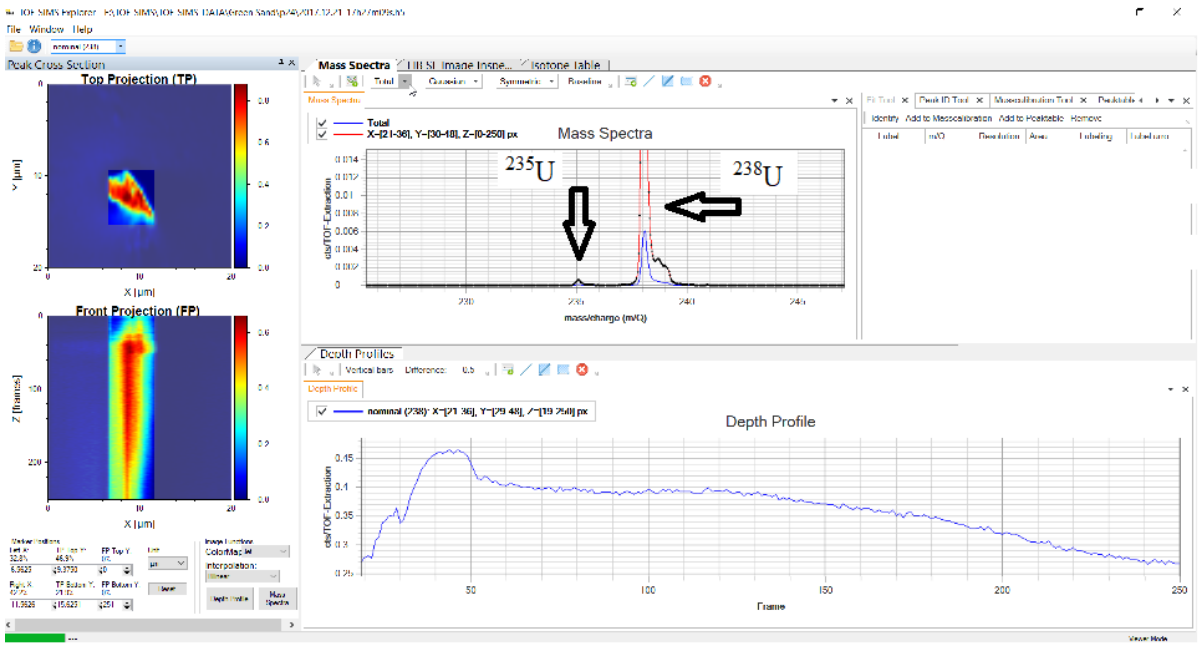

Fig. 4. TOF-SIMS analysis of uranium particle, the isotopes ^{235}U and ^{238}U can be clearly seen.

References

[1] Itzhak Halevy, Uri Admon, Ernesto Chinea-Cano, Aryeh M. Weiss, Naida Dzigal, E. Boblil, Michal Dagan, Itzhak Orion, and Roman Radus, *Progress in Nuclear Science and Technology* Volume # (2017) accepted

O2

Laser Spectroscopy and Detection of Actinides/Lanthanides in Solutions

Igor Izosimov[1]

[1] *Joint Institute for Nuclear Research, Joliot-Curie 6, 141980 Dubna, Russia,*
e-mail: izosimov@jinr.ru

This work is devoted to applications of the time-resolved laser-induced luminescence (*TRLIF*) spectroscopy and time-resolved laser-induced chemiluminescence *(TRLIC)* spectroscopy for detection of lanthanides and actinides. Pu, Np, and some U compounds do not produce direct luminescence in solutions, but when excited by laser radiation, they can induce chemiluminescence [1-4] of chemiluminogen (luminol in our experiments). It is shown that multi-photon scheme of chemiluminescence excitation makes chemiluminescence *(TRLIC)* not only a highly sensitive but also a highly selective tool for the detection of lanthanides/actinides. Results of the experiments on Eu, Sm, U, Pu, and Np detection in different solutions are presented.

References

[1] I.N. Izosimov, *Phys. Part. Nucl.* **38**, 203 (2007). DOI: 10.1134/s1063779607020025
[2] I.N. Izosimov, N.G. Firsin, N.G. Gorshkov and S.N. Nekhoroshkov, *Hyperfine Interact.* **227**, 281(2014). DOI: 10.1007/s10751-013-0990-7
[3] I.N. Izosimov, *Journal of Rad. and Nucl. Chem.* **304**, 211 (2015). DOI: 10.1007/s10967-014-3601-4
[4] I.N. Izosimov, *Procedia Chemistry* **21**, 473 (2016). DOI:10.1016/j.proche2016.10.066

O3

Isotopic analysis of uranium particles by laser ablation – ICP-MS

A.-L. Ronzani[1, 2], A. Hubert[1], F. Pointurier[1], J. Aupiais[1], N. Dacheux[2]

[1]CEA, DAM, DIF, F-91297 Arpajon, France, e-mail : anne-laure.ronzani@cea.fr
[2]ICSM, CEA, CNRS, ENSCM, Univ Montpellier, Site de Marcoule, 30207 Bagnols sur Cèze, France

Particle analysis, i.e. measurement of the isotopic composition of micrometric particles, is a major analytical tool for nuclear safeguards. Recently, laser ablation - inductively coupled plasma mass spectrometry (LA-ICP-MS) was evaluated for direct actinide isotope analysis in single particles. Some of the advantages of LA include minimal to no sample preparation, minimization or elimination of chemical reagent and wastes; rapid analysis leading to high sample throughput; and spatial resolution around a few micrometers, which allows individual particles analysis. However, the quantity of uranium present inside each particle is extremely low (around few picograms); the analysis of these particles requires a measurement technique very sensitive as the multi-collection ICP-MS Thermo "Neptune Plus".

One of the main issues in LA-ICP-MS analysis of particles is the signal irregularity. Actually, ablation of micrometric particles produces transient and short signals (a few seconds to a few tens of seconds) with high and abrupt intensity variations (cf. Fig. 1). Some variations last for less than one or two seconds with a highest intensity than the remaining signal (red circle on Fig. 1), therefore they strongly influence the isotope ratio calculation and might introduce some deviation from the true value. In order to calculate isotopic ratios, laser ablation signal need special mathematical processing, which will be described in this presentation. The signal aspect is strongly influenced both by the laser (energy, frequency…) and ICP-MS settings (integration time, …). We observe that some settings favor the apparition of short and abrupt intensity variations (cf. Fig. 1 – graphic on the right).

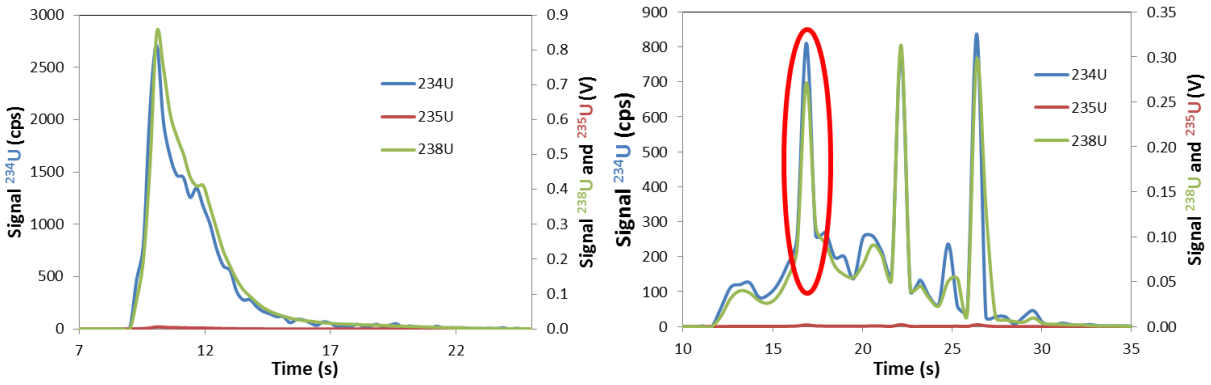

Fig. 1: Examples of laser ablation signals; right: relatively smooth signals with limited variations of intensities, left: very unstable signals with rapid variations of the intensity.

Another issue is the bias in isotopic ratio measurements due to differences in temporal response of the various detectors of the multi-collector ICP-MS. This bias is very significant when ions from the isotopes of interest are collected with different types of detectors: electron multipliers or Faraday cups. Different correcting methods will be discussed.
All those isotopic ratio processing have been applied to sub-micrometer particles and results will be compared with values given by other technologies within our laboratory (SIMS, fission tracks - TIMS).

O4

Microscopic behavior of hydrogen on PuO_2 (110) surface: A DFT study

Huilong Yu, Shaotao Zheng, Tao Tang, Tao Tang, Yan Shi, Daqiao Meng

Institute of Materials China Academy of Engineering Physics, Mianyang City Sichuan Province, China, 621907, e-mail: yuhuilong2002@126.com

Plutonium is an important nuclear material in some nuclear reactors as a source of energy, which is generated in an operating nuclear reactor due to transmutation of uranium. Plutonium is a chemically reactive metal. Plutonium shows enormous and reversible reaction rates exposed to a hydrogen containing atmosphere, forming plutonium hydride. The safe handling and storage of plutonium metal requires an understanding of plutonium corrosion by hydrogen. In the presence of air or oxygen, plutonium metal surface rapidly becomes covered with a protective layer of plutonium dioxide (PuO_2). PuO_2 layer may be exposed to hydrogen atmosphere during plutonium handling and long storage process, the key factor of the reaction between plutonium and hydrogen.

The adsorption, dissociation and diffusion of hydrogen on PuO_2 (110) surface have been investigated by density functional theory corrected for onsite Coulombic interactions (GGA+U). In order to find out the energetically more favorable adsorption site, optimum dissociation and diffusion path, adsorption energy of hydrogen on various sites, the dissociation and diffusion energy barrier are derived and compared. The results show that H_2 molecules are weakly adsorbed on PuO_2 (110) surface, while H atoms are strongly bonded at the top of O atom sites. One possible dissociation pathway of H_2 molecule is investigated using the climbing nudged-elastic-band (cNEB) approach. The calculated barriers show that the dissociation of H_2 molecule on PuO_2 (110) surface is kinetically the most favorable and can occur even below room temperature [1]. Atomic H diffusion from surface to subsurface is investigated; the results indicate that it is energetically more favorable for H atom to be on the surface [2]. Hydrogen permeation through purity PuO_2 surface is mainly inhibited from hydrogen atom diffusion from surface to subsurface.

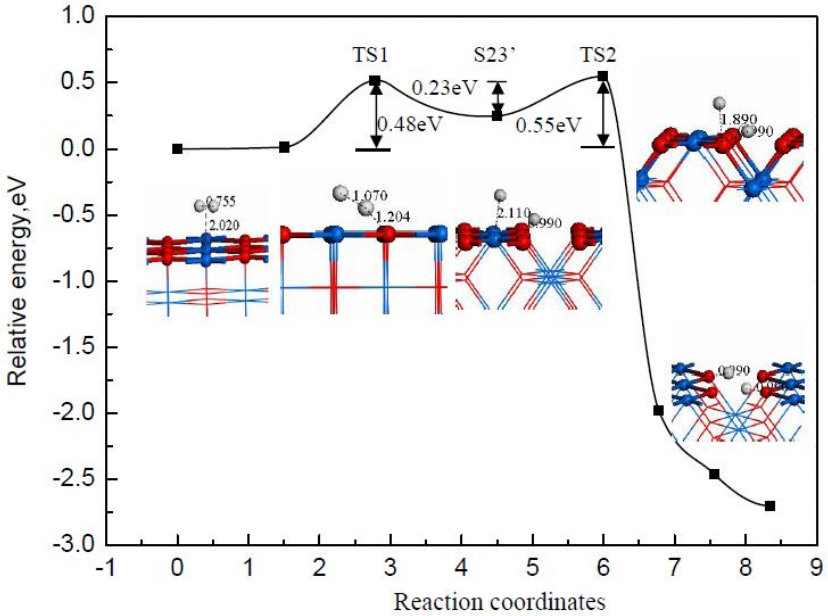

Figure 1. Potential energy diagram of H_2 dissociation on PuO_2 (110) surface. The inserted figures are the side view of the physisorbed simulation model, the transition simulation model, and the two H atoms coadsorbed simulation model.

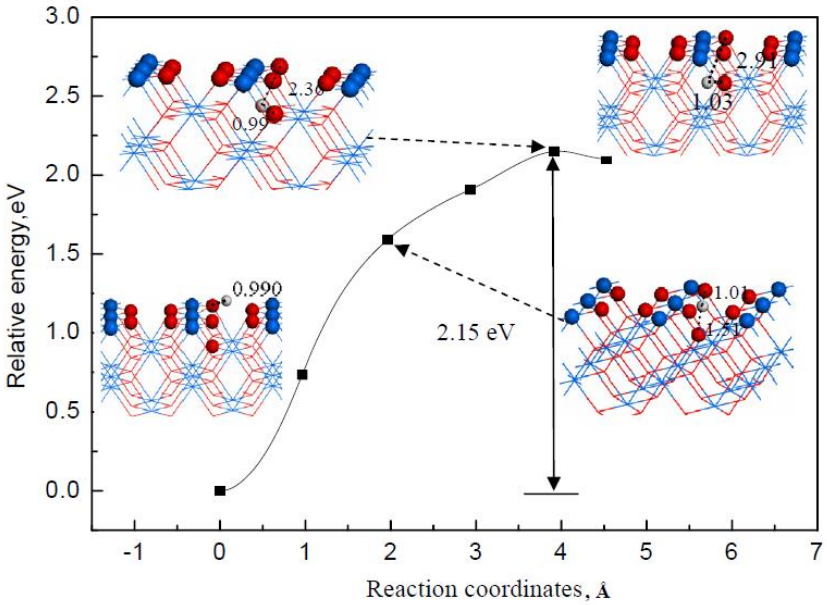

Figure 2. The minimum-energy path for H diffusion from surface to subsurface. Zero points energy corrections are not included.

References

[1] H.L. Yu *et al.*, Journal of Alloys and Compounds **567-573**, 654 (2016).

[2] H.L. Yu *et al.*, Journal of Alloys and Compounds **287-291**, 666 (2016).

O5

An Experimentalist's Viewpoint: The Tremendous Strengths and Occasional Weaknesses of Actinide Cluster Calculations

J.G. Tobin

University of Wisconsin-Oshkosh, Oshkosh, WI, USA 54902
e-mail: tobinj@uwosh.edu

Over the course of the last several years, cluster calculations have been used in a myriad of ways to analyze spectroscopic results from actinides systems and gain insight into the electronic structure of these actinides systems. For example, the calculated 6d Unoccupied Density of States (UDOS) in Uranium Tetrafluoride and Uranium Diode were probed using U L3 (2p) X-ray Absorption Near Edge Structure (XANES) as well as U N7 (4d) X-ray Absorption Spectroscopy (XAS), as shown in Figure 1 below. [1]

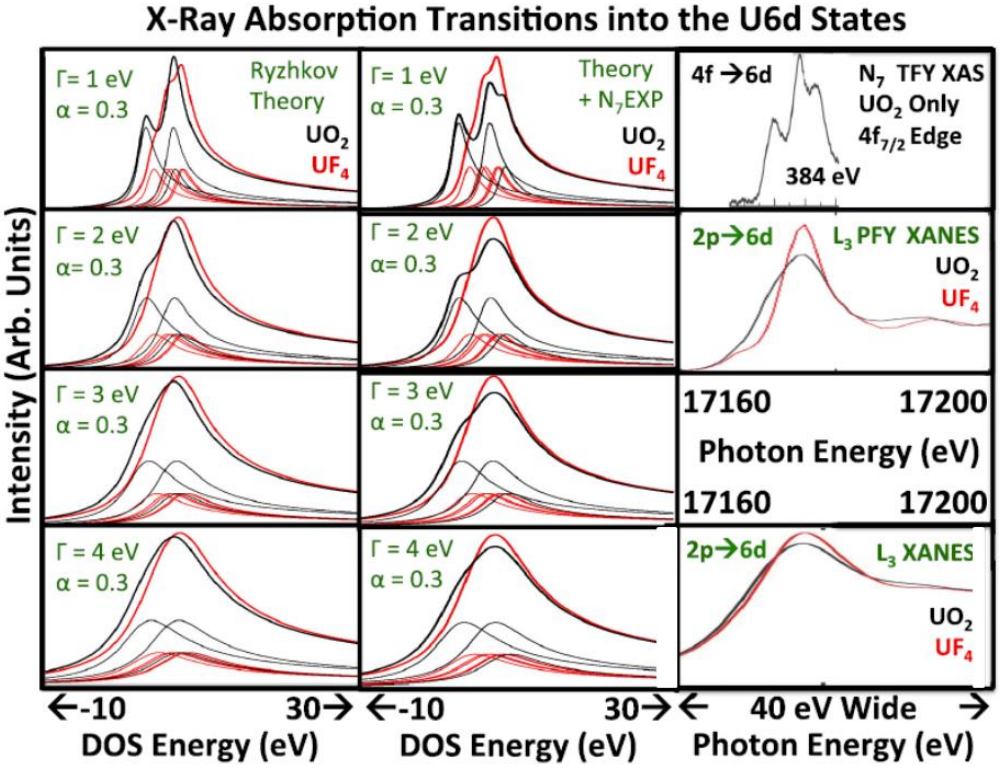

Figure 1. Comparison of the experimental XAS/XANES measurements of UO_2 and UF_4 (3rd column) with simulated spectra generated with Doniach-Sunjic line shapes and based upon the cluster calculations of Ryzhkov *et al.* for UO_2 and UF_4 [2,3]. UO_2 (UF_4) curves are shown in black (red). The first column is based solely upon the calculated 6*d* unoccupied density of states (UDOS) of Ryzhkov *et al.*, using DS line shapes, where α is the asymmetry parameter and Γ is the half-width at half-maximum of the Lorentzian part of the DS function. The value of α has been held constant at 0.3, while Γ has been varied systematically. In the middle column, the distribution of UO_2 6*d* states has been modified to match the UO_2 N7 XAS spectrum in the third column. The energy of the states has been modified as follows: $-2.33 \rightarrow -2.33; -5.85 \rightarrow -5.85; -6.09 \rightarrow -7.85$. Thus, only the single highest-energy state has been moved. The third column contains the experimental results, for transitions into the 6*d* UDOS, from the 4*f*7/2(N7) and 2*p*3/2(*L*3) initial states. From UF_4 PFY *L*3 edge jump width (width corresponding to 10%–90% intensities), it is found that the FWHM = 3.7, which corresponds to Γ = 1.85 eV. Thus, for the PFY *L*3 spectra, the comparison is made to the Γ = 2 case. For the "regular" *L*3 XANES, the FWHM is on the order of 10 eV, and the comparison is made with the Γ = 4 eV case. See Ref 1 for details.

Cluster calcutions have also been used successfully to study the development from atomic to bulk electronic structure in Pu (Figure 2 [4,5]) and issues associated with the 2p Occupied Density of States (ODOS) in Uranium Tetrafluoride. (Figure 3 [6])

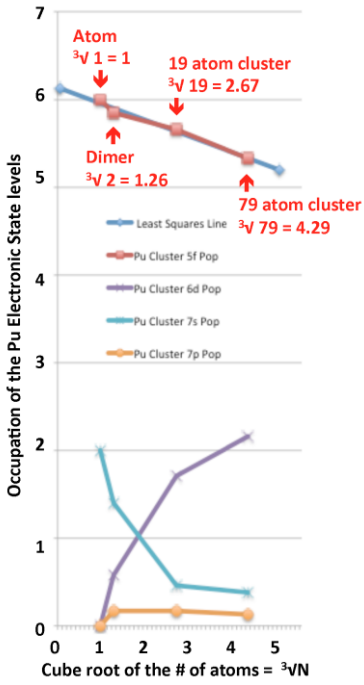

Figure 2 Plot of Pu 5f, 6d, 7s, and 7p average occupations vs. the cube root of the number of Pu atoms in the cluster. See Ref 2 for details.

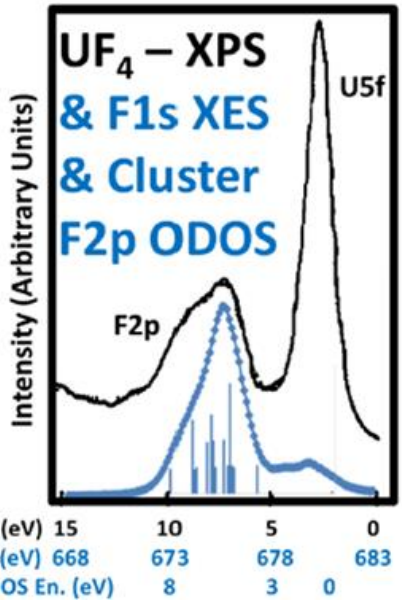

Figure 3 Comparison of the XES results for UF_4 with the X-ray Photoelectron Spectroscopy (XPS) of UF_4 from Thibaut *et al.* [7] and the ODOS derived from the calculations of Ryzhkov [2,3], for a $(UF_8)^{4-}$ cluster. Note that while the energy steps are identical, each of the x-axes can be shifted relative to the others. The XES peak is at hv = 675 eV. See Ref 6 for details.

However, there now appear to be some interesting discrepancies between what has been observed experimentally and the predictions of cluster theory. In particular, the 1s XAS of Uranium Tetrafluoride [8] and the 4d XAS branching ratio (BR) ratio predictions for oxidized uranium. [1] These issues will be addressed in the talk.

References

[1] J. G. Tobin, S.-W. Yu, C. H. Booth, T. Tyliszczak, D. K. Shuh, G. van der Laan, D. Sokaras, D. Nordlund, and T.-C. Weng, and P. S. Bagus, Phys. Rev. B **92**, 035111 (2015).
[2] Yu. A. Teterin, K. I. Maslakov, M. V. Ryzhkov, O. P. Traparic, L. Vukcevic, A. Yu. Teterin, and A. D. Panov, Radiochemistry **47**, 215 (2005).
[3] A. Yu. Teterin, Yu. A. Teterin, K. I. Maslakov, A. D. Panov, M. V. Ryzhkov, and L. Vukcevic, Phys. Rev. B **74**, 045101 (2006).
[4] M. V. Ryzhkov, A. Mirmelstein, S.-W. Yu,B. W. Chung,[c] and J. G. Tobin, International Journal of Quantum Chemistry **113**, 1957 (2013).
[5] M.V. Ryzhkov, A. Mirmelstein, B. Delley, S.-W. Yu, B.W. Chung, J.G. Tobin, Journal of Electron Spectroscopy and Related Phenomena **194**, 45 (2014).
[6] J.G. Tobin, S.-W. Yu, R. Qiao, W.L. Yang, and D.K. Shuh, "F1s X-ray Emission Spectroscopy of UF4," Progress in Nuclear Science and Technology, submitted 2017.
[7] Elisabeth Thibaut, Jean-Pol Boutique, Jacques J. Verbist, Jean-Claude Levet and Henri Noel, J. Am. Chem. Soc. 104, 5266-5273 (1982).
[8] J. G. Tobin, S.-W. Yu, R. Qiao, W. L. Yang, C. H. Booth, D. K. Shuh, A. M. Duffin, D. Sokaras, D. Nordlund, and T.-C. Weng, Phys. Rev.**B** 92, 045130 (2015).

O6

Thermal expansivity and thermal conductivity of Th and Ac from first principles calculations

Dominik Legut,[1] Lukáš Kývala[1], Urszula D. Wdowik[2],

[1] IT4 Innovations Center, VSB-Technical University of Ostrava, 17. Listopadu 15, CZ 708 33, Czech Republic, e-mail: dominik.legut@vsb.cz
[2] Institute of Technology, Pedagogical University, ul. Podchorazych 2, 30-084 Cracow, Poland

Actinides such as Ac and Th have gained renewed experimental and theoretical interest which stems from their potential application in radiotherapy and novel nuclear fuels. Therefore, a comprehensive density functional theory studies have been undertaken to explore the effect of spin-orbit and strong electron interactions on the electronic structure, elastic, dynamical, and thermo-physical properties of these materials. The well-established codes [1, 2, 3] have been used for this purpose. Both phonon and electron contributions to the thermal conductivity have been examined enabling explanation of the Th thermal conductivity being the highest among other actinides. Various phases of Ac (*hcp*, *bcc*, *fcc*, and *sc*) were investigated within the approach of quasi-harmonic theory to determine the phase transition in Ac as a function of pressure and temperature. Results of these calculations lead to somewhat different conclusions than those reported by Rubio-Ponce *et al.* [4]. Theoretically determined mechanical and thermodynamical properties of Th correlate very well with the experimental ones, which suggest that similar properties could be accurately determined also for elemental Ac.

Acknowledgement
This work was supported by the European Regional Development Fund in the IT4Innovations national supercomputing center - Path to Exascale project, No. CZ.02.1.01/0.0/0.0/16_013 /0001791 within the Operational Programme Research, Development and Education and by the Ministry of Education, Youth and Sports from the National Programme of Sustainability (NPU II) project "IT4Innovations Excellence in Science - LQ1602".

References

[1] G. Kresse and J. Furthmüeller, *Comput. Mater*. Sci. **6**, 15 (1996).
[2] A. Togo and I. Tanaka, *Scr. Mater*., **108**, 1-5 (2015).
[3] [3] G. K.H.Madsen and D. J.Singh, Comp. Phys. Comm. **175**, 67 (2006).
[4] [4] A. Rubio-Ponce, J. Rivera, and D. Olguın, Phys. Status Solidi B **252**, 695 (2015).

O7

Dependence of Mechanical Properties of Actinides on Nano-Grain Structure and Alloying Addition Distribution

V.V. Dremov, A.V. Karavaev, F.A. Sapozhnikov, G.V. Ionov

Russian Federal Nuclear Center – Zababakhin Institute of Technical Physics (RFNC-VNIITF), 13, Vasiliev st., Snezhinsk, Chelyabinsk region, 456770, Russia, e-mail: V.V.Dryomov@vniitf.ru

Previously in [1] we applied the atomistic simulations approach with the modified embedded atom model (MEAM) for interatomic interaction to the direct large-scale molecular dynamics simulation of dislocation dynamics in *fcc* δ-phase Pu-Ga alloys. We had demonstrated predictive capabilities of Classical MD in simulations of strength properties of δ-phase Pu-Ga alloys. The simulations of dislocation dynamics allowed us to evaluate the yield stress dependence on Ga concentration and its evolution due to radioactive aging. Both results proved to be in a pretty good agreement with experimental data. Present work continues our study of the mechanical properties of the δ-phase Pu-Ga alloys. Within previously developed stress relaxation technique here using the large-scale CMD simulations we study elastic-plastic behavior of the material focusing on the influence of the sub-micro grain structure of the samples and non-uniform alloying addition distribution. For that we generated sub-micro grain poly-crystal MD samples of *fcc* Pu 4 at. % Ga alloys of ~ 0.2 μm in size containing ~ 250 million atoms. The samples were generated with two disaligned grains replicated in all directions by the periodic boundary conditions (see Fig. 1). Gallium atoms were added to the sample as disordered substantial solution with different distributions: uniform through the sample or non-uniform that mimics the distribution of the gallium in as cast samples (see Fig. 2). After the thermalization at the ambient conditions the samples contained essentially no other crystal structure defects except grain boundaries.

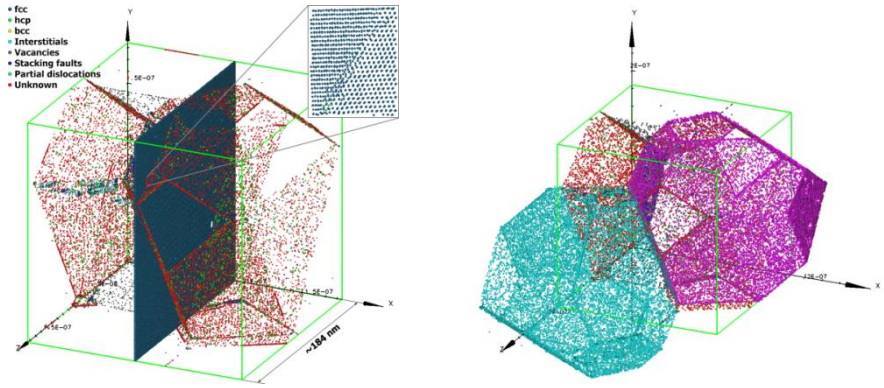

Fig. 1. Poly-crystal sample for the large-scale CMD simulations of the stress relaxation process. The *fcc* lattice is shown only in the 1.5 nm width layer. The atoms forming the grain boundaries are shown by red circles. Periodic boundary conditions are used in all directions. On the right by cyan and magenta colors two disaligned grains are shown. The microstructure of the sample was recognized with the Adaptive Template Analysis (ATA) [2].

The well-thermalized samples were subjected to instantaneous shear deformations of various directions and amplitudes in order to study their elastic-plastic properties using stress relaxation technique [1]. Instantaneous shear deformations cause shear stresses which in turn produce in the material extended lattice defects mainly edge dislocations and stacking fault planes. In all the cases the main sources of the extended defects are the grain boundaries and their intersections. The total shear stresses in the samples decrease due to the motion and interaction of the extended defects.

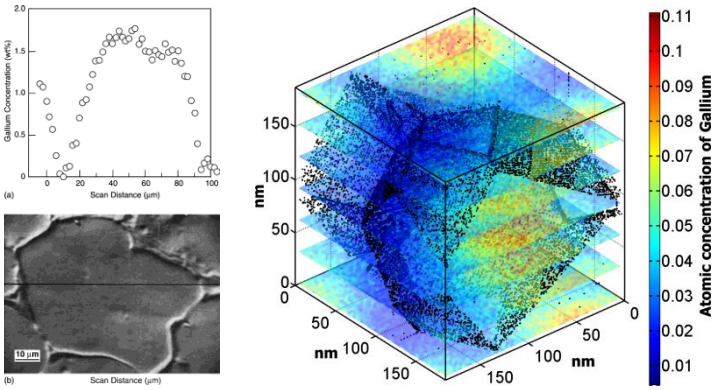

Fig. 2. Micro-segregation of gallium in the δ-phase Pu-Ga alloys due to casting. On the left – gallium distribution in the grain of Pu-1 wt. % Ga alloy along black line in bottom figure [4,5], on the right – gallium distribution in MD sample imitating micro-segregation due to casting.

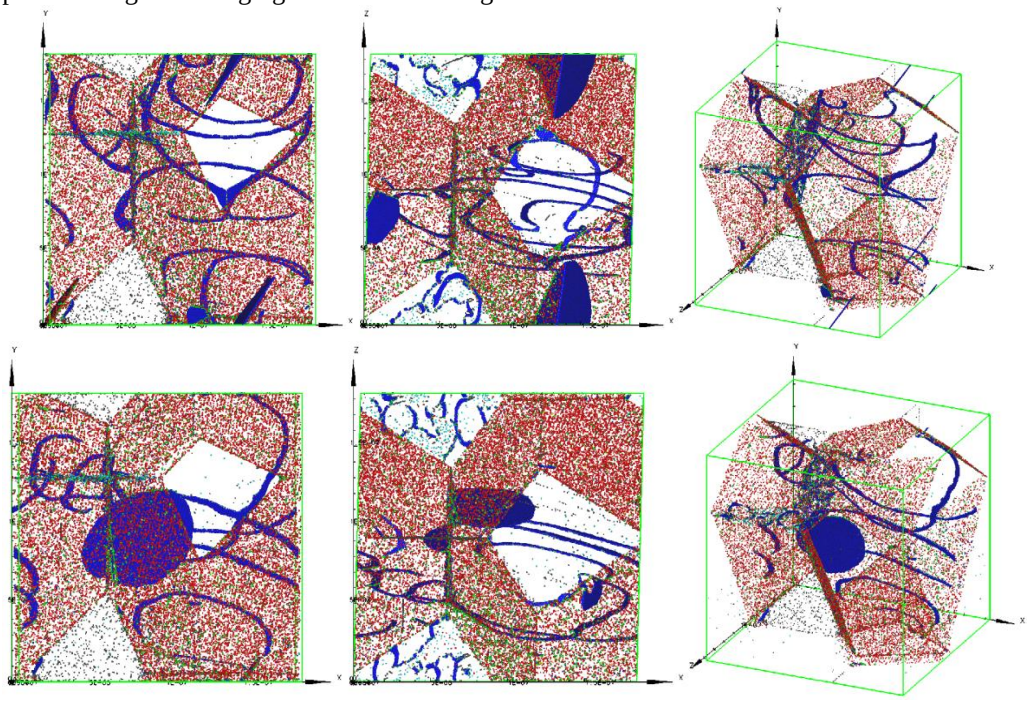

Fig. 3. Comparison of the microstructures of the samples in the same instant of the simulations for the same initial shear deformation $\varepsilon_{xz} = 0.025$: on the top – the sample with uniform gallium distribution, on the bottom – the sample with gallium micro-segregation.

As expected, the lower (nearly zero) gallium concentration on the grain boundaries leads to the lower threshold for the edge dislocation and stacking fault formation. At the same time the mobility of the extended defects is higher in the lower gallium concentration regions. As the result the shear stress relaxation in the samples with the gallium micro-segregation is faster than in the samples with uniform gallium distribution.

References

[1] A.V. Karavaev *et al.*, *J. Nucl. Mater.* **496**, 85 (2017).
[2] F.A. Sapozhnikov *et al.*, *Rus. J. Phys. Chem. B* **2**, 238-245 (2008).
[3] D. L. Clark, S. S. Hecker, G. D. Jarvinen, M. P. Neu, in: L. R. Morss, N. Edelstein, J. Fuger, J. J. Katz (Eds.), The Chemistry of the Actinide and Transactinide Elements, 3rd Edition, Springer, 2006, Ch. 7, pp. 979-989.
[4] M.R. Harvey *et al.*, *Micron* **5**, 417 (1975).
[5] J.L. Robbins, *J. Nucl. Mater.* **324**, 125-133 (2004).

O8

A unifying DFT+U approach for plutonium modeling

Boris Dorado,[1] Bernard Amadon[1], François Bottin[1], Johann Bouchet[1]

[1] CEA, DAM, DIF, F-91297 Arpajon, France, e-mail: boris.dorado@cea.fr

The theoretical description of the plutonium phase diagram still represents a major challenge to modern electronic structure methods. It exhibits six different allotropic phases at ambient pressure, with each phase transition marked by a significant change in the electronic behavior.

For the δ phase, a comprehensive knowledge has gradually been building up and the correct description of spectroscopic, magnetic, and structural properties could be obtained using the DMFT approach, which is a dynamical method that can account for the valence fluctuations that govern the ground state of δ plutonium [1].

In addition, the effective Coulomb interactions in plutonium were calculated very recently with DMFT and were found to be around 1 eV [2], which is much smaller than the "commonly accepted value" of 4 eV. It was also shown that the Hund's exchange, together with the spin-orbit coupling, yield an improved and accurate description of all phases of plutonium, thus opening the way to a unifying theory of plutonium.

In the present study, we investigate the influence of these weak electron correlations on the ground state properties of α, δ, and ε phases of plutonium, calculated with DFT+U, which is a static approximation of the DMFT. We show that the DFT+U and DMFT approaches yield similar structural properties, provided the GGA functional is used and the spin-orbit coupling is accounted for. This allows us to use the "simple" DFT+U approximation instead of the "expensive" DMFT to perform *ab initio* molecular dynamics calculations in plutonium at three different temperatures (300K, 600K and 900K) for all three phases and to extract the phonon spectra using the TDEP method [3].

References

[1] M. Janoschek *et al.*, *Sci. Adv.* **e1500188**, 1 (2015)
[2] B. Amadon, *Phys. Rev. B* **94**, 115148 (2016)
[3] O. Hellman *et al.*, *Phys. Rev. B* **87**, 104111 (2013)

O9

The phase transitions in plutonium studied by an LDA + Gutzwiller method

Mingfeng Tian,[1] Haifeng Song[1], Gongmu Zhang[1], Xi Dai[2]

[1] Institute of Applied Physics and Computational Mathematics, 2 Fenghao east road, Haidian district, 100094 Beijing, China, e-mail: mftian@iapcm.ac.cn
[2] Beijing National Laboratory for Condensed Matter Physics and Institute of Physics, Chinese Academy of Sciences, Beijing, China

The electronic structure and total energy of plutonium has been studied by combining density functional theory with the Gutzwiller variation approach (LDA + Gutzwiller), which can include the strong correlation effect among the 4f electrons in plutonium properly. We use LDA + G method calculated the equilibrium volume and bulk modulus of δ-Pu and ε-Pu (see Tab. 1 and Tab. 2), our results are quite consistent with the experimental data.

Tab. 1. The equilibrium volume and bulk modulus of δ-Pu

δ-Pu	LDA+G	Experiment (595K)	LDA
Equilibrium volume (Å^3)	25.6	24.92[1]	16.9
Bulk modulus (GPa)	34.9	30-35[2]	146.3

Tab. 2. The equilibrium volume and bulk modulus of ε-Pu

ε-Pu	LDA+G	Experiment (765K)	LDA
Equilibrium volume (Å^3)	23.9	24.04[1]	15.5
Bulk modulus (GPa)	10.6		227.6

We calculated the 5f-electrons density of states for plutonium (see Fig. 1), our results are consistent with experiments [3].

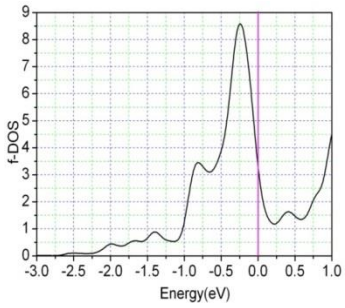

Fig. 1. LDA + G calculated 5f-electrons density of states for plutonium.

By further providing a newly finite temperature generalization of the LDA + G method (using the mean-field potential approach, [4]), the entropy contributed by electronic quasiparticles and lattice vibration both included, we obtain the Gibbs free energy of plutonium, from which we get the δ-ε transition at finite temperature and pressure (see Fig. 2), and finding good agreement with the experiments.

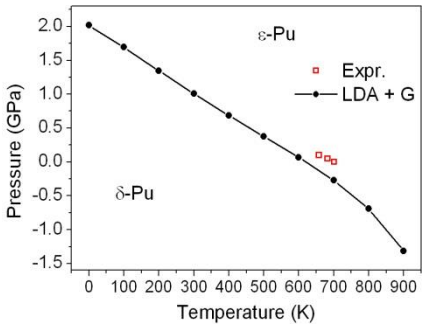

Fig. 2. LDA + G calculated the δ-ε phase transitions in plutonium

References

[1] Edited by O. J. Wick, *Plutonium Handbook A Guide to the Technology*, Gordon and Breach, New York, (1967).
[2] Edited by H. Blank and R. Lindner, *Moment in Plutonium and Other Actinides*, North-Holland, Amsterdam, 687 (1976).
[3] Arko, A. J., Joyce, J. J., Morales, L., Wills, J. & Jashley, *Phys. Rev. B* **62**, 1773 (2000).
[4] Mingfeng Tian, Haifeng Song *et al.*, *Phys. Rev. B* **91**, 125148 (2015).

O10

Spin-triplet superconducting phases at the border of ferromagnetic transitions: The case of UGe_2

J. Spałek[1*], M. Fidrysiak[1†], and E. Kądzielawa-Major[1§]

[1] *Marian Smoluchowski Institute of Physics, Jagiellonian University, ul. Łojasiewicza 11, 30-348 Kraków, Poland*

The discovery of superconductivity (SC) in the series of ferromagnetic uranium compounds UGe_2 [1], URhGe [2], UCoGe [3], and UIr [4] provides us with a challenge of finding the proper mechanism of SC pairing, consistent with their ferromagnetism (FM). Equally challenging is to understand the SC appearance at the borders of discontinuous phase transitions between the two ferromagnetic (high-moment, FM2 – low-moment, FM1) phases, as is the case for UGe_2 or between ferromagnetic and paramagnetic (PM) phases, which appears in UIr. What is also unique is the circumstance that SC phase appears at best only marginally on the PM side.
UCoGe has a very small magnetic moment $m \sim 0.039\ \mu_B$/U [5], so in that case the quantum-spin-fluctuation induced pairing invoked some time ago may be appropriate [6]. On the other hand, UGe_2 has the moment essentially larger in both FM2 ($m \sim 1.5\ \mu_B$/U) and FM1 ($m \sim 1\ \mu_B$/U) phases. Under these circumstances the local correlations, in conjunction with the Hund's ferromagnetic coupling, may become important for explaining concomitantly both ferromagnetism and superconductivity in that orbitally degenerate system of 5*f* electrons hybridized with conduction (*c*) electrons, here modeled by an extended Anderson-lattice model (ALM).
Very recently, we have put forward the idea of the correlations + Hund's-rule-interaction combined pairing for UGe_2 [6], as well as have implemented it to test its predictions in a semiquantitative manner. In Fig. 1(a)-(f) we summarize the principal results [7] obtained from the multi-orbital version of proposed earlier Statistically Consistent Gutzwiller approximation (SGA) [8]. The explanation is provided in the Figure Caption. The evolution of the phases as a function of the relative magnitude V of *f-c* hybridization mimics the experimentally controllable parameter – the pressure exerted on the system. The agreement between our theory and experiment is quite good. Note particularly the fact that the discontinuous changes in in superconducting gap are connected to the corresponding magnetic-moment jumps (also, A, A_1, and A_2 of SC phases are taken from the corresponding labeling of superfluid phases of ^{3}He).
In Fig. 2 we have plotted the correlation contribution coming from the *f-f* interaction represented by the Hubbard term ($\sim U$) and the Hund's rule exchange ($\sim J$). They are of comparable amplitude at the main (A_1) phase appearance, and therefore we may say that the system is an example of the *Hund's metal.*
In summary, we have formulated a model, which explains successfully the principal ferromagnetic and superconducting properties of UGe_2. In a separate contribution we discuss those properties in the Zeeman magnetic field [9].

The work was supported by National Science Centre, Grant No. DEC-2012/04/A/ST3/00342. We also thank P. Kubiczek for discussions on the early stage of this work.

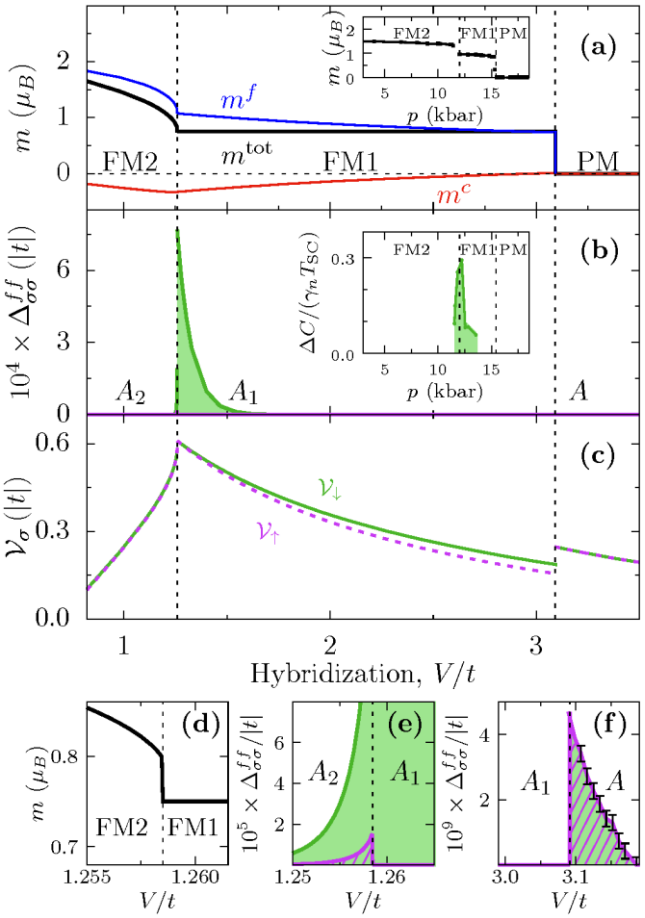

Fig. 1. Calculated phase diagram for the orbitally-degenerate ALM as a function of *f*-*c* hybridization V (adapted from Ref. [7]). (a) Total-, *f*-electron, and *c*-electron magnetic moments per formula unit (black, blue, and red lines, respectively). (b) Equal-spin SC gap components $\Delta_{\downarrow\downarrow}$ and $\Delta_{\uparrow\uparrow}$ (green and purple shadings, respectively). (c) Effective SC coupling constants for equal-spin-triplet pairing. (d)-(f) Close-ups of first-order transitions. Insets: experimental magnetization per U [1] (upper) and normalized specific-heat discontinuity at the SC transition for UGe_2 [10].

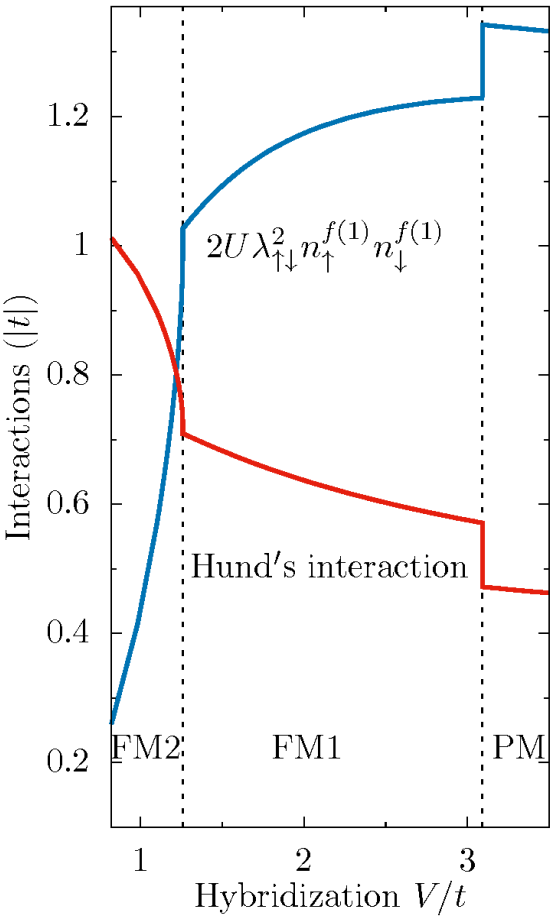

Fig. 2. Hybridization-dependence of the ground-state expectation values of *f*-*f* on-site Hubbard repulsion (blue line) and Hund's interaction (red line). Note that these energies become comparable close to the metamagnetic FM2→FM1 phase transition, *i.e.*, in the regime, where SC is the most pronounced.

References

[1] S. S. Saxena *et al.*, Nature **406**, 587 (2000); N. Tateiwa *et al.*, J. Phys.: Condens. Matter **13**, L17 (2001);
[5] C. Pfleiderer and A. D. Huxley, Phys. Rev. Lett. **89**, 147005 (2002).
[2] D. Aoki *et al.*, Nature **413**, 613 (2001).
[3] N. T. Huy *et al.*, Phys. Rev. Lett. **99**, 067006 (2007).
[4] T. C. Kobayashi *et al.*, Physica B **378**, 355 (2006).
[5] N. Tateiwa *et al.* Phys. Rev. B **96**, 035125 (2017).
[6] T. Hattori *et al.*, Phys. Rev. Lett. **108**, 066403 (2012); Y. Tada *et al.*, J. Phys.: Conf. Series **449**, 012029 (2013).
[7] E. Kądzielawa-Major, M. Fidrysiak, P. Kubiczek, and J. Spałek, arXiv:1712.08028.
[8] J. Jędrak and J. Spałek, Phys. Rev. B **83**, 104512 (2011); M. M. Wysokiński, M. Abram, and J. Spałek, Phys. Rev. B **90**, 081114(R) (2014); *ibid.*, **91**, 081108(R) (2016).
[9] M. Fidrysiak, E. Kądzielawa-Major, D. Goc-Jagło, and J. Spałek, Poster (this conference).
[10] N. Tateiwa *et al.*, Phys. Rev. B **69**, 180513 (2004).

* jozef.spalek@uj.edu.pl † maciej.fidrysiak@uj.edu.pl § ewa.kadzielawa@doctoral.uj.edu.pl

O11

Anisotropic response of high-density specific heat and magnetocaloric effect of single-crystalline UGe_2 on magnetic field

Adam P. Pikul, Tomasz Plackowski, Robert Troć

[1] *Institute of Low Temperature and Structure Research, Polish Academy of Sciences, P Nr 1410, 50-422 Wrocław, Poland e-mail: A.Pikul@intibs.pl*

The discovered under-pressure superconductor UGe_2, crystallizing in the orthorhombic $ZrGa_2$-type structure, is one of the most intensively studied uranium-based intermetallic during more than last decade. Its long-range ferromagnetic ordering (T_C = 52 K), with the saturated magnetic moment μ_s = 1.4 μ_B, has been widely described in the literature in the past as manifesting itinerant character of the uranium 5f electrons. Hence, the coexistence (or interplay) of the relatively strong ferromagnetism and superconducting state discovered in UGe_2 upon applying high pressure of 1.0–1.6 GPa [1] has been a subject of a several theoretical approaches based on the band character of the 5f electrons [2,3].

As we have shown in Ref. [4], the unusual behavior of this germanide might be explained by assuming dual nature of these electrons, considered generally by a few independent theoretical groups [5,6] in the past. In particular, our bulk physical properties data obtained in a wide range of temperatures and magnetic fields, supplemented by spectroscopic and theoretical investigations [4,7–10] suggest that the system can be described as possessing two subsystems of the 5f electrons: "localized" – responsible for the fairly strong and highly anisotropic magnetic and transport properties and "itinerant" – being a source of strong spin fluctuations achieving a maximum at about T^* = 26 K (≈ ½T_C) at ambient pressure and being responsible for superconductivity under applied pressure. Our approach seems to be consistent with a number of various novel experiments and theoretical considerations (for review and discussion see Refs. [4,11]). In this contribution we present results of another two experiments carried out on single-crystalline UGe_2, namely specific heat and magnetocaloric effect measurements, both performed for two crystallographic directions and in various applied fields. All the experimental data presented here were obtained on the samples cut from exactly the same large single crystal as those described in Refs. [4,7–10]. Temperature dependence of the specific heat and field variation of the isothermal magnetocaloric effect of the so-obtained single crystals were measured at temperatures from 15 to 300 K and in magnetic fields up to 10 T using a homemade apparatus and utilizing innovatory, simple and robust technique developed by one of us (TP) [12]. The most important feature of that method is exceptional ability to measure precisely the heat flux between the sample and its surroundings and to measure specific heat with 2% accuracy and very high density of statistically independent data. High signal-to-noise ratio (in the range of 10^3 to 10^4) allows to detect very small anomalies (~0.1 %), such as e.g. melting of the flux line lattice in superconductors, sharp first-order anomalies and their hysteresis, vortex melting, crossover to irreversibility etc.

As can be inferred from Fig.1, displaying temperature variations of the specific heat of UGe_2 measured around T_C and T^*, the anomalies related to these two characteristic temperatures exhibit very different sensitivity on the magnetic field applied: while for $H||a$-axis both features are quickly suppressed by $\mu_0 H$ (the peak at T_C is hardly visible already in ~ 2.5 T), for $H||b$-axis the ferromagnetic order at T_C and the spin fluctuations at T^* are well visible even in 10 T. Most importantly, high resolution of the performed experiments allowed us to distinguish for the first

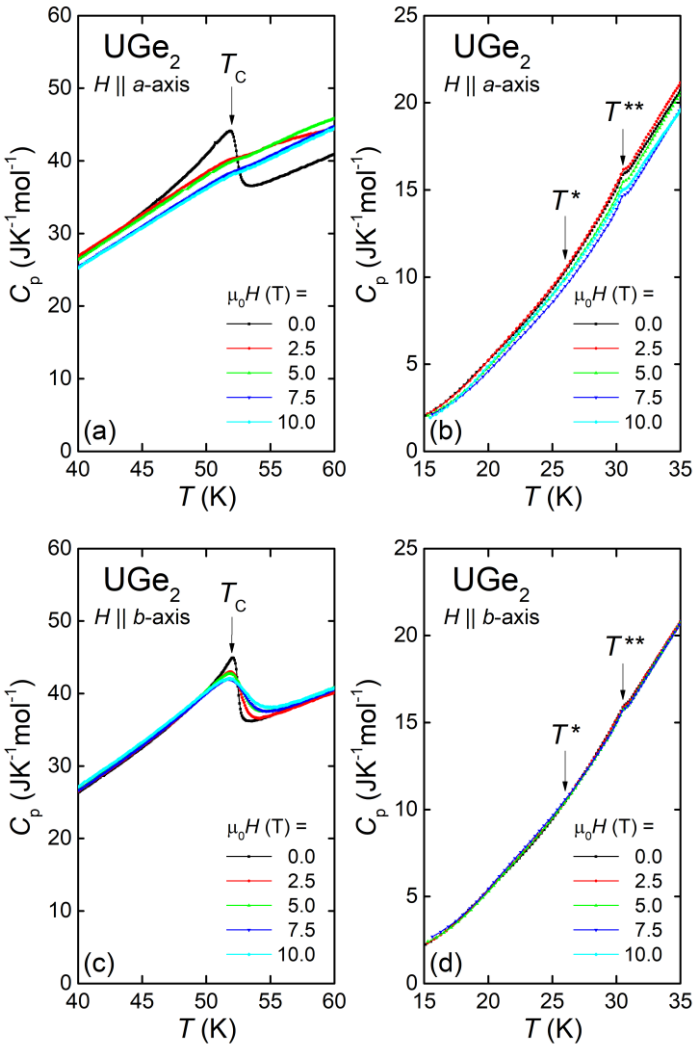

Fig. 1. Temperature dependences of the specific heat of single-crystalline UGe_2 measured around the characteristic temperatures in various magnetic fields applied along the *a*- and *b*-axis.

time another characteristic temperature of the UGe_2 system, namely T^{**} = 30.5 K. For a long time this anomaly was hidden by the broad hump at T^*. Going back to the Hall effect measurements reported earlier [9], there is apparent a coincidence between T^{**} and the temperature of the Fermi surface reconstruction suggested in Ref. [9].
This finding sheds new light on the complex nature of UGe_2 and requires further studies, including some re-investigations of the bulk physical properties of that system.

References

[1] A. Huxley *et al.*, *Phys. Rev. B* **63**, 144519 (2001).
[2] S. Kakani, M. L. Kalra, S. L. Kakani, *J. Supercond. Nov. Magn.* **21**, 301 (2008).
[3] J. Linder *et al.*, *Phys. Rev. B* **77**, 184511 (2008).
[4] R. Troć, Z. Gajek, A. Pikul, *Phys. Rev. B* **86**, 224403 (2012).
[5] P. Santini, R. Lemański, P. Erdős, Adv. Phys. **48**, 537 (1999).
[6] G. Zwicknagl, P. Fulde, *J. Phys.: Condens. Matter* **15**, S1911 (2003).
[7] R. Troć, *Acta Phys. Pol. B* **34**, 407 (2003).
[8] M. Biasini, R. Troć, *Phys. Rev. B* **68**, 245118 (2003).
[9] V. H. Tran *et al.*, *Phys. Rev. B* **69**, 195314 (2004).
[10] H. Misiorek *et al.*, *J. Phys.: Condens. Matter* **17**, 679 (2005).
[11] E. Kądzielawa-Major *et al.*, arXiv:1712.08028
[12] T. Plackowski, Y. Wang, A. Junod, Rev. Sci. Instrum. **73**, 2755 (2002).

O12

Local-correlation-driven spin-triplet superconductivity in UGe_2 in applied magnetic field

M. Fidrysiak[1*], E. Kądzielawa-Major,[1†] D. Goc-Jagło[1‡], and J. Spałek[1§]

[1] *Marian Smoluchowski Institute of Physics, Jagiellonian University, ul. Łojasiewicza 11, 30-348 Kraków, Poland*

The phenomenon of coexistent superconductivity (SC) and ferromagnetism (FM), discovered in uranium compounds (*e.g.,* UGe_2 [1] and UCoGe [2]), has raised the question of the microscopic mechanism responsible for the spin-triplet pairing in this class of materials. Even though SC appears near the first-order magnetic transitions in both systems, a particularly weak ferromagnetism in UCoGe (magnetic moments ~0.039 μ_B/U [3]) makes the pairing by FM fluctuations a viable candidate [4]. However, as the moment in UGe_2 is 1-2 μ_B/U, the fluctuation-induced pairing might not apply to that material. Recently, we have argued [5] that, for the larger-moment case of UGe_2, a qualitatively different microscopic mechanism [5], based on local correlations combined with Hund's rule exchange, is capable of stabilizing variety of equal-spin-triplet SC states (analogous to A, A_1, and A_2 phases of superfluid ^{3}He). The latter mechanism yields the maximal SC amplitude near the pressure-induced transition between the large-moment (FM2) and the smaller-moment (FM1) phases, in agreement with experiment. A further verification of the pairing mechanism should involve a comprehensive check of its consistency with other features of the complex phase diagram of U-based compounds and, in particular, with the observed evolution of metamagnetic and SC transitions under applied magnetic field and at finite temperature.

In this contribution we extend our previous analysis [5] by including Zeeman magnetic field in an orbitally degenerate periodic Anderson model (PAM), describing the system of hybridized conduction (c) carriers with correlated f-electrons. The model is solved within the multi-orbital variant of Statistically Consistent Gutzwiller Approximation (SGA) [6]. Exemplary results of magnetic-field evolution of the FM and SC states are shown in Fig. 1. The parameters have been selected so that, at zero field, the system falls into the low-moment FM1 phase, coexisting with the A_1-type SC, just above the FM2$\underline{\rightarrow}$FM1 transition [5]. At nonzero field, $H=H_x$, the first-order transition to the larger-moment FM2+A_2 state takes place. Notably, a weak SC persists also for $H > H_x$, which is consistent with measurements on UGe_2 [7] (showing that just above $p_x \approx 12.5$ kbar, the upper critical field H_{c2} exceeds H_x). In Fig. 2 we plot the SC amplitudes and the total magnetic moment as a function of f-c hybridization magnitude V (mimicking the pressure change) for zero- and nonzero-applied magnetic field. The main effect of the Zeeman field is shifting the FM2-FM1 boundary towards larger values of hybridization/pressure, as observed in UGe_2.

The work was supported by National Science Centre, Grant No. DEC-2012/04/A/ST3/00342.

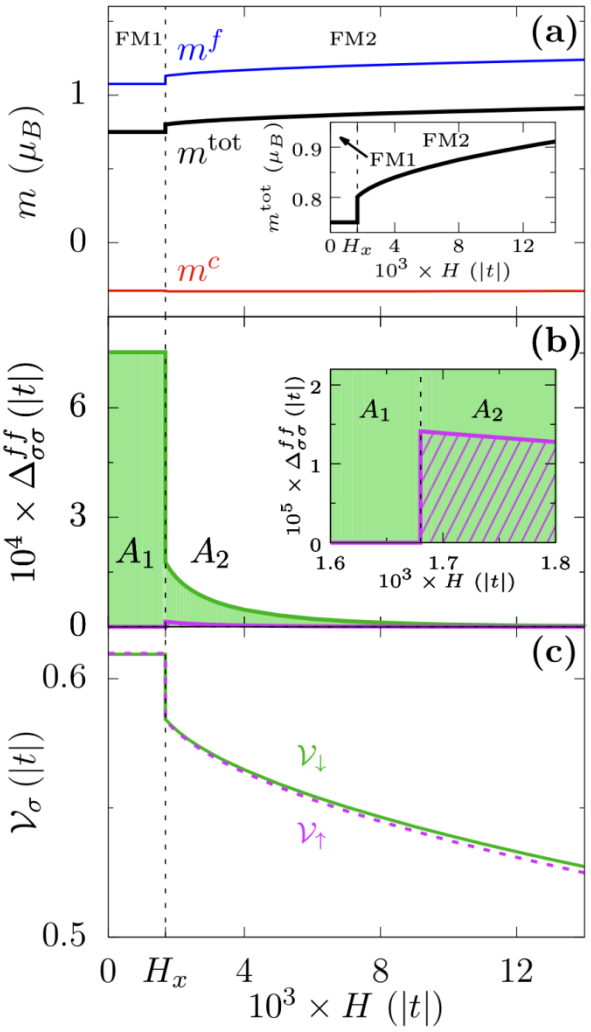

Fig. 1. Magnetic-field dependence of magnetic and superconducting properties for the doubly-degenerate PAM. The *f*-*c* hybridization $V/|t|$ = -1.26, where t is the nearest-neighbor *c*-electron hopping. The rest of the parameters coincide with those used in Ref. [5]. (a) Total magnetization (black line) and its *f*- and *c*-electron components (blue and red lines, respectively). (b) Equal-spin-triplet SC gap amplitudes $\Delta_{\downarrow\downarrow}$ and $\Delta_{\uparrow\uparrow}$. (c) Equal-spin-triplet SC coupling constant components. Magnetic (FM2, FM1), and superconducting (A_1, A_2) phases are marked. Insets show close-ups of the transition regions.

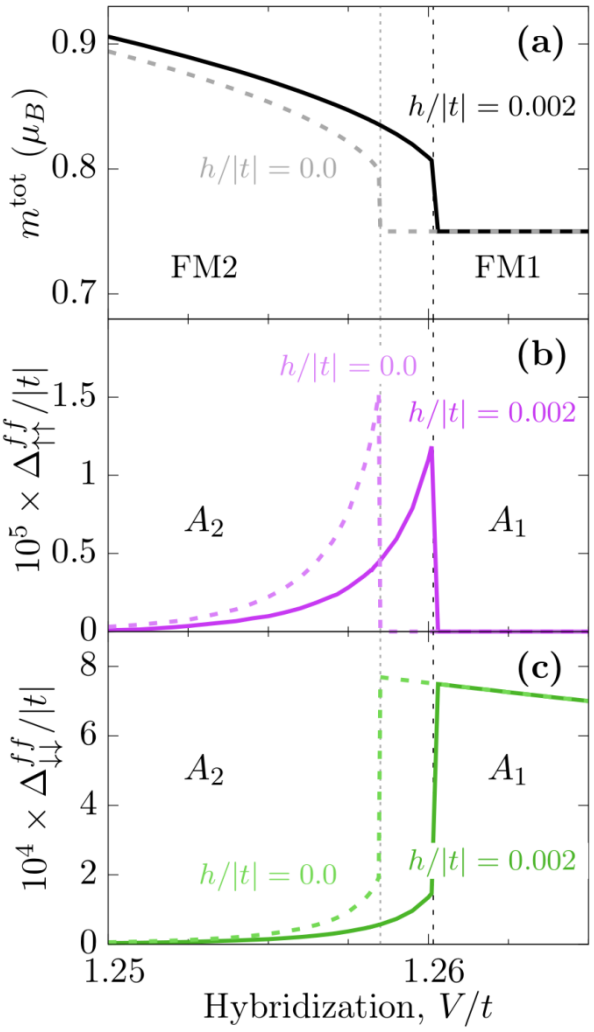

Fig. 2. Hybridization-dependence of (a) total magnetization $m^{\rm tot}$, and (b)-(c) equal-spin SC gap amplitudes $\Delta_{\downarrow\downarrow}$ and $\Delta_{\uparrow\uparrow}$, with and without applied magnetic field (solid and dashed lines, respectively). The main effect of the field is to shift the joint metamagnetic and superconducting transition to larger values of hybridization.

References

[1] S. S. Saxena *et al.*, Nature **406**, 587 (2000).
[2] N. T. Huy *et al.*, Phys. Rev. Lett. **99**, 067006 (2007).
[3] N. Tateiwa *et al.* Phys. Rev. B **96**, 035125 (2017).
[4] T. Hattori *et al.*, Phys. Rev. Lett. 108, 066403 (2012).
[5] E. Kądzielawa-Major, M. Fidrysiak, P. Kubiczek, and J. Spałek, arXiv:1712.08028; J. Spałek, M. Fidrysiak, and E. Kądzielawa-Major, Talk (this conference).
[6] J. Jędrak and J. Spałek, Phys. Rev. B **83**, 104512 (2011); M. M. Wysokiński, M. Abram, and J. Spałek, Phys. Rev. B **90**, 081114(R) (2014); *ibid.*, **91**, 081108(R) (2016).
[7] I. Sheikin *et al.*, Phys. Rev. B **64**, 220503(R); A. D. Huxley, Physica C **514**, 368 (514).

* maciej.fidrysiak@uj.edu.pl † ewa.kadzielawa@doctoral.uj.edu.pl
‡ danuta.goc-jaglo@uj.edu.pl § jozef.spalek@uj.edu.pl

O13

Tracking Al impurities in UBe_{13}: impact on structure and physics

Alfred Amon,[1] Matej Bobnar,[1] Marcel Naumann,[1] Frank Arnold,[1] Eteri Svanidze,[1] Horst Bormann,[1] Paul Simon,[1] Iryna Zelenina,[1] Reiner Ramlau,[1] Wilder Carillo,[1] Elena Hassinger,[1] Walter Schnelle,[1] Ulrich Burkhardt,[1] Andreas Leithe-Jasper,[1] Yuri Grin[1]

[1] Max-Planck-Institute for Chemical Physics of Solids, Nöthnitzerstr.40, 01187 Dresden, Germany
e-mail: alfred.amon@cpfs.mpg.de

The heavy-fermion superconductor UBe_{13} has fascinated and puzzled scientists since its discovery in the 1980's.[1] Displaying the highest Sommerfeld coefficient of U-based compounds with $\gamma \approx 1.1$ J K^{-2} $molU^{-1}$, its unconventional superconducting properties have been the subject of numerous studies and are not fully understood till today.[2-4] The influence of magnetic and nonmagnetic dopants on the physical properties has been extensively investigated: While most dopants lead to a suppression of superconductivity, Th introduces a second phase transition below the critical temperature T_c. The addition of small amounts of B (isoelectronic to Al) leads to a strong enhancement of the specific heat jump $\Delta C/\gamma T_c$. [5-9]
It was observed that there exists a large spread in the reported values for the lattice parameter and the critical temperature, especially between single crystals, grown from Al-flux, and arc-melted polycrystalline samples (Fig. 1). Similar observations have even led to the conjecture that *two* types (high T_c and low T_c) of UBe_{13} might exist. [10] Literature has considered the possibility of Al incorporation in UBe_{13} only in side notes so far, despite the potential impact this might have on the interpretation of experimental results.[10, 11]
This encouraged us to launch an extensive investigation into the sample dependence of UBe_{13} and the role of aluminium. Employing X-ray diffraction, solid state NMR, specific heat measurements, high-resolution electron microscopy and X-ray spectroscopy we were able to unambiguously detect and locate Al incorporations in UBe_{13} and, furthermore, determine its influence on the normal and superconducting states. We show that Al readily enters the crystal structure of UBe_{13} by substituting Be. The solubility of Al shows a strong temperature dependence which is reflected in the low temperature physics of UBe_{13} comparing crystals at different annealing stages. The obtained results draw a coherent picture and shed light on the longstanding puzzle about the role of Al and the sample dependence of UBe_{13}.

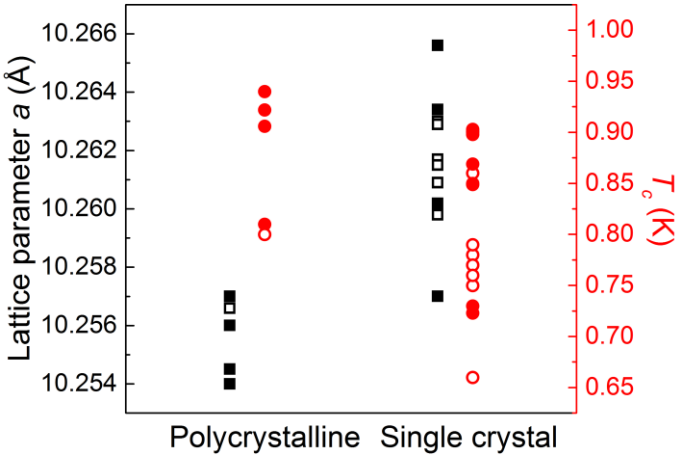

Fig. 1. Reported (full symbols) and our measured values (open symbols) for the lattice parameter *a* (left axis, black squares) and the critical temperature T_c (right axis, red circles) for UBe_{13}.

References

[13] H.R. Ott *et al.*, *Phys. Rev. Lett.* **50(20)**, 1595 (1983).
[14] H.R. Ott *et al.*, *Phys. Rev. Lett.* **52(21)**, 1915 (1984).
[15] N. Oeschler *et al.*, *Acta Phys. Pol. B.* **34(2)**, 255 (2003).
[16] K. Hattori *et al.*, *J. Phys. Soc. Jpn.* **86**, 113702 (2017).
[17] J.L. Smith *et al.*, *J. Appl. Phys.* **55**, 1996 (1984).
[18] A.L. Giorgi *et al.*, LT-17 (contributed papers), 229 (1984).
[19] J.L. Smith *et al.*, *J. Magn. Magn. Mater.* **63-64**, 464 (1987).
[20] W.P. Beyermann *et al.*, *Phys. Rev. B.* **51**, 404 (1995).
[21] R.H. Heffner *et al.*, *J. Appl. Phys.* **70**, 5782 (1991).
[22] C. Langhammer *et al.*, *J. Magn. Magn. Mater.* **177-181**, 443 (1998).
[23] J.L. Smith *et al.*, *Philos. Mag. B* **65**, 1367 (1992).

O14

Electronic transport of the Ti rich U hydrides

Volodymyr Buturlim[1], Ladislav Havela[1], Mykhaylo Paukov[1,2], Oleksandra Koloskova[1], Daria Drozdenko[1], Milan Dopita[1], Peter Minarik[1], Silvie Mašková[1], Michal Falkowski[1]

[1]Charles University, Faculty of Mathematics and Physics, Ke Karlovu 5, 12116 Prague, Czech Republic, e-mail: buturlim@mag.mff.cuni.cz
[2]Immanuel Kant Baltic Federal University, Gaidara 6, 236029, Kaliningrad, Russia

Electronic structure of Uranium compounds can vary dramatically. The main factors that influence it are the smallest distance between Uranium atoms, determining the overlap of the 5*f* states, and the 5*f*-ligand hybridization. An efficient way of tuning is hydrogen absorption, which expands the crystal lattice. Unfortunately hydrides are typically obtained in the form of fine powder, which makes some experiments (e.g. transport) difficult. Here we describe an exceptional case of a monolithic hydride, which allowed to deploy a complete set of low temperature experimental techniques.

In the context of hydrogenation study of U-Ti alloys, we succeeded to synthesize a cubic uranium Laves phase UTi_2H_x, which does not exist without hydrogen. In fact, it is the only U- T (T – transition metal) hydride which adopts the cubic Laves structure. This group of Laves-phase hydrides can absorb a variable amount of hydrogen as was showed by the studies of L- T systems (L – Lanthanide element). The study of $ThZr_2H_y$ [1] suggests that the hydrogen content can range within y = 1.8 - 6.7, this tunes the ground state. Thus UTi_2H_x with $x \approx 5$ H/f.u. exhibiting the smallest $d_{U\text{-}U}$ = 368.2 pm does not order magnetically. Increasing x can yield $d_{U\text{-}U}$ = 371.9 pm and ferromagnetic ground state (T_C = 54 K)[2]. The first hydride is located rather close to the verge of magnetism, where the electron-electron correlations are prominent. Although magnetic susceptibility reflects weak traces of UH_3 ($T_C \approx$ 170 K) and UTi_2H_x ($T_C \approx$ 54 K), the dominant feature is the divergence when approaching T = 0 K (see Fig. 1a). The strongly correlated character is reflected in a prominent upturn of C/T vs T at low temperatures (see Fig. 1b), which is first emphasized and then only slowly suppressed by magnetic fields. The Sommerfeld coefficient can be estimated at 263 mJ/mol U K^2.

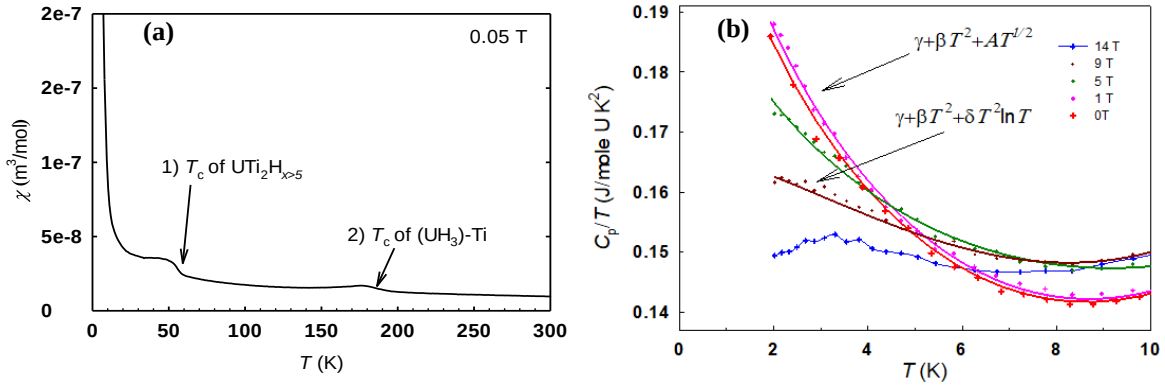

Fig. 1. Magnetic susceptibility of $UTi_2H_{x\approx5}$ measured in 0.05 T, the arrows indicate onsets of the following ferromagnetic impurities (left), specific heat in the *C/T vs. T* representation, which shows the upturn attributed tentatively to weakly interacting spin fluctuations (with $AT^{1/2}$ term, fit for magnetic fields 0, 1, 5 T) and the non-interacting spin fluctuation model with logarithmic term used only for 9 T (right).

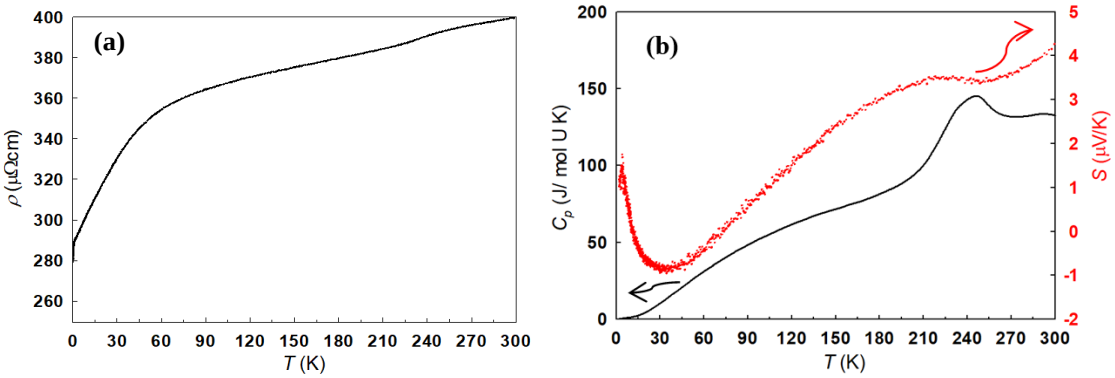

Fig. 2. Temperature dependence of electrical resistivity (a) and comparison of the temperature variation of the thermoelectric power with specific heat (b) of the $UTi_2H_{x\approx5}$.

In the vicinity of the onset of magnetism, the temperature dependence of electrical resistivity is of primary interest. Indeed, our study performed down to 0.3 K exhibits a non-Fermi liquid behavior (Fig. 2a). The aT^n power law has the exponent n close to 1. Fitting gave n = 1.08, which increases to 1.24 in the field of 6 T. We are, however, aware that quantitative analysis of material with high residual resistivity (288 μΩcm is likely due to fractional occupancies of H positions) may be misleading. The broad knee around 50 K can be due to spin fluctuation phenomena. Another weaker anomaly at 230 K is visible also on thermoelectric power $S(T)$. It can be tentatively explained by diffusion of hydrogen at elevated temperatures (hydrogen lattice melting).

This work was supported by the Czech Science Foundation under the grant No. 18-02344S. Part of the work was supported by the project "Nanomaterials center for advanced applications", Project No. CZ.02.1.01/0.0/0.0/15_003/0000485, financed by ERDF.

References

1. W. Bartscher, J. Rebizant, J.M. Haschke, Equilibria and thermodynamic properties of the $ThZr_2$-H system, J. Less Common Met. 136 (1988) 385–394. doi:10.1016/0022-5088(88)90441-9.
2. V. Buturlim, L. Havela, S. Sowa, M. Paukov, D. Drozdenko, M. Dopita, P. Minarik, S. Mašková, Laves phase UTi_2 stabilized by hydrogen and its magnetic properties, Phys. B Condens. Matter. (2017). doi:10.1016/J.PHYSB.2017.10.027.

O15

Novel Canonical Heavy Fermion Compound

E. Svanidze[1], A. Amon[1], M. Nicklas[1], A. Leithe-Jasper[1], Yu. Grin[1]

[1] Max-Planck-Institut fur Chemische Physik fester Stoffe, Noethnitzer Strasse 40, 01187 Dresden, Germany, e-mail: svanidze@cpfs.mpg.de

The field of heavy fermion physics emerged nearly four decades ago and has since become one of the central research directions of condensed matter physics. While significant progress has been made in understanding heavy fermion behavior and accompanying phenomena, the global trends still remain unclear. One of the avenues in the search for heavy fermions has focused on compounds with high coordination, and, therefore, low concentration of uranium atoms. This approach has proven fruitful in the case of antiferromagnetic U_2Zn_{17} and UCd_{11}, as well as unconventional superconductor UBe_{13}. The two former compounds are also the only two canonical heavy fermions. In this work, we present the discovery of the third canonical heavy fermion $U_{11}Hg_{45}$. This compound exhibits an antiferromagnetic transition at $T_N = 2$ K, which can be suppressed by application of magnetic field. A high value of the Sommerfeld coefficient $\gamma = 0.6$ J/U mol K^2 is likely related to the high itineracy of the f-electrons, as evidenced by the high value of the Rhodes-Wohlfarth ratio along with the small entropy of the antiferromagnetic transition.

O16

Exploring and Expanding High Oxidation States of Actinides

John K. Gibson[1], Monica Vasiliu[2], Wibe A. de Jong[3], Kirk A. Peterson[4], Phuong D. Dau[1], Yu Gong[1], David A. Dixon[2]

[1] *Chemical Sciences Division, Lawrence Berkeley National Laboratory, One Cyclotron Road, MS 70A-1150, Berkeley, California 94720, USA, email: JKGibson@lbl.gov*
[2] *Department of Chemistry, The University of Alabama, Tuscaloosa, Alabama 35487, USA*
[3] *Computational Research Division, Lawrence Berkeley National Laboratory, Berkeley, California, 94720, USA*
[4] *Department of Chemistry, Washington State University, Pullman, Washington 99164, USA*

Oxidation states (*OS*) are among the most fundamental of chemical properties. The actinides are characterized by a wide range of well-established *OS*, from +2 to +7 in the particular case of Pu [1,2]. The appearance of high *OS* distinguishes the actinides from the homologous lanthanides and can essentially be ascribed to the higher relative energies of the 5f versus 4f orbitals, which renders the actinide *OS* key characteristics to understand the nature of these elements and variations across the actinide series. Elementary gas-phase molecular ions have been generally demonstrated as a realm to identify new high *OS*, such as in $Pr^{V}O_2^+$ [3] which is the only known pentavalent lanthanide species, and in $Ir^{IX}O_4^+$ [4] which distinctively exhibits the highest known *OS* in the entire periodic table. In view of these results, new actinide oxide molecules and complexes have been studied by experiment and theory to better understand the realm of high actinide *OS*, and identify new actinide *OS* [5,6]. A particular emphasis is the synthesis and properties of elementary binary oxide molecules that can be accurately evaluated by high-level *ab initio* relativistic theoretical approaches for comparison with experimental observations.

Among the recently synthesized and characterized species are NpO_4^- and PuO_4^-, in both of which the oxidation state is +7 with a square planar geometry as shown for PuO_4^- in Figure 1 [7]. Water chemisorption to yield the hydrolysis products results in retention of the heptavalent *OS* in $NpO_3(OH)_2^-$ but reduction to hexavalent Pu in $PuO_3(OH)_2^-$, a result that reveals the slightly higher stability of Np^{VII} versus Pu^{VII}. A particularly notable result is that addition of an electron to neutral $Pu^{V}O_4$ counterintuitively results in *oxidation* to Pu^{VII}, a phenomenon attributable to the redox active nature of dioxygen as O_2^-, O_2^{2-} or $2(O^{2-})$.

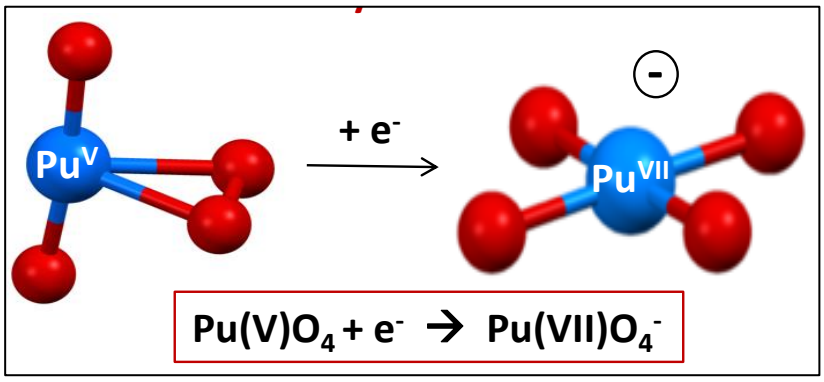

Fig. 1. Addition of an electron to PuO_4 results in oxidation from Pu(V) to Pu(VII) [7].

New *OS* have been prepared in BkO_2^+ and CfO_2^+, both of which are prototypical linear actinyl(V) ions, $\{O=An=O\}^+$ [8]. The synthesis of berkelyl(V) and californyl(V), the first known Bk(V) and Cf(V) species, demonstrates that the 5f electrons remain substantially more chemically accessible late into the series as compared with the 4f electrons of the homologous trivalent lanthanides. The results furthermore extend distinctive actinyl chemistry beyond Am (see Table 1) and reveal an unexpected increase in stability of the AnO_2^+ species beyond CmO_2^+, as indicated by a rise in $\{OAn^+\}$-O bond dissociation energies. It is predicted that EsO_2^+ is also a pentavalent actinyl; einsteinyl(V) is a challenging but enticing synthetic target. Both fermyl and mendelevyl are predicted to be local, albeit not global, energy minima. The new *OS* for the difficult-to-study late actinides are particularly important for more fully characterizing the distinctive nature of these elements, revealing the characteristic chemical involvement of the 5f electrons, and developing advanced computational approaches to more reliably predict chemical properties of even heavier elements that may not be amenable to experimental studies due to extreme scarcity and rapid radioactive decay. As is apparent in Table 1, rich chemistry is predicted for the late AnO_2^+ species.

Table 1. Known (in black) actinide *OS*, and predicted *OS* for AnO_2^+ (in red) [8].*

Ac	Th	Pa	U	Np	Pu	Am	Cm	Bk	Cf	Es	Fm	Md	No	Lr
	2		2	2	2	2			2	2 *2*	2 ***2***	 ***2***	**2** ***2***	
3	3	3	3 *3*	3 *3*	3 *3*	**3** *3*	**3** ***3***	**3** *3*	**3** *3*	**3**	**3**	**3**	3	**3** ***3,***<u>3</u>
	4	4	4	4	**4**	4	4	4	4				<u>4</u>	
		5 **<u>5</u>**	5 **<u>5</u>**	**5** **<u>5</u>**	5 **<u>5</u>**	5 **<u>5</u>**	**<u>5</u>**	**<u>5</u>**	**<u>5</u>**	**<u>5</u>**	<u>5</u>	<u>5</u>		
			6	6	6	6								
				7	7									

*Most stable are in **bold**; actinyls are <u>underlined</u>; *italics* indicate η^2-(O_2) coordination.

Acknowledgements: *Research supported by the U.S. Department of Energy, Office of Basic Energy Sciences, Heavy Element Chemistry Program at LBNL under Contract No. DE-AC02-05CH11231 and at WSU through Grant No. DE-FG02-12ER16329. D.A.D. acknowledges the support of U.S. DOE, OBES, Geochemistry program through a subcontract from the Pacific Northwest National Laboratory, and thanks the Robert Ramsay Fund at the University of Alabama.*

References

[1] C. J. Windorf *et al.*, Journal of the American Chemical Society **139**, 3970 (2017).
[2] C. Keller *et al.*, Angewandte Chemie International Edition **8**, 279 (1969).
[3] Q. N. Zhang *et al.*, Oxides. Angewandte Chemie International Edition **55**, 6896 (2016).
[4] G. J. Wang *et al.*, Nature **514**, 475 (2014).
[5] R. Maurice *et al.*, Inorganic Chemistry **54**, 2367 (2015).
[6] P. D. Dau *et al.*. Inorganic Chemistry **55**, 9830 (2016).
[7] J. K. Gibson *et al.*, Journal of Physical Chemistry A **121**, 9156 (2017).
[8] P. D. Dau *et al.*, Chemistry - A European Journal **23**, 17369 (2017).

O17

Minor actinide separation using new N-donor ligands

Stepan Kalmykov, Petr Matveev, Yuri Ustinyuk

Lomonosov Moscow State University, Department of Chemistry, 119991 Moscow, Russia

Eu/Am and Am/Cm separation is an important and challenging task for nuclear chemists and engineers. The strategy for the back-end of the nuclear fuel cycle is to separate americium isotopes for burn-up in fast neutron nuclear reactors while relatively short-lived isotopes of rare earth elements and Cm could be disposed in near surface geological repositories. This would avoid potential long-term impact of deep geological repositories on the environment.

The aim of the study is to apply hydrophobic/hydrophilic ligands system based on derivatives of N,N'-dialkyl-N,N'-diaryldiamides 1,10-phenantroline-2,9-dicarbonic acid in various solvents and tetraethylamide diglycolic acid (TEDGA) for effective solvent extraction separation of Am(III) and Cm(III) from nitric acid solutions with record high separation factors SFAm/Cm≥5.

The structure and properties of more than 50 new polydentate ligands were modeled using DFT approach to define the general regularities that define complexation properties with electronic effects of substituents, size of coordination cavity and conformational hardness of the ligand. Based on DFT calculations the highest selectivity for Am/Cm separation is predicted for the diamides of 1.10-phenantrolyne-2,9-dicarbonic acid (A, R = NO2, CF3, CN). This prediction was confirmed experimentally in a series of batch solvent extraction tests with various Am and Cm total concentrations and acidities.

The radiation stability of ligands (external gamma-source) was studied as well as radiolysis products were detected by ESI-MS. The highest value of radiation stability was established for CN derivative that makes this ligand promising for large scale applications.

The cascade of mixer-settler extraction units was calculated to achieve complete Am/Cm separation with purity of at least 99.9%.

O18

Probe of plutonium oxide nanoparticles at the large-scale facility

Evgeny Gerber,[1,2,3] Anna Romanchuk[3], Ivan Pidchenko[1,2], Christoph Hennig[1,2], Alexander Trigub[4], Stephan Weiss[2],Stepan Kalmykov[3], and Kristina Kvashnina [1,2]

[1] *Rossendorf Beamline at ESRF – The European Synchrotron, CS40220, 38043 Grenoble Cedex 9, France, e-mail: evgeny.gerber@esrf.fr*
[2] *Helmholtz Zentrum Dresden-Rossendorf (HZDR), Institute of Resource Ecology, PO Box 510119, 01314 Dresden*
[3] *Lomonosov Moscow State University, Department of Chemistry, 119991 Moscow, Russia*
[4] *National Research Centre "Kurchatov Institute", 123182 Moscow, Russia*

Plutonium is a chemical element of a most significant concern at the nuclear legacy sites. The problem of the plutonium migration plays an important role in the environmental radioactivity because of its high radiological toxicity. It was shown previously that plutonium migrates in the subsurface environment on the kilometer scale at some previously contaminated sites [1-2]. During the last few years due to the evolution of spectroscopic and microscopic techniques it was found that so called "colloidal Pu(IV) polymers" actually represents as aggregates of PuO_2 nanoparticles with size ~ 2 nm. [3-4]. Investigation of plutonium oxides nanoparticles is complicated, as plutonium can exist in four partially unstable oxidation states in aqueous solution: III, IV, V, VI under environmental conditions. At the same time, presence of Pu in different oxidation states in PuO_2 structure is still an open question.

This contribution will show first results of plutonium oxide nanoparticles studies at the large-scale facility – The European Synchrotron (ESRF) by X-ray spectroscopy and X-ray diffraction methods. Plutonium nanoparticles were prepared by rapid chemical precipitation using precursors in the different oxidation states. These precursors were obtained by chemical reduction or oxidation of Pu stock solution. The obtained nanoparticles were characterized by high energy resolution fluorescence detection (HERFD) [5] X-ray absorption spectroscopy, extended X-ray absorption fine structure (EXAFS) and X-ray diffraction (XRD) techniques. The experiments were performed at the Rossendorf Beamline (ROBL) at the ESRF, dedicated to actinide science, where we recently installed a novel X-ray emission spectrometer with ground-breaking detection limits. The recently upgraded ROBL beamline at the ESRF provides now a unique opportunity to study actinide materials by several experimental techniques - HERFD, XES, RIXS [6], EXAFS and XRD simultaneously. We will show how the detailed information about local and electronic structure and plutonium oxidation state in different nanoparticles can be obtained using the variety of methods at large scale facilities.

References

[1] A.B. Kersting *et al.*, *Nature* **397**, 56, (1999).
[2] A.P. Novikov *et al.*, *Science* **314**, 638 (2006).
[3] B.A. Powell *et al.*, *Environ. Sci. Technol.* **45**, 2698 (2011).
[4] A.R. Romanchuk *et al.*, *Geochim. Cosmochim. Acta.* **121**, 29 (2013).
[5] K.O. Kvashnina *et al.*, *Phys. Rev. Lett.* **111**, 253002 (2013).
[6] K.O. Kvashnina *et al.*, *J. Electron. Spectrosc. Relat. Phenom.* **194**, 27 (2013).

O19

Single-ion magnets based on uranium compounds

Laura C.J. Pereira, Joana T. Coutinho, Maria A. Antunes, Manuel Almeida

C^2TN, DECN, Instituto Superior Técnico, Universidade de Lisboa, Estrada Nacional 10, 2695-066 Bobadela LRS, Portugal, e-mail: lpereira@ctn.tecnico.ulisboa.pt

Nowadays, one of the most pressing technological needs is to find more efficient ways to store and process digital information. Magnets are a multi-billion euros annual industry with a multitude of uses, such as in computer hard drives, credit and ID cards, motors, and highly specialized instruments, such medical MRI, X-rays or synchrotrons. Also, quantum-based computing is almost practical evidence. The key point is the creation of molecular devices using one or a few magnetic molecules. Single molecule magnets (SMM) based on f-elements have gained increasing relevance since they display magnetic bistability generated by an energy barrier for magnetisation reversal and consequently have memory effect [1]. The fact that these compounds present the highest energy barriers and blocking temperatures makes them the ideal candidates for molecular devices that could store and process information above cryogenic temperatures. Actinides-based SMMs are also very interesting since they present much larger spatial extension of orbitals than lanthanides allowing stronger exchange couplings [2-4]. Recently we have carried out an investigation on uranium-SMMs based on mononuclear species and called single-ion magnets (SIM) allowing a rational study by comparing different compounds to clearly understand the factors that govern the slow relaxation, such as the coordination environment and magnetic anisotropy, while enlightening the relaxation mechanisms.

Two different uranium systems have been studied, depending on their supporting ligands, the hydrotris(3,5-dimethylpyrazolyl)borate ($TpMe^2$) and the triazacyclononane (tacn). Particularly relevant was the result obtained for the complex $[U^{III}(TpMe_2)_2(bipy^{\bullet})]$ [5], a compound that contains a radical monoanionic bipyridine ($bipy^{\bullet -}$) as co-ligand, where the extra magnetic moment of the radical ligand couples with the central ion leading to slow relaxation even at zero field and enhancing the thermally activated relaxation barrier. Recently we have also shown how with an appropriate choice of the coordination environment the presence of a radical ligand enhances the magnetic behavior of an U(IV) compound, $[\{(SiMe_2NPh)_3\text{-tacn}\}U^{IV}(\eta^2\text{-}N_2Ph_2^{\bullet})]$ [6], inducing the appearance of slow magnetic relaxation under zero static magnetic field by changing the parity of the molecule from non-Kramers to Kramers.

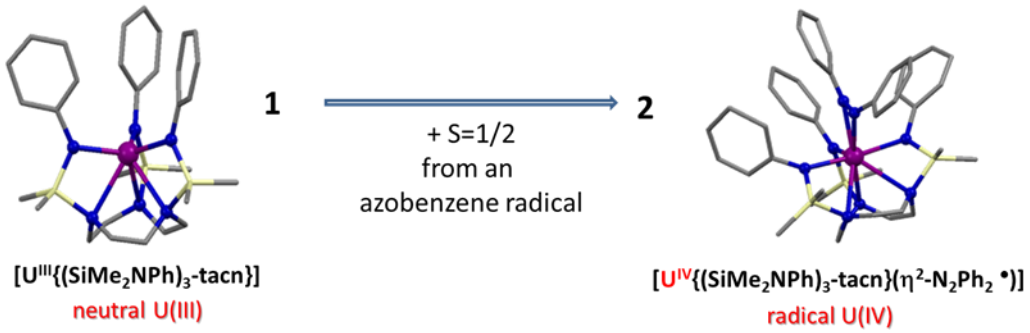

In this work our recent advances in this topic will be presented by illustrating some synthetic strategies to prepare uranium SIMs in a selected set of compounds with different U environments, enabling to probe the effects of structural parameters, like ion oxidation state,

coordination geometry, ligand field strengths, and the radical nature of the ligands on the magnetic properties of such compounds.

Acknowledgements
FCT (UID/Multi/04349/2013); COST Action CA15128 (MolSpin).

References
[1] H.L.C. Feltham, and S. Brooker, *Coord. Chem. Rev*. 2014, 276, 1-33.
[2] Nicola Magnani, Christos Apostolidis, Alfred Morgenstern, Eric Colineau, Jean-Christophe Griveau, Hélène Bolvin , Olaf Walter, Roberto Caciuffo, *Angew. Chem. Int. Ed*. 2011, 50, 1696 –1698.
[3] N. Magnani, E. Colineau, J.-C. Griveau, C. Apostolidis, O. Walter, R. Caciuffo, *Chem. Commun*., 2014, 50, 8171; N. Magnani, Int. J. Quantum Chemistry, 2014, 114, 755–759.
[4] K.R. Meihaus, S. Minasian, W.W. Lukens Jr., S.A. Kozimor, D.K- Shuh, T. Tyliszczak, and J.R. Long, *J. Am. Chem. Soc.*, 2014, 136, 6056.
[5] M.A. Antunes, L.C.J. Pereira, I.C. Santos, M. Mazzanti, J. Marçalo, M. Almeida, *Inorg. Chem*. 2011, 50, 9915-9917; J.T. Coutinho, M.A. Antunes, L.C.J. Pereira, J. Marçalo, M. Mazzanti, H. Bolvin, M. Almeida, Dalton Trans. 2012, 41, 13568–13571; M.A. Antunes, I.C. Santos, H. Bolvin, L.C.J. Pereira, M. Mazzanti, J. Marçalo, M. Almeida, *Dalton Trans*., 2013, 42, 8861–8867; d) J.T. Coutinho, M.A. Antunes, L.C.J. Pereira, J. Marçalo, M. Almeida, *Chem Comm*. 2014, 50, 10262-10264.
[6] M.A. Antunes, J.T. Coutinho, I.C. Santos, J. Marçalo, M. Almeida, J.J. Baldoví, L.C.J. Pereira, A. Gaita-Ariño, and E. Coronado, *Chem.Eur.J*. 2015, 21, 17817-17826.

O20

Spark Plasma Sintering of uranium carbides and silicides

Mathieu Pasturel,[1] N. Brisset,[1] Antonio P. Gonçalves,[2] Sanjib Chowdury,[2] Stéphanie Fryars,[1] Francis Gouttefangeas,[1] Loïc Joanny,[1] Olivier Tougait[1,3]

[1] Univ Rennes, CNRS, ISCR – UMR 6226, CMEBA, F-35000 Rennes, France,
e-mail: mathieu.pasturel@univ-rennes1.fr
[2] C2TN, Instituto Superior Técnico, Universidade de Lisboa, Estrada Nacional 10, 2695-066 Bobadela LRS, Portugal
[3] Univ. Lille, CNRS, Centrale Lille, ENSCL, Univ. Artois, UMR 8181 – UCCS – F-59000 Lille, France

Spark plasma sintering (SPS) combines the effect of a pressure (up to few hundred MPa, depending on the matrix material) applied on the powder, elevated sintering temperature (up to 2000°C for graphite moulds) and high heating/cooling rates (up to few hundred $K.min^{-1}$) reachable by flowing a high intensity electrical current through the conducting mould and the sample if the latter is not an insulator. From these features, it enables the sintering of a wide variety of materials with controlled microstructure, from polymers [1] to refractory materials [2,3], and different shapes, from simple pellets to complex pieces [4].

This technique might thus be of interest in the field of nuclear materials. On the one hand it can help in producing highly dense pellets of nuclear fuels while on the other hand highly porous pellets can be expected for a fast release of exotic isotopes from irradiation targets. Among them, we will focus on the binary silicide U_3Si_2, envisaged as an Accident Tolerant Fuel candidate [5], and on the binary carbides UC and UC_2, both used as irradiation targets [6] and considered as GenIV reactor fuels [7].

We will present our preliminary structural (X-ray diffraction) and microstructural (scanning electron microscopy, electron backscattering diffraction) analyses of spark plasma sintered U_3Si_2 and UC_x (x = 1 or 2), focusing on the influence of sintering pressure and temperature on the density of the pellets, and will compare them to literature data [8,9]. Our work targeted the determination of the minimum pressure and temperature enabling the sintering and the preparation of sintered pellets with the highest achievable density. The reactivity of the materials towards the mould internal cladding will also be evaluated.

References

[1] M. Omori *et al.*, *Mater. Sci. Eng. A* **287**, 183 (2000).
[2] S. Chanthapan *et al.*, *Int. J. Refract.Metals Hard Mater.* **31**, 114 (2012).
[3] O. Guillon *et al.*, *Adv. Eng. Mater.*, **16**, 830 (2014).
[4] C. Manière *et al.*, *Scripta Mater*. **124**, 126 (2016).
[5] J.M. Harp *et al.*, *J. Nucl. Mater*. **466**, 728 (2015).
[6] V.N. Panteleev *et al.*, *Eur. Phys. J. A* **42**, 495 (2009).
[7] R.A. Karam *et al.*, *Trans. Am. Nucl. Soc*. **11**, 245 (1968).
[8] D.A. Lopes *et al.*, *J. Nucl. Mater*. **496**, 234 (2017).
[9] D. Salvato *et al.*, *Ceram. Int.* **43**,866 (2017).

O21

The influence of gaseous impurities on the initial kinetics of uranium-hydrogen reaction

Gan Li [a], Wenhua Luo [a], Chen Yin [b]

[a] Science and Technology on Surface Physics and Chemistry Laboratory, Mianyang 621907, China,
[b] China Academy of Engineering Physics, Mianyang 621900, China

Abstract: The presence of gaseous impurities such as O_2, CO and CO_2 in hydrogen can drastically affect the initial kinetics of the uranium–hydrogen reaction. Understanding how these oxidizing gaseous impurities inhabit the initial hydriding of uranium metal is important fundamentally for many technological applications. In this work, the adsorption isotherms of CO, CO_2 and O_2 on UO_2 powder were measured using static volumetric method, and their effects on the induction time for uranium-hydrogen reaction were investigated by measuring pressure drop combined with in-situ micrographic observation. The Langmuir and Freundlich equations were found to describe well the adsorption behavior of CO and CO_2 on UO_2, respectively, with the adsorption strength following the ordering of O_2>CO_2>CO. The effects of oxidizing gases on the induction time are closely related to their adsorption properties, with inhibition efficiency following the ordering of CO_2>CO>O_2. The induction time is almost direct proportion to CO or O_2 concentration, whereas varies differently as CO_2 concentration depending on its concentration region. The inhibition mechanism of CO or CO_2 is mainly attributed to their preferred occupation of active adsorption sites on the uranium surface, whereas that of O_2 is relatively complex, and may be related to two surface chemical processes: the formation of water precursor state and the diffusion of adsorbed O particles. Based on the inhibition mechanism and gas adsorption property, a simple model was derived, which describes better the influence behavior of CO and CO_2 on the induction time.

Key words: hydriding kinetics, uranium, induction time, oxygen-containing impurities

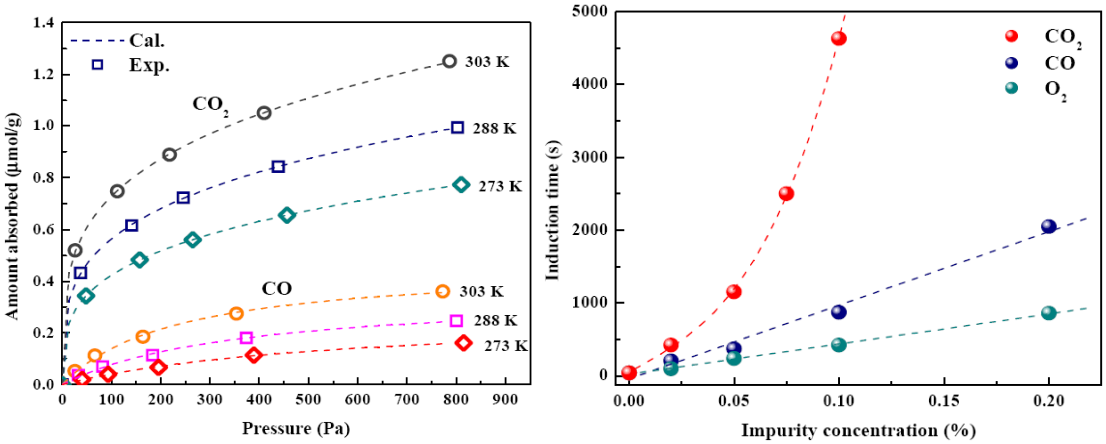

Fig.1 Adsorption isotherms of CO and CO_2 on UO_2 (left) and induction time for uranium-hydrogen reaction as a function of CO, CO_2 and O_2 concentration(right)

O22

Study of the microstructure evolution in monoclinic U-Nb alloy during aging using in-situ X-ray diffraction

Yanzhi Zhang [1], Xiaolin Wang [2], Xinjian Zhang [3]

[1] Science and Technology on Surface Physics and Chemistry Laboratory, Mianyang 621907, China, e-mail: zhangyanzhi@caep.cn
[2] China Academy of Engineering Physics, Mianyang 621900, China
[3] Institute of Materials, China Academy of Engineering Physics, Mianyang 621907, China

The evolution of microstructure in monoclinic U-Nb alloy during aging has been studied using in-situ X-ray diffraction. The experimental results show that the microstructure of monoclinic phase changes evidently with temperatures. The interplanar spacing of (110) and (021) reduce surprisingly with temperature increasing and recover to the origin values at higher temperature. The changes of diffraction peak's position suggest that the maximum constriction of interplanar spacing exceeds the range of macroscopic elastic deformation, which may induce the micro twinning deformation producing in some grains of alloy. The large change in lattice can also produce serious anisotropic lattice distortion, especially in coarse-grained sample because of lower grain boundary density result in lower accommodation. Therefore, we suggest that the effect of lattice distortion on microstructure may be the reason for low-temperature aging strengthening of the alloy. The experimental results can assist in understanding the mechanism of low-temperature aging in monoclinic structure U-Nb alloy.

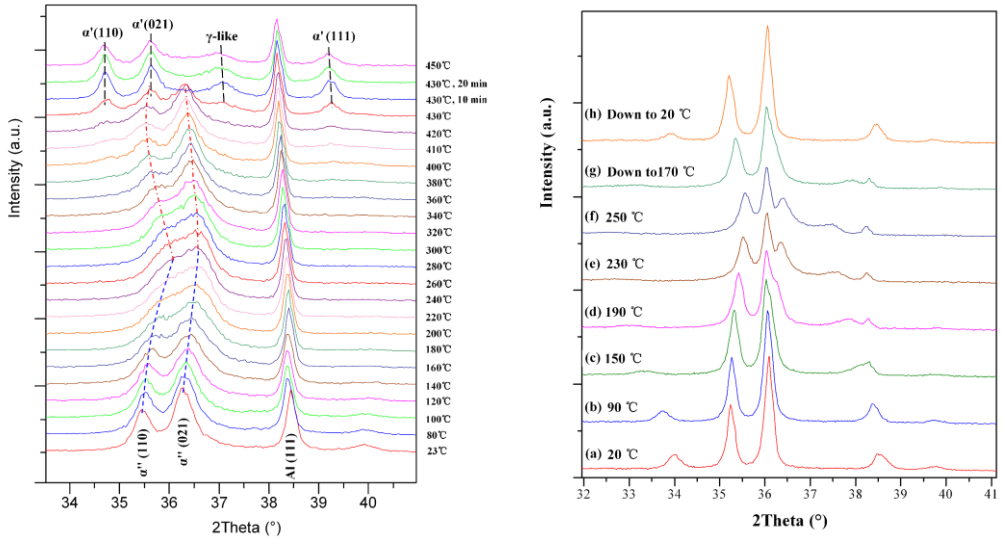

Fig.1 The diffraction peaks changes of fine-grained sample (left) and coarse-grained sample (right) with temperature

O23

Structure and properties of a novel boride $ThNi_{12}B_6$

G. Rogl[1,2,3], P. Rogl[1], H. Michor[2], G. Giester[4], A.P. Gonçalves[5]

[1]Institute of Materials Chemistry and Research, University of Vienna, Waehringerstrasse 42, A-1090 Wien, Austria
[2]Institute of Solid State Physics, TU Wien, Wiedner Hauptstraße 8-10, A-1090 Wien, Austria
[4]Institute of Mineralogy and Crystallography, University of Vienna, Althanstrasse 14, A-1090 Wien, Austria
[5]Centro de Ciências e Tecnologias Nucleares (C2TN), Campus Technologico e Nuclear, Sacavem, Lisboa, Portugal

Abstract

The distribution of boride compounds in the ternary systems rare earth (RE) - iron metal (IM) - boron reveals the general formation of borides preferably in the rare earth metal poor part of the diagrams, however, from rather few Fe-containing ternary borides we see an increasing number of Ni-containing boride compounds.
The investigation of the system Th-Ni-B prompted a novel ternary compound $ThNi_{12}B_6$. X-ray structure analyses of single crystals obtained by mechanical fragmentation of an as cast alloy revealed a fully ordered $CeNi_{12}B_6$-type structure (space group space group $Cmc2_1$, No. 36; a=0.95638(1) nm, b=0.73852(1) nm,c=1.10195(1) nm; R_{F2} = 0.0305).
Specific heat, C_p, and electrical resistivity, ρ, have been determined in the low temperature regime. $C_p(T)$ displayed a smooth dependence without any feature of a phase transition yielding a Debye temperature of θ_D = 506 K. The temperature dependent electrical resistivity ρ(T) shows metallic behavior and could be fitted with the Bloch-Grüneisen model revealing a θ_D = 413 K and a residual resistivity of 13.8 μΩcm.
Static and dynamic hardness were measured in dependence of the applied load and give evidence of a rather hard material. In addition elastic moduli measurements were performed with two different equipments. The Debye temperature, calculated with Mott's equation from elastic properties, is in good accord with those gained via specific heat and electrical resistivity.

O24

Stability of plutonium monoxide from first-principles calculation

Ruizhi Qiu,[1] Xin Wang, Yongbin Zhang, Bingyun Ao, Kezhao Liu

[1] *Institute of Materials, China Academy of Engineering Physics, Huafengxincun No.9, Jiangyou 621908, China, e-mail: qiuruizhi@itp.ac.cn*

The resolution of questions about the existence of condensed plutonium monoxide (PuO) has long been hindered by lack of thermochemical data [1]. Here we perform first-principles calculation to investigate the reaction Pu_2O_3 + Pu → 3 PuO and find that PuO is thermodynamically unstable under ambient pressure (see Fig. 1) [2].

We also find PuO could be stabilized by pressure and impurities, such as carbon. The reaction Pu_2O_3 + Pu → 3 PuO becomes exothermal under pressure above 12 GPa (see Fig. 1). The origin of the stabilization under pressure lies in the delocalization of Pu-5*f* states and the increasing hybridization between Pu-5*f*/6*d* and O-2*p* states [2].

To illustrate the stabilization of PuO by carbon impurity, we performed first-principles calculations on the special quasirandom structures of plutonium monoxycarbide (PuO_xC_{1-x}) to investigate the physical property of monoxycarbide and its dependence on *x* [3]. The solubility limit of oxygen is explored by examining the thermodynamical stability of plutonium monoxycarbide and monoxycarbide is found to be stable for $0 \leq x \leq 0.776$, which agrees well with the experiment (see Fig.2). The stability of PuO_xC_{1-x}, or in other words, the stabilization of plutonium monoxide by carbon impurity, is ascribed to the established Pu 5*f*/6*d*-C 2*p* hybridization around the Fermi level. Moreover, the anomalous variation of experimental lattice parameter was also reproduced by our calculations (see Fig.2). It was interpreted from the interplay between the increase of ionic radius and the shorter Pu-O bond with respect to Pu-C bond, rather than the reported intuitive mechanism of filling the vacancies and then replacing the carbon atoms.

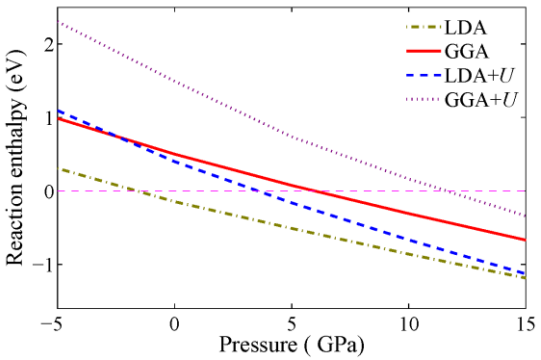

Fig. 1. The reaction enthalpy as a function of pressure from LDA/GGA and LDA/GGA + *U*.

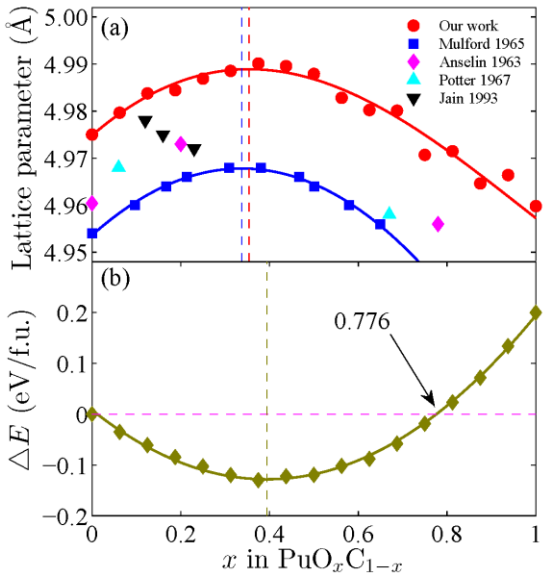

Fig. 2. (a) The lattice parameters of PuO_xC_{1-x} with respect to *x*. The red circle represents the calculated data and the blue square, magenta diamond, cyan triangle, and black downward triangle represent the experimental data. The calculated data and the experimental data from Mulford1965 are fitted to the fourth-order polynomial. (b) Reaction energy ΔE of *x*/3 Pu2O3 + *x*/3 Pu + (1-*x*) PuC → PuO_xC_{1-x} and the fitted curve from a second-order polynomial fitting. The fitted curves and the corresponding peak positions are represented by the solid and dashed lines, respectively.

References

[1] D. Larson, J. Haschke, *Inorg. Chem.* **Vol.20**, 1945 (1981).
[2] R. Qiu, Y. Zhang, B. Ao, *Sci. Rep.* **Vol.7**, 12167 (2017).
[3] R. Qiu, X. Wang, Y. Zhang, B. Ao, K. Liu, *submitted* (2017).

O25

UH_2– a new ferromagnetic uranium hydride analogous to ThH_2, NpH_2 and PuH_2

Ladislav Havela[1], Mykhaylo Paukov[1], Milan Dopita[1], Lukas Horak[1], Daria Drozdenko[1], Martin Divis[1], Ilja Turek[1], Dominik Legut[2], Thomas Gouder[3], Alice Seibert[3], Frank Huber[3]

[1]Faculty of Mathematics and Physics, Charles University, Ke Karlovu 5, 12116 Prague, Czech Republic, e-mail: havela@mag.mff.cuni.cz
[2]IT4Innovations Center, VSB-Technical University of Ostrava, CZ-70833 Ostrava, Czech Republic
[3]European Commission, Joint Research Centre (JRC), Directorate for Nuclear Safety and Security, Postfach 2340, D-76125 Karlsruhe, Germany

Uranium forms with hydrogen two different hydrides with the same UH_3 stoichiometry. The metastable transient form, α-UH_3, represented as bcc uranium filled with H atoms, is fast converted to the stable form β-UH_3, which is also cubic, with U atoms occupying two different crystallographic positions. Both are ferromagnets with the Curie temperature close to 165 K.
In the course of photoelectron spectroscopy study of UH_3 (reported at JdA 2017) we synthesized thin films of U hydrides by reactive sputter deposition. Although the deposition process may in principle destabilize the hydrogen bonding (by heating from the sputter source or by kinetic energy of deposited atoms), it proved feasible in the past [1] and also we succeeded to obtained clean UH_3 films, which consisted of highly textured grains of β-UH_3, and which had the corresponding Curie temperature. Following our research of U hydrides alloyed with Mo, which gives significant T_C enhancement, we attempted also reactive co-sputtering of U and Mo. In this case, however, the hydrides were not formed for significant Mo concentrations, which suggested problems with stability (H bonding enthalpy).
So as to facilitate hydrogen retention, we tested deposition on cooled (170 K) substrate. This indeed led to formation of (U,Mo)H_3. As next we attempted the reactive sputter deposition of pure U on a cooled substrate. In contrast to all previous depositions, where fused silica was used, here we used a Si wafer, covered by Mo film approx. 30 nm thick, to prevent formation of U-Si phases. After the deposition of U hydride was completed (estimated thickness 400 nm), the film was tested by XPS, confirming absence of oxygen and all other contaminants. UPS yielded valence band spectra very similar to UH_3 collected before. Then the film was capped by 15 nm of Mo, removed from the UHV equipment and studied off situ by XRD and magnetometry.

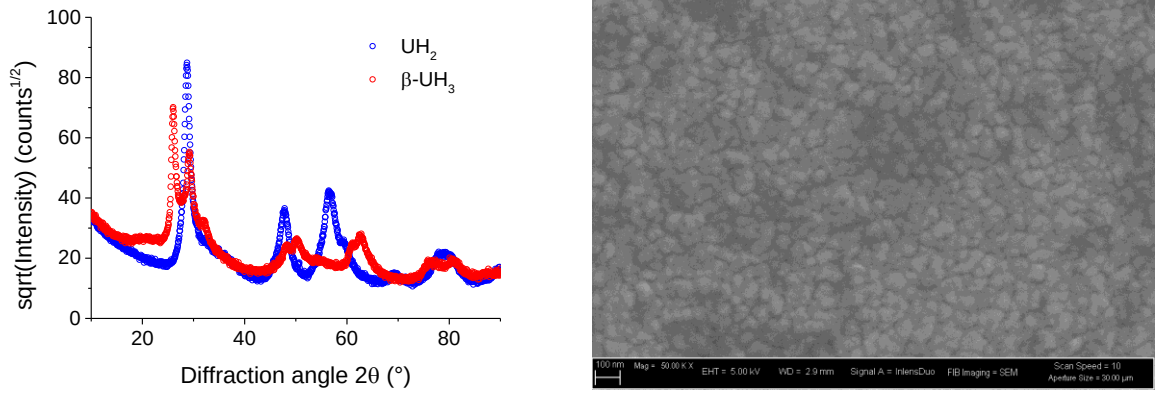

Fig. 1. XRD pattern of UH_2 (blue) compared with β-UH_3 (red), obtained in the parallel beam geometry with constant angle of incidence 1 deg. The SEM micrograph (right) show the grains with a typical size 50-100 nm.

The XRD study (Fig.1) gave no agreement with any of the known UH_3 structures, instead another cubic structure, CaF_2 type, *fcc* structure (*Fm-3m*) with a = 5.3598 ± 0.0014 Å was indicated. It may point to UN_2 (a ≈ 5.31 Å) as a possible species, while isostructural UO_2 is significantly larger (a = 5.471 Å). The lattice parameter is however close to isostructural PuH_2 (a = 5.359 Å) and NpH_{2+x} (a = 5.343-5.355 Å). The fluorite structure is moreover adopted by AcH_2, ThH_2 as a metastable form (a = 5.492 Å), and is shared by numerous rare-earth dihydrides as LaH_2 and YH_2. Hence we can conclude that absence of *fcc* dihydride is actually anomalous and it should be existing for U at least as a metastable type. As shown by the NpH_{2+x} case, additional hydrogen can be accommodated if octahedral positions are occupied [2]. The XRD pattern gives also an information on the in-plane residual strain (-1.54 ± 0.09 GPa) and gives a mean grain size 250 nm, which correlates well with expected columnar grains 400 nm long and with 50-100 nm lateral size.

As common uranium trihydrides yield relatively very high T_C values for moderate U-U distances (3.31 and 3.60 Å for β- and α-UH_3, respectively, we were naturally interested in magnetic properties. The shortest U-U distances are actually somewhat larger, 3.78 Å. Results of magnetic studies seen in Fig.2 reveal T_C ≈ 125 K. The ferromagnetic state is also the ground state obtained from ab-initio calculations. The hysteresis loops are over 9 T wide in the low-temperature limit.

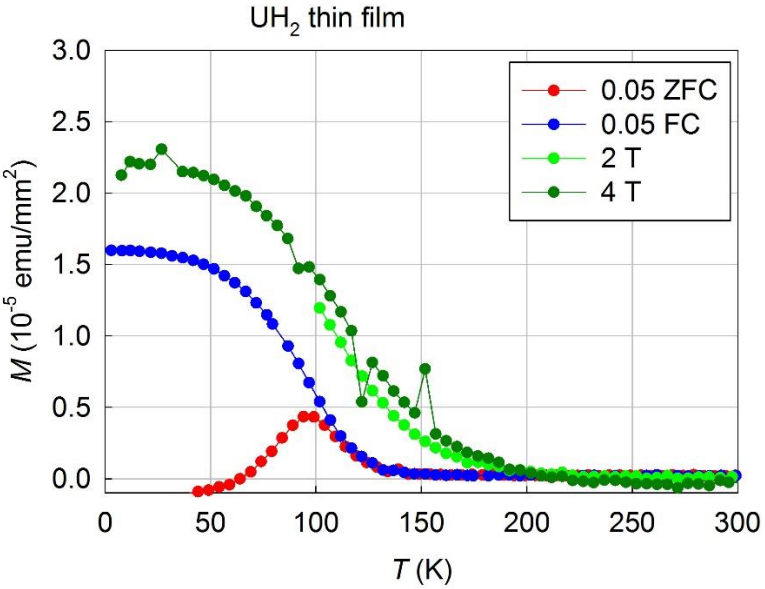

Fig 2. Temperature dependence of magnetization in several magnetic fields measured using a SQUID magnetometer.

We can summarize that new *fcc* uranium hydride was synthesized. Its ground state is ferromagnetic. The key role in stabilization plays likely the effect of substrate (Si has a = 5.431 Å) in combination with low temperature deposition. Details will have to be determined in a forthcoming study.

This work was supported by the Czech Science Foundation under the grant No. 18-02344S. The work at JRC Karlsruhe was supported by the European FP7 TALISMAN project, under contract with the European Commission. Part of the work was supported by the project "Nanomaterials centre for advanced applications", Project No. CZ.02.1.01/0.0/0.0/15_003/0000485, financed by ERDF.

References

[1] T. Gouder *et al.*, *Phys.Rev. B* **70** (1979) 235108.
[2] A.T. Aldred *et al.*, *Phys.Rev. B* **19** (1979) 300-305.

O26

Discontinuous behavior of Uranium compounds in magnetic field

Leonid Sandratskii[1]

[1]*Max Planck Institute of Microstructure Physics, Weinberg 2, D-06120 Halle, Germany, e-mail:lsandr@mpi-halle.de*

It is characteristic for the U compounds to have sharp discontinuous increase of the magnetization in continuously increasing applied magnetic field. This behavior is very often anisotropic and different for different directions of the applied field. The presence of the regions of sharp changes of the magnetization is important characteristic of the physics of the system. The prominent examples are the field-reentrant superconductivity of URhGe [1] or broken hidden order of the puzzling compound URu_2Si_2 [2].

The discontinuity of magnetization has different nature in different compounds. Despite reach collected experimental data the studies on the basis of the density-functional-theory are very rare.

To perform such a study the computational machinery must be able to deal with (i) magnetic field arbitrary directed with respect to the atomic lattice, (ii) noncollinearitu of the magnetic moments of different atoms, (iii) noncollinearity of the spin and orbital moments of the same atom. It is important to investigate how the magnetic behavior depends on the orbital-polarization correction designed to improve the value of the atomic orbital moment and on the on-cite electron correlations within the framework of the LDA+U scheme.

In this talk I report and interpret the results of the in-field calculations for a number of U compounds with different magnetic characteristics. The applied magnetic field couples to both spin and orbital moments and acts in the competition with exchange interaction, magnetic anisotropy, and Dzyaloshinskii-Moriya interaction. The in-field properties of the systems depend crucially on the hierarchy of the interactions.

This study was partly motivated by recent work by Miyake et al. on UPtGe [3].
The discussions with A. Miyake are gratefully acknowledged.

References

[1] A. Miyake, D. Aoki, G. Knebel, V. Taufour, and J. Flouquet, J. Phys: Conf. Series 200, 012122 (2010).
[2] W. Knafo *et al.*, Nat. Commun. 7, 13075 (2016).
[3] A. Miyake, A. Nakamura, Y. Shimura, Y. Honma, D. Li, F. Honda, M. Tokunaga, D. Aoki, doi.org/10.11316/jpsgaiyo.71.1.0_2062.

O27

XMCD studies of UH_3-based ferromagnets: $(UH_3)_{1-x}Mo_x$ and $(UH_3)_{1-x}Zr_x$

Amir Hen,[1] Silvie Maskova,[2] Mykhaylo Paukov,[2] Volodymyr Buturlim,[2] Itzhak Halevy,[3] Fabrice Wilhelm,[1] Andrei Rogalev,[1] and Ladislav Havela[2]

[1]European Synchrotron Radiation Facility (ESRF), B.P.220, F-38043 Grenoble, France
E-mail: amir.hen@mail.huji.ac.il
[2]Department of Condensed Matter Physics, Charles University, KeKarlovu 5, 12116 Prague, Czech Republic
[3]Physics Department, Nuclear Research Center Negev, P.O. Box 9001, IL84190 Beer-Sheva, Israel

Understanding the interaction of uranium and hydrogen is of great importance, e.g. in the field of nuclear energy safety – the formation of uranium hydrides affects the mechanical integrity of uranium, forming a very fine pyrophoric powder. On the other hand, hydrides, in general, provide a tool for investigating the effects of lattice expansion (it can be viewed as application of negative pressure), which, in the case of uranium, might lead to formation of *5f* moments and magnetic ordering [1].
UH_3 is the first reported *5f* ferromagnetic system; synthesized more than half a century ago [2]. UH_3 exists in two structural modifications: the ferromagnetic β-UH_3 ($T_C \approx 165$ K) and the thermodynamically unstable α-UH_3. Attempts to stabilize the α-UH_3 phase upon alloying successfully yielded two stable compounds [1, 3]: $(UH_3)_{1-x}Zr_x$ and $(UH_3)_{1-x}Mo_x$. The Zr based one keeps the α-UH_3 structure whereas the Mo hydride is found to be a nanocrystalline material featuring β-UH_3 crystal structure (see fig.1). Despite their different crystal structures, both hydrides have quite similar basic bulk magnetic characteristics. Both compounds are ferromagnetically ordered below T_C slightly higher compared to the stable β-UH_3 and their macroscopic physical properties have been thoroughly investigated [4].

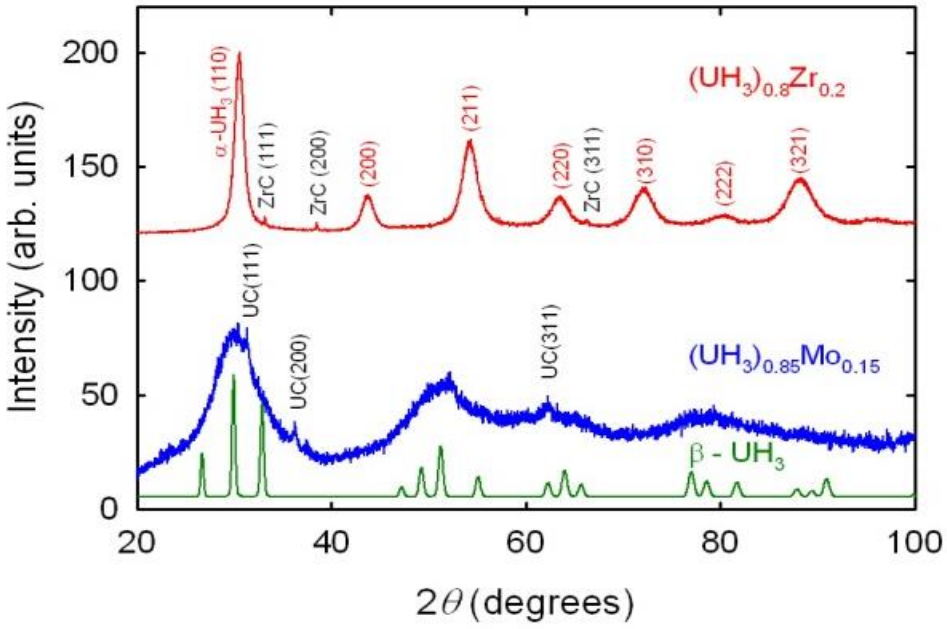

Fig. 1. XRD pattern for Zr- and Mo-alloyed hydrides showing the crystal structure differences [3].

Here we present element selective magnetic measurements of $(UH_3)_{1-x}Mo_x$ and $(UH_3)_{1-x}Zr_x$ powders using X-ray Magnetic Circular Dichroism (XMCD) at the $M_{4,5}$-edges of Uranium and at the $L_{2,3}$-edeges of Zirconium and Molybdenum. Normalized Uranium XMCD

spectra together with the corresponding XANES spectra are reproduced in Fig. 2. Using the so called magneto-optical sum rules we were able to determine the spin (~-0.76 μ_B, ~-0.57 μ_B) and orbital (~1.72 μ_B , ~1.4 μ_B) moments of Uranium in the Zirconium and Molybdenum alloyed samples, respectively. These results are in a rather good agreement with bulk measurements. On the other hand, theoretical calculations also predict large spin and orbital *5f* moments of Uranium which are antiparallel, and an induced sizeable moments on the alloying atoms (Mo, Zr) [5].

XMCD measurements revealed several differences in the magnetic properties between these two hydrides. Whereas an ordered magnetic moment was indeed found on Mo atoms, Zr atoms seem to do not acquire a moment (the XMCD signal is below the present detection limit). The measured magnetic moments on Uranium atoms in the samples also differ by about ~0.2 μ_B and the unoccupied part of the *5f* band appears to be narrower for the Mo alloyed sample.

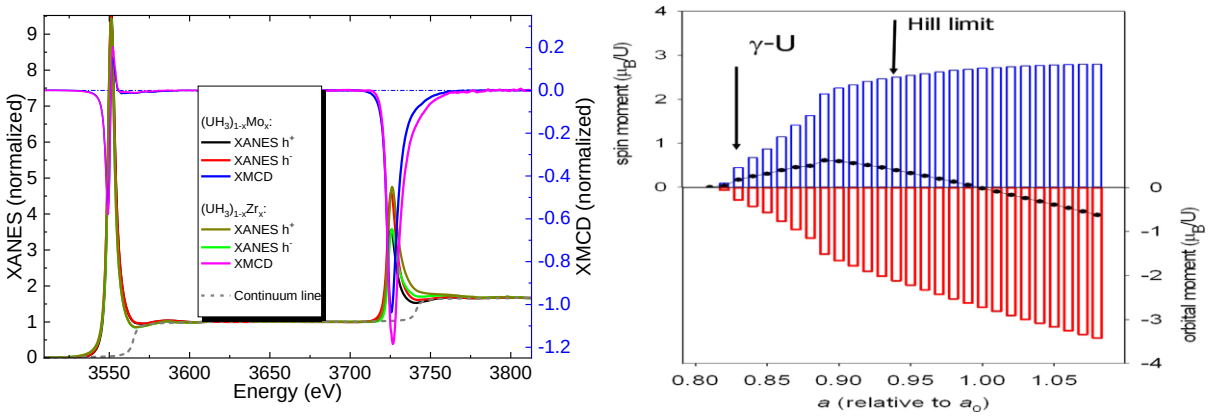

Fig. 2. Left – XANES and XMCD measurements of $(UH_3)_{1-x}Mo_x$ and $(UH_3)_{1-x}Zr_x$ measured at uranium's $M_{4,5}$ absorption edges. Right – Variations of U spin and orbital moments in α-UH_3, calculated by means of the FPLO method, as a function of the lattice parameter (a) normalized to the experimental value a_0. The black dots indicate the total U moments [taken from 5].

Acknowledgement:
This work was supported by the Czech Science Foundation under the grant No. 18-02344S and by the by the European Synchrotron Radiation Facility (ESRF) via project MA-3660.

References

[1] I. Tkach *et al. Physical Review B* **91**, 115116 (2015)
[2] R. Troć and W. Suski, *Journal of Alloys and Compounds* **219**, 1-5 (1995)
[3] I. Tkach *et al. Physical Review B* **88**, 060407(R) (2013)
[4] M. Paukov *et al. Journal of Science: Advanced Materials and Devices* **1**, 185 (2016)
[5] L. Havela *et al. Journal of Magnetism and Magnetic Materials* **400**, 130 (2016)

O28

Magnetic properties of the Np-Ge binary system

E. Colineau[1], P. Boulet[2], F. Wastin[1], J.-C. Griveau[1], R. Eloirdi[1] and R. Caciuffo[1]

[1] European Commission, Joint Research Centre (JRC), Directorate for Nuclear Safety and Security, Postfach 2340, D-76125 Karlsruhe, Germany, e-mail: eric.colineau@ec.europa.eu
[2] Institut Jean Lamour, UMR 7198 CNRS-Université de Lorraine, 2 Allée André Guinier, BP50840, F-54011 Nancy cedex, France

In the Uranium - Germanium binary system, 6 phases have been confirmed to exist and show either paramagnetism (UGe, U_5Ge_4, UGe_3) or ferromagnetism in UGe_2 (T_C = 53 K), U_3Ge_5 (T_C = 94K) and UGe_{2-x} (T_C = 47 K) [1]. The additional occurrence of superconductivity (T_{sc}^{max} = 0.7 K) at high pressure (1-1.5 GPa) in UGe_2 and its coexistence with ferromagnetism [2] has led to extensive experimental and theoretical work about ferromagnetic superconductors.
An equivalent number of phases have been reported for the Neptunium - Germanium analogue system: $NpGe_3$, $NpGe_{2-x}$ ($ThSi_2$ and AlB_2 types), NpGe, Np_5Ge_4 and Np_5Ge_3 [3]. Whereas $NpGe_3$ is a paramagnet, $NpGe_{2-x}$ order ferromagnetically (T_C = 121 K for the $ThSi_2$ type [4] and T_C = 157.4 K for the AlB_2 type [5]), but the physical properties of the other half of the series were not known up to now.
In this contribution, we report on the magnetic properties of NpGe, Np_5Ge_4 and Np_5Ge_3. Figure 1 shows the temperature dependence of the magnetization recorded in NpGe, indicating the onset of ferromagnetic ordering below T_C = 202 K. The marked difference between the Field-Cooled and Zero-Field-Cooled curves reveal the existence of magnetic domains in the sample. In the temperature range between T_C and room temperature, the magnetic susceptibility follows a Curie-Weiss law, from which the effective moment μ_{eff} = 2.2 μ_B (slightly reduced compared to the free ion Np^{3+}) and the paramagnetic Curie temperature θ_p = 190 K (positive, as expected for a ferromagnet and close to T_C) can be inferred. Ferromagnets with relatively high Curie temperatures are not very common in actinides and Np_5Ge_3 also appears to order ferromagnetically with a comparable Curie temperature, T_C = 208 K. On the contrary, Np_5Ge_4 orders antiferromagnetically at T_N = 108K.

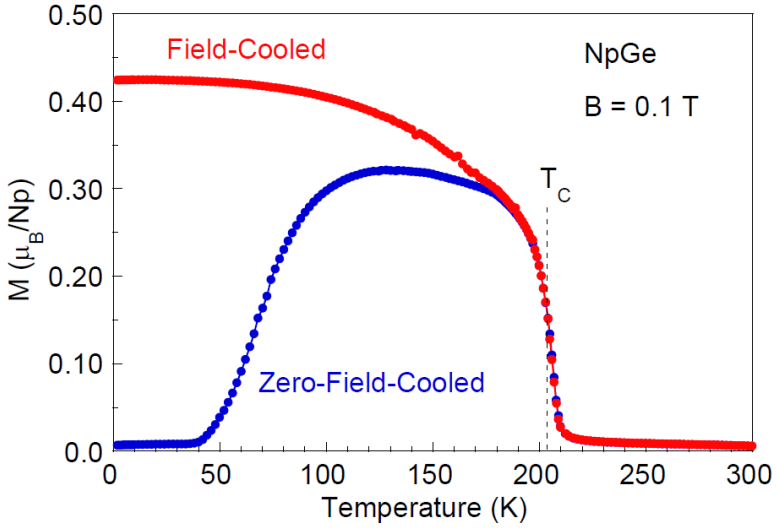

Fig. 1. Magnetization of NpGe in an applied field B = 0.1 T. The blue curve has been obtained by first cooling the sample down to 2 K with B = 0, whereas the red curve has been measured by first applying B = 0.1 T at room temperature and then cooling with the applied field, preventing the formation of magnetic domains.

The two latter compounds undergo a second magnetic transition at $T^* \approx 44$ K and 60 K, respectively. The magnetic phase diagrams of these compounds will be presented and compared to their Uranium analogues and the properties of the whole series discussed in relation with their crystallographic structures.

References

[1] R. Troć *et al.*, *Philos. Mag. B52*, **805**, 805 (2002) and references therein.
[2] S.S. Saxena *et al.*, *Nature.* **406**, 587 (2000).
[3] P. Boulet *et al.*, *J. Solid State Chem.* **156**, 313 (2001).
[4] P. Boulet *et al.*, *J. Alloys Comp.* **337**, 44 (2002).
[5] P. Boulet *et al.*, *Acta Physica Polonica B* **34**, 1421 (2003).

O29

Development of Rapid Semi-empirical Quantum Models for Plutonium Surface Corrosion

Nir Goldman,[1*] Balint Aradi[2], Rebecca Lindsey[1], Larry Fried[1]

[1] *Lawrence Livermore National Laboratory, 7000 East Ave., L-288, Livermore, CA 94550*
e-mail: ngoldman@llnl.gov
[2] *Bremen Center for Computational Materials Science, Universität Bremen, P.O.B. 330440, D-28334, Bremen, Germany*

Plutonium metal is highly complex from a physical and chemical perspective, with six allotropes between ambient and melting conditions [1]. The metastable face-centered-cubic (fcc) δ-phase is of particular interest for engineering applications in part due to its high ductility, in contrast to the unalloyed α-phase ground-state, which is monoclinic and brittle [2]. However, corrosion from gases in the ambient atmosphere of the application environment presents significant challenges due to the high degree of reactivity of the material and the ubiquity of these gases in experimental setups. Surface hydrogenation in particular is problematic, where the Pu-hydride product can catalyze violently exothermic oxidation reactions and even induce pyrophoricity [3]. Despite these pressing issues, relatively little is known about the chemical mechanism for corrosion, and experimental studies would greatly benefit from detailed atomistic knowledge of the chemical reactivity of hydrogen on δ-Pu surfaces. Accurate modeling of the breaking and forming of bonds in condensed phases frequently requires the use of quantum simulation approaches, such as Kohn-Sham Density Functional Theory (DFT). DFT calculations, though, are extremely computationally intensive, and are generally limited to exceedingly small system sizes and time scales. Properties of f-electron solids can be particularly difficult to determine [4], where the computational cost due specifying the electronic spin-states (e.g., anti-ferromagnetic vs. ferromagnetic) and electron correlations precludes the calculation of time-dependent dynamics, reaction barriers, and other properties. Purely empirical classical molecular dynamics force fields, where atomic forces are computed by parameterized potential energy surfaces, are usually highly computationally efficient but tend to yield poor results outside of their fitting regime, and do not allow for the simultaneous determination of electronic properties. Thus, there exists a strong need for atomistic simulation approaches that can achieve acceptable accuracy while exhibiting a high degree of computational efficiency.

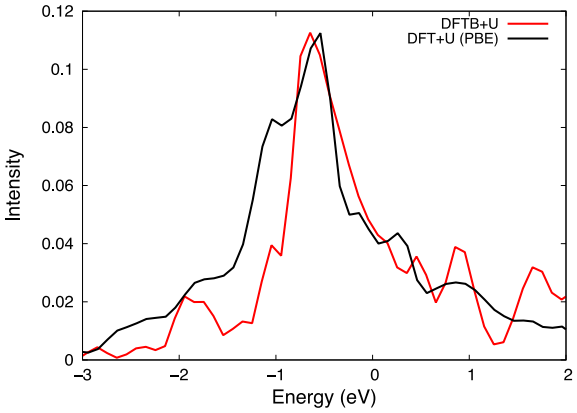

Fig. 1:Electronic density of states for bulk δ-Pu. Our DFTB model (red line) yields accurate results compared to DFT (black line).

To this end, we have created a density functional tight binding (DFTB) semi-empirical quantum approach for the hydrogen/δ-Pu system. DFTB utilizes a balance of empiricism with approximate quantum mechanics to yield computational times that are approximately three orders of magnitude more efficient than Kohn-Sham DFT while retaining most of its accuracy [5]. In this work, we have determined a many-body empirical repulsive energy by force matching linear combinations of Chebyshev polynomials [6] to previously computed DFT results on hydrogen/δ-Pu [4]. The use of a purely linear empirical function allows for optimal

parameters to be determined in a single step, making optimizations for any number of systems extremely rapid. This is in contrast to force field functions that require non-linear optimization methods, which can get trapped in local minima (e.g., Levenberg-Marquardt) or can be too computationally intensive to be of use (e.g., simulated annealing).

We find that the computed total electron density of states from our DFTB model compares well to that from Kohn-Sham DFT for bulk δ-Pu (Figure 1), as well as to the reaction barriers and total energy of reaction for H_2 dissociation on the (100) surface. We have then used our model to compute molecular dynamics simulations of an H_2 molecule adsorbed on the (100) and (111) surfaces, as well as minimum energy paths for hydrogen sub-surface diffusion. Our results indicate that the energetic barriers for diffusion through the (100) surface are relatively high (~2 eV), due to the formation of a stable intermediate wherein the hydrogen ion is tetrahedrally coordinated by four plutonium atoms (Figure 2). In contrast, diffusion through the (111) surface has relatively low energetic barriers (~0.6 eV) because the hydrogen ion is generally coordinated by fewer Pu atoms (Figure 3). This indicates the possibility of corrosive hydriding reactions being more prevalent for δ-Pu (111) crystalline faces. Our DFTB method represents a simple way to perform accurate atomic-level simulations that would be computationally cost-prohibitive with standard quantum calculation approaches. Our efforts are particularly pertinent to studies that rely on these types of calculations for interpretation and validation of their results, such as experimental determination of chemical reactivity on surfaces and in condensed phases.

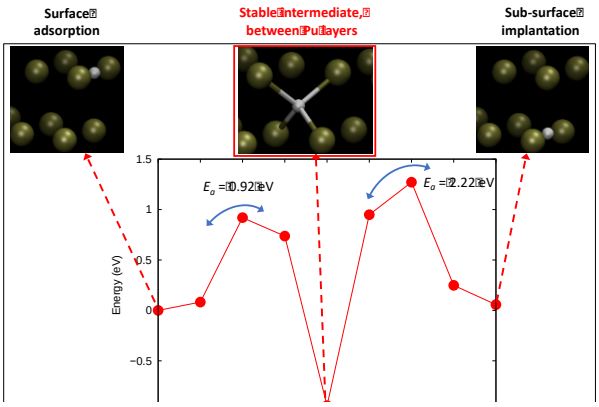

Fig. 2: Minimum energy pathway for hydrogen diffusion through the δ-Pu (100) surface. A low energy minimum occurs between layers, where the hydrogen ion is tetrahedrally coordinated.

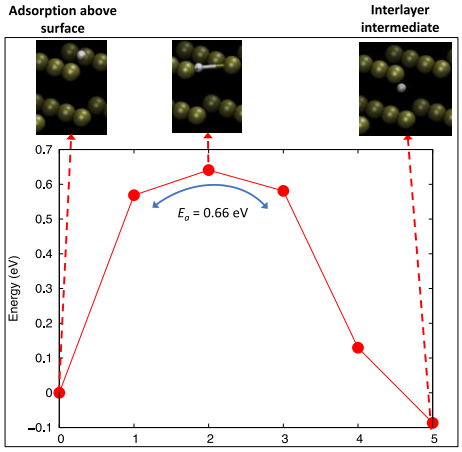

Fig. 3: Minimum energy pathway for diffusion tinto the δ-Pu (111) surface. We compute significantly lower energetic barriers relative to the (100) surface.

** This work performed under the auspices of the U.S. Department of Energy by Lawrence Livermore National Laboratory under Contract DE-AC52-07NA27344.*

References

[1] R. Atta-Fynn and A. K. Ray, *Europhysics Letters*, **85**, 27008 (2009).
[2] A. Arsenlis, W. G. Wolfer, and A. J. Schwartz, *Journal of Nuclear Materials*, **336**, 31 (2005).
[3] B. Sun, H. Liu, H. Song, G. Zhang, H. Zheng, Z.-G. Zhao, P. Zhang, *J. Chem. Phys*., **140**, 164709 (2014).
[4] N. Goldman and M. A. Morales, *J. Phys. Chem. C*, **121**, 17950 (2017).
[5] M. Elstner, D. Porezag, G. Jungnickel, J. Elsner, M. Haugk, T. Frauenheim, S. Suhai, and G. Seifert, *Phys. Rev. B*, **58**, 7260 (1998).
[6] R. K. Lindsey, L. E. Fried, and N. Goldman, *J. Chem. Theory Comput.*, **13**, 6222 (2017).

O30

Actinoid Metal-Boron-Carbon Systems: Phase Equilibria, Crystal Structures and Physical Properties in Th – B - C

Peter Rogl[1], Raimund Podloucky[2], Henri Noel[3], Gerald Giester[4]

[1]*Institute of Materials Chemistry & Research, University of Vienna, A-1090 Wien, Austria*
[2]*Institute of Physical Chemistry, University of Vienna, A-1090 Wien, Austria*
[3]*Laboratoire de Chimie du Solide et Materiaux, UMR-CNRS 6226, Université de Rennes I, F-35042 Rennes, France*
[4]*Institute of Mineralogy and Crystallography, University of Vienna, A-1090 Vienna, Austria.*

As generation IV nuclear fuels include actinoid carbides in combination with B_4C control rods, interest has been revived in the corresponding phase relations for the An-B-C systems. Preliminary studies of phase relations in the ternary systems {Th,U,Np,Pu}-B-C prompted the formation of two main isotypic series of ternary compounds {Th,U,Np,Pu}BC (UBC-type, space group *Cmcm* or ThBC-type, space group $P4_122$) and {Th,U,Np,Pu}B_2C (ThB_2C-type, space group *R*-3*m*); for details see also review given in [1]. Since then isothermal sections have been established for all four systems revealing further compounds, the crystal structures of which have recently been defined from single crystal and powder X-ray intensity data.
Phase equilibria in the system Th-B-C, established at 1400 ºC, reveal four ternary thorium boron carbides: ThBC, ThB_2C, $Th_3B_2C_3$, "$ThBC_2$". Whereas the structures of the former are already established [1], the crystal structure of the latter (hitherto described as "$ThBC_2$"), has now been defined from single crystal data as a new and unique orthorhombic structure type with the proper formula $Th_2B_2C_3$ (space group *Pnnm*, #58; a=1.30655(9) nm, b=0.39757(3) nm, c=0.36507(3) nm). The crystal structure of $Th_2B_2C_3$ is characterized by C-branched infinite chains ...B-C1-B-B-C1-B... whereby each boron atom is additionally linked to a C2-atom. Boron atoms are in a typical triangular prismatic metal coordination, C1-atoms center a bi-pyramid, Th_4B_2, and C2-atoms are surrounded by 5 pyramidal Th-atoms and one B-atom. Bonding from carbon atoms to thorium appears to correspond to the sum of radii for C2, whereas distances d_{Th-B} slightly exceeds the sum of the radii. According to the formula $Th_2B_2C_3$ (formerly "$ThBC_2$"), the phase relations for the Th-B-C system have been revised.
Density functional theory calculations were made for all thorium boron carbides as well as for the homologous uranium boron carbides (including also isotypic CeB_2C) within the pseudopotential approach of VASP utilizing the general gradient approximation for the exchange correlation functional. Structural parameters optimized were in good agreement with the experimental values. Relativistic calculations by including spin-orbit coupling were performed for the electronic structure. Atomic volumes and charges were computed by the concept of Bader yielding the ionic charges and the charge transfer among the atoms. Particularly the analysis of the electronic structure for $Th_2B_2C_3$ shows features of chains and corresponding structural subunits with σ-like bonding. The DFT heat of formations were studied along the sections which involve all the ternary {Th,U} boron carbides: ThB_4 - αThC_2 and αB - ThC as well as for the corresponding U-sections.

References

[1] P. Rogl, "*Ternary Systems M-B-C*", (G. Effenberg Ed.), ASM-MSI, Ohio, USA, 1998, pp. 1-520.

O31

Influence of hydrogen absorption on crystal structure and magnetic properties of the UNi(Al,Ga) solid solution

Silvie Maskova[1], Khrystyna Miliyanchuk[1,2], Anatoliy Senyshyn[3], Lev Akselrud[2], Ladislav Havela[1]

[1]*Department of Condensed Matter Physics, Charles University, Ke Karlovu 5, 12116 Prague, Czech Republic, e-mail: maskova@mag.mff.cuni.cz*
[2]*Department of Inorganic Chemistry, Ivan Franko National University of Lviv, Kyryla i Mefodiya St. 6, 79005 Lviv, Ukraine*
[3]*Forschungsneutronenquelle Heinz Maier-Leibnitz (FRM II), Technische Universität München, 85747 Garching, Germany*

U-based ternary compounds, which were studied in large isostructural series, allow large variations of the 5*f*-localization due to variable 5*f*-5*f* overlap and the 5*f*-hybridization with the *d*- and *p*-states. An additional tuning parameter is the H absorption, working primarily as a negative pressure. At 5*f*-band systems it leads to enhancement of magnetic properties in most of cases [1]. Hydrogenation of a band antiferromagnet UNiAl (ZrNiAl structure type), leading to $UNiAlH_{2.3}$, is increasing the Néel temperature from 19 K to 95 K. UNiGa (ZrNiAl structure type) is a local-moment antiferromagnet, T_N = 39 K. Hydrogen absorption in UNiGa could not be achieved in the past. In the present work we undertook a study of the hydrides of the UNiAl-UNiGa system, and found that the H absorption can be reached even for high Ga concentrations. The hydrogenation of all compounds from the series was performed at hydrogen pressure 100 bar by heating up to T = 473 K and subsequent cooling with the rate 0.1 K/min.
UNiAl can absorb up to 2.3 H/f.u. The desorption experiment showed that the amount of absorbed hydrogen decreases with increasing Ga concentration (2.3 H/f.u. for UNiAl, 2.15 H/f.u. for $UNiAl_{0.4}Ga_{0.6}$ and 1.53 H/f.u. for UNiGa). One characteristic desorption temperature implies one type of H site. Hence we can assume single type of H position. The desorption products were checked by XRD, which proved the reversibility of hydrogenation. Magnetic susceptibility studies reveal certain increase of critical temperatures in the hydrides (Fig. 1), but the increment becomes smaller with increasing Ga concentration as a result of smaller H absorption and concomitant structure changes.

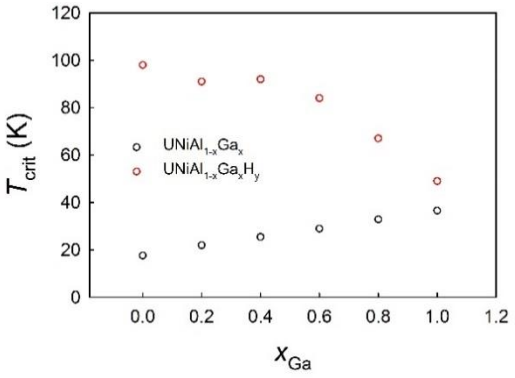

Fig. 1. The concentration dependence of the Néel temperature of UNi(Al,Ga) and their hydrides.

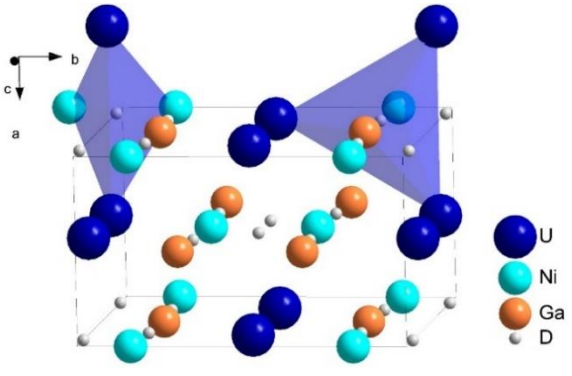

Fig 2. The crystal structure of $UNiGaD_{1.49}$.

There exist several different structure models for the hydrides/deuterides of UNiAl. According to one model, the hydrogenation does not change the type of the crystal structure. It only leads to the deformation of the unit cell. The unit cell volume is increased by approx. 12 %. It is the result of the expansion in the basal plane ($\Delta a/a$ = 7 %), which is partly compensated by the contraction along the *c*-axis. The analysis of X-ray and neutron diffraction data indicates a positional shift of U atoms from (0.572,0,1/2) in UNiAl to (0.666,0,1/2) in $UNiAlH_{2.3}$ [2]. More structure changes were suggested in [3], including an additional shift of Ni atoms along the *c*-direction. The structure thus remains double-layered, but the layers of uranium atoms are separated by the layers containing all nickel and aluminum atoms. The refined values of the atomic coordinates U (0.659(9),0,1/2) and Al (0.347(23),0,0) result in the formation of regular hexagonal nets, i.e. into a symmetry increase. We have revisited the UNiAl-H case, and our data agree well with those published before [2]. Yet, a better fit was obtained in the case of fixed *x*-coordinates for both U and Al (i.e. 2/3 and 1/3, respectively). Thus, the obtained structure can be described by the ternary ordered derivative of AlB_2 structure type LiBaSi (space group *P*-6*m*2). The crystal structure of the hydrides with the Ga content 0.3-0.5 at./f.u. is better described presuming disorder in the Ni and Al/Ga positions, leading to the AlB_2 structure type (space group *P*6/*mmm*). Further increase of Ga content yields the crystal structure of the hydride related to the crystal structure of terminal hydride $UNiGaH_{1.53}$ (space group *Immm*). Its crystal structure was solved by neutron powder diffraction. For the neutron diffraction experiment we have synthesized also the deuteride $UNiGaD_{\sim 1.5}$. The diffraction patterns for $UNiGaD_{\sim 1.5}$ and $UNiGaH_{\sim 1.5}$, collected at room temperature, were indexed in orthorhombic symmetry. The refined crystal structure of $UNiGaD_{1.49}$ is shown on Fig. 2. Deuteration/hydrogenation results in the symmetry decrease compared to the hexagonal parent intermetallic UNiGa. The volume expansion ($\Delta V/V$) reaches 8.6 % and 8.9 % for deuteride and hydride, respectively, and is strongly anisotropic. Also here a lattice expansion in the basal plane is accompanied by a decrease of the lattice parameter *c*. Deuterium atoms occupy two positions: 8*l* inside the trigonal bipyramid [U_3NiGa] and 4*i* inside the tetrahedron [U_2Ni_2], whereas the only hydrogen position 8*l* was found in the hydride (supported by the desorption experiment showing one H position). The metallic matrix of the deuteride/hydride can be regarded as orthorhombically distorted ordered derivative of the AlB_2 structure type.
No additional reflections were observed in the neutron diffraction pattern for $UNiGaD_{\sim 1.5}$ collected at T = 4 K. Hence we can assume a model with identical magnetic and crystallographic unit cell. The shortest U-U distance is reduced from 3.48 Å to 3.37 Å in the deuteride, so the U-moments should be reduced.

Acknowledgement

This work was supported by the Czech Science Foundation under the grant No. 18-02344S. Part of the work was supported by the project "Nanomaterials centre for advanced applications", Project No. CZ.02.1.01/0.0/0.0/15_003/0000485, financed by ERDF. This work is based upon experiments performed at the SPODI instrument operated by FRM II at the Heinz Maier-Leibnitz Zentrum (MLZ), Garching, Germany.

References

[1] S. Maskova, L. Havela, E. Santava, and K. Miliyanchuk, *J. Phys.: Conf. Ser.* **200**, 032040 (2010).
[2] H.N. Bordallo, H. Nakotte, A.V. Kolomiets, A. Christianson, L. Havela, A.J. Schultz, H. Drulis, W. Iwasieczko, *Physica* B **276-278**, 706 (2000).
[3] T. Yamamoto, Y. Ishii, H. Kayano, *J. Alloys Comp.* **269**, 162 (1998).

O32

Recent developments in UC_x targets at C^2TN

S. Chowdhury,[1] M.S. Henriques,[2] L. Maria,[1] A. Cruz,[1] T. Stora,[3] A.P. Gonçalves[1]

[1] Centro de Ciências e Tecnologias Nucleares (C^2TN), Instituto Superior Técnico, Universidade de Lisboa, Estrada Nacional 10, 2695-066 Bobadela LRS, Portugal e-mail: sanjib@ctn.tecnico.ulisboa.pt
[2] Institute of Physics, ASCR, Na Slovance 2, 182 21 Prague, Czech Republic
[3] CERN – European Organization for Nuclear Research, CH-1211 Genève 23, Switzerland

Background:
Radioactive ion beams at ISOLDE, CERN, are produced through nuclear reactions induced by the interaction between an intense proton beam and a thick target material [1]. The target should operate at high temperatures and must quickly release the isotopes. Bulk, micrometric, UC_x-based targets are the current reference at ISOLDE, but a significant increase on the release of exotic isotopes can be obtained from submicron and nanostructured porous materials.
Key isotopes for cancer research are 211-At and 212-Bi. 211-At would be the most important alpha particle emitting radionuclide if widely available, emitting alpha particles without high energy beta particles, which are advantages over 131-I. 212-Bi can be used in targeted alpha therapy. Therefore, there is a need of high yield productions of such isotopes. Nano grain UC_x target materials can be the solution.

Key Method:
Electrospinning is a process of making fiber from viscous solutions. It is a top-down technique based on electro spun of a polymer in solution into ultrafine fibers [2]. In the electrospinning process, a high voltage is used to originate a charged jet of polymer solution out of a needle orifice. Before reaching the collector, the solvent evaporates and interconnected web are collected on the collector. The two electrodes (needle and collector) are connected to oppositely charged power supply. The polymer solution at the tip of the needle, held by its surface tension, is subjected to the high electric field. An induction charge appears on the surface of the liquid, which takes a hemispherical shape due to mutual charge repulsion, contraction of the surface charges and surface tension. If the voltage increases, the hemispherical surface elongates and changes into a conical shape, known as the Taylor Cone. With further increasing of electric field, the cone continues to elongate until a critical value is reached, where the repulsive force overcomes the surface tension and the fluid jet is ejected from the tip of the Taylor cone. After discharging, the polymer solution undergoes 1) bending instability and 2) elongation process that allows and results in the jet to become thin and long.

Experiments and Results:
Uranium precursor nanofibers were made by the electrospinning method. The solutions for electrospinning were prepared by dissolving three different types of uranium precursors (acetate, acetylacetonate and formate) and cellulose acetate in glacial acetic acid and 2,4-pentanedione in 1:1 ratio. The effect of the solution characteristics, including the concentrations of the starting materials and C/U ratio, on the as-spun materials was investigated. The consequence of other electrospinning process parameters, like voltage and distance to targets were also studied. The fibers formed by electrospinning were heated at 550^{o}C to decompose the polymer. A slowly heating (1^{o}C/ min) was used to keep the fiber form. The decomposed material was further heat treated at 1750^{o}C in induction furnace to reduce the oxide. The electrospun precursors and the heat-treated materials were characterized by scanning electron microscopy, X-ray diffraction, thermogravimetry, and transmission electron microscopy.

Schematic setup for electrospinning

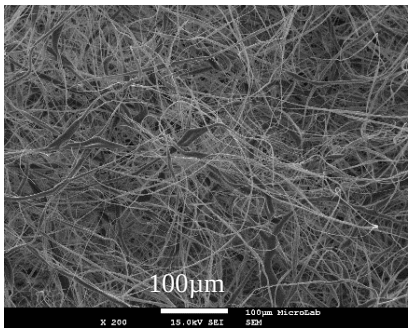

Fig. of. SEM images of fibers for U-formate precursor.

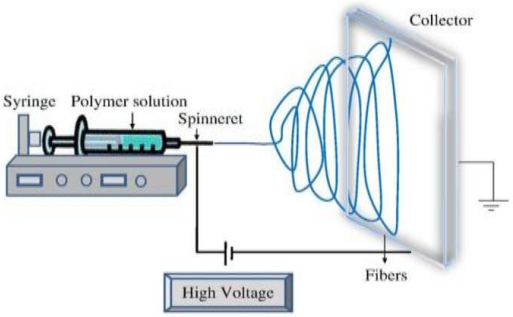

Source: Ning Zhu, Xiongbiao Chen *"Biofabrication of Tissue Scaffolds"*, in book entitled *"Advances in Biomaterials Science and Biomedical Applications"*

References

[1] T. Stora *et al.*, *U.S. Patent 20110235766 A1*, September 29 (2009).
[2] D. H. Reneker *et al.*, *Polymer*, May 13, Vol. 46, pp. 2387-2425 (2008).

O33

Influence of Niobium content on the hydriding behavior of binary uranium alloys

Peng Shi,[1] Lijun Zhu[1], Jiangrong Yang[1], Hefei Ji[1], and Ruiwen Li[1]

[1] *China Academy of Engineering Physics, Mianyang Sichuan, 621907, P. R. China*
e-mail: shipeng@caep.cn

Understanding the corrosion behavior of uranium in atmosphere is very important for the safe handling of uranium. Among which, the uranium hydriding behavior is one of the key points because of the pyrotous nature of uranium hydride and have attracted lots of research interest in the last few decades. Previous research shows that, many different factors, including oxide over-layer, impurities and inclusions [1], alloying elements [2] could influence the hydride nucleation sites and reaction rates. Until now, the underlying mechanism for the interaction between uranium and hydrogen is still not fully understood.

In this report, we will show some recent experimental results on the hydriding behavior of dilute U-Nb alloys. Specimens with different niobium content (namely, U-*x* wt.% Nb, *x* = 0,1, 2, 2.5 and 4) were prepared with arc-furnace method. The hydriding rates were studied by a PVT method, the nucleation sites were analyzed by an ex-situ microscope method.

From the reaction kinetic data we find that, the induction time was increased by the increase in the niobium content. As is known, the solubility enthalpy of hydrogen in uranium and niobium is +7 and -35 kJ/mol, respectively. In other words, the TSS (Terminal Solid Solubility) of hydrogen in U-*x* wt.%Nb is increased with the content of niobium, this may partially contribute to the increase of the induction time. Another interesting experimental finding is that, a reverse decrease in the induction time was seen for U-2.5Nb, compared with U-2Nb. A possible explanation is given like this; U-2Nb is composed of needle-like martensite. In contrast, U-2.5 Nb is composed with a mixture of needle-like and band-like martensite. This indicates that, a higher number density of interface defects might exit in U-2.5Nb alloy, which possibly help trapping of hydrogen atoms and shorten the induction time.

References

[1] W. J. Siekhaus *et al., Journal of Alloys and Compounds* 645, S225-S229 (2015).
[2] Ji, Hefei *et al.. Journal of Nuclear Materials* 464, 43-47 (2015).

O34

Revisiting the Pu(V) and Pu(VI) carbonate systems by CE-ICPMS

J.C. Alexandre[a,b], N. Dacheux[b], J. Aupiais[a]

[a] *CEA, DAM, DIF, F-91297 Arpajon, France, email : jean-charles.alexandre@cea.fr*
[b] *ICSM, CEA, CNRS, ENSCM, Univ Montpellier, Site de Marcoule, 30207 Bagnols sur Cèze, France*

Plutonium is one of the most radiotoxic elements. Its presence in the environment is mainly due to the human activity (atmospherics nuclear weapons tests, accidents, …) Due to its long-term persistence in the environment, the knowledge of its chemical behavior (migration, retention, interaction with organic matter, living organisms) is of the greatest importance.
The present work, in this context, concerns the complexation of plutonium (V) and (VI) by inorganic ligands (CO_3^{2-}) in surface waters (rivers, seas, etc.) by a speciation technique coupling capillary electrophoresis and ICPMS. This study on the Pu(V) and Pu(VI) carbonate systems aims at bringing new data and giving some weight to the actual values recommended by the OECD.
The coupling between these two apparatus (CE-ICPMS) applied to the Pu (V) and Pu (VI) speciation allows determining the thermodynamic data associated to the Pu - carbonates systems. Currently, the results obtained concern the complexation of Pu (V) and Pu (VI) with carbonates ligands at various conditions of temperature and concentration of ligand. The data obtained are consistent with the literature values for Pu(VI) and Pu(V) carbonate systems at 25 °C. Brand new values of enthalpy and entropy of the reaction with Pu(V) and carbonate are proposed.
Concerning the Pu(VI)-carbonate system, data are obtained at 25°C in 0.37 M $NaClO_4$ medium. The overall mobilities determined by CE-ICPMS allows determining the formation constants and the coefficients of the Specific Interaction Theory (SIT) of the 1:1, 1:2, and 1:3 complexes in the conditions cited above (table 1). The following values obtained in this work are extrapolated to ionic strength null: $log_{10}\beta^0_{PuO_2CO_3} = 9.34 \pm 0.44$, $log_{10}\beta^0_{PuO_2(CO_3)_2^{2-}} = 15.02 \pm 0.12$, and $log_{10}\beta^0_{PuO_2(CO_3)_3^{4-}} = 18.07 \pm 0.46$. These values are more precise than the ones recommended by the OECD: $log_{10}\beta^0_{PuO_2CO_3} = 9.5 \pm 0.5$, $log_{10}\beta^0_{PuO_2(CO_3)_2^{2-}} = 14.7 \pm 0.5$, and $log_{10}\beta^0_{PuO_2(CO_3)_3^{4-}} = 18.0 \pm 0.5$. Moreover, the SIT coefficients recommended by the OECD were all obtained by analogy with UO_2^{2+} and NpO_2^{2+} and not experimentally. The values determined by the present work are in the following table:

Table 1 : stability constants β_n^0 and SIT coefficients for the reaction of formation $PuO_2^{2+} + nCO_3^{2-} \rightleftharpoons PuO_2(CO_3)_n^{(2n-2)-}$ in 0.37 M $NaClO_4$ at 25 °C.

	$log_{10}\beta^0$		SIT coefficients in $NaClO_4$ medium	
State or reaction	This work	OECD	This work	OECD
PuO_2^{2+}	-	-	0.43±0.20	0.46±0.05
$PuO_2^{2+} + CO_3^{2-} \rightleftharpoons PuO_2CO_3$	9.34 ± 0.44	9.5 ± 0.5	0	0
$PuO_2^{2+} + 2CO_3^{2-} \rightleftharpoons PuO_2(CO_3)_2^{2-}$	15.02 ± 0.12	14.7 ± 0.5	0.14±0.14	-0.02±0.09
$PuO_2^{2+} + 3CO_3^{2-} \rightleftharpoons PuO_2(CO_3)_3^{4-}$	18.07 ± 0.46	18.0 ± 0.5	0.18±0.20	-0.01±0.11

A divergence is noticed for $\varepsilon_{PuO_2(CO_3)_3^{4-}, Na^+} = 0.18 \pm 0.20$ which was found to be close to that recommended for $\varepsilon_{UO_2(CO_3)_3^{4-}, Na^+} = -0.01 \pm 0.11$.

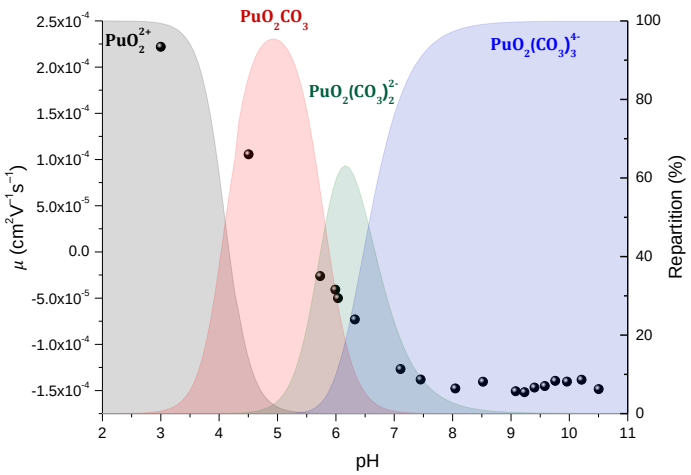

Fig. 1: repartition diagram of Pu(VI) carbonates species in I = 0.37 M $NaClO_4$ at 25 °C and comparison with the overall electrophoretic mobility.

Data on the Pu(V)-carbonate system are obtained at various temperatures in 0.37 M $NaClO_4$ medium. As for the previous system, the formation constants for the 1:1, 1:2, and 1:3 complexes are determined from the overall mobilities obtained by CE-ICPMS (table 2). The following values are obtained at 25°C and extrapolated to zero ionic strength: $log_{10}\beta^0_{PuO_2CO_3^-} = 5.023 \pm 0.044$, $log_{10}\beta^0_{PuO_2(CO_3)_2^{3-}} = 6.260 \pm 0.155$, and $log_{10}\beta^0_{PuO_2(CO_3)_3^{5-}} = 5.371 \pm 0.101$. These values are more precise than those recommended by the OECD: $log_{10}\beta^0_{PuO_2CO_3^-} = 5.120 \pm 0.140$ and $log_{10}\beta^0_{PuO_2(CO_3)_3^{5-}} = 5.025 \pm 0.920$ (value recommended for 1:2 complex by analogy with $NpO_2(CO_3)_2^{3-}$: $log_{10}\beta^0_{PuO_2(CO_3)_2^{3-}} = 6.534 \pm 0.083$). Moreover, the formation constants obtained at various temperatures allow determining new thermodynamic data for this system. The following table sums up the results obtained on the Pu(V)-carbonate system:

Table 2: stability constants β^0_n and thermodynamic constants for the reaction of formation $PuO_2^+ + nCO_3^{2-} \rightleftharpoons PuO_2(CO_3)_n^{(2n-1)-}$ in 0.37 M $NaClO_4$ at 25 °C.

	$log_{10}\beta^0$		This work	
Reaction	This work	OECD	ΔrH° (kJ.mol^{-1})	ΔrS° (J.mol^{-1}.K^{-1})
$PuO_2^+ + CO_3^{2-} \rightleftharpoons PuO_2CO_3^-$	5.023 ± 0.044	5.120 ± 0.140	22.70 ± 4.00	171.71 ± 13.42
$PuO_2^+ + 2CO_3^{2-} \rightleftharpoons PuO_2(CO_3)_2^{3-}$	6.260 ± 0.155	6.543 ± 0.083*	5.42 ± 15.88	142.02 ± 53.31
$PuO_2^+ + 3CO_3^{2-} \rightleftharpoons PuO_2(CO_3)_3^{5-}$	5.371 ± 0.101	5.025 ± 0.920	2.99 ± 5.41	112.24 ± 18.17

*value recommended by analogy with $NpO_2(CO_3)_2^{3-}$

The results obtained on both Pu(V) and Pu(VI) carbonate systems show that the coupling between CE and ICP-MS provides results precise and in good agreement with the ones of the literature which allows considering it as an efficient technic for the determination of the actinides speciation and the thermodynamic data associated.

O35

Oxidation of uranium in liquid water under initial vacuum contained conditions

Antonios Banos[1], Tom Scott[1]

[1] *University of Bristol, Interface Analysis Centre, School of Physics, HH Wills Physics Laboratory, Tyndall Avenue, Bristol, BS8 1TL, United Kingdom, email: ab13306@bristol.ac.uk*

Intermediate level radioactive waste (ILW) has been accumulated in the UK's legacy ponds and silos for over 60 years. Remediation of these plants has been listed as one of the top priorities of the Sellafield decommissioning programme. ILW retrieval, disposal and confinement is a most critical subject owing to the waste's form, activity and relative abundance. ILW is mainly comprised of activated and contaminated metals and materials, such as reactor components, fuel-cladding and conditioned fuel parts [1]. Uranium metal, which acted for many decades as the UK's primary fuel for civil nuclear power generation, can be found in significant quantities in ILW. Thus, uranium and uranium-containing components have been corroding for prolonged periods under water-immersed and/or contained storage conditions. Uranium will readily react with water to produce uranium dioxide (UO_2) and hydrogen gas (H_2). If H_2 does not escape to be diluted in the atmosphere, but instead remains trapped in the near vicinity of the metal, a complex ternary U-H_2O-H_2 reaction system will occur. Uranium hydride (UH_3) has been identified as a potential reaction product of the corrosion process. Hydride formation occurs due to the increasing concentration of hydrogen gas, generated from the reaction of uranium, Magnox (Magnox-AL80) and other metals. The highly-pyrophoric and unstable nature of UH_3 in air poses considerable safety risks, due to the potential of a thermal excursion (leading to radionuclide release) under retrieval and handling of this material. In this work, we endeavour to simulate the corrosion conditions found in the ponds and silos by immersing initially-polished uranium sample in water under initial vacuum-contained conditions. The system is investigated at four different temperatures (25°C, 45°C, 55°C and 70°C). Kinetics of the reaction is monitored using a specially-designed set-up comprised of a stainless steel reaction vessel and a data-logging pressure controller attached to one end. Information on the whole reaction is recorded and the rate of corrosion through gas generation is evaluated. Three main questions wait to be answered:

Is UH_3 identified? For this reason, post-examination of reacted surfaces was conducted using secondary ion mass spectrometry (SIMS), focused ion beam (FIB) milling and X-ray diffraction (XRD).

If UH_3 is identified, can it be quantified? Temperature programmed desorption (TPD), combined with residual gas analysis (RGA), was undertaken on the reacted samples to analyse the emerging gases from sample degassing and yield information about the reaction products of the system.

If UH_3 can be quantified, what are the parameters affecting its formation and quantity?

Data indicating that UH_3 forms on the water-covered uranium surfaces under contained conditions will be presented (Figure 1). The parameters facilitating this formation will be discussed.

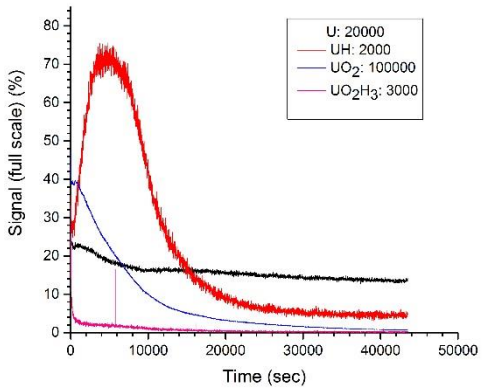

Fig. 1: Secondary ion mass spectrometry (SIMS) depth profile for a uranium sample reacting with liquid water at 70 °C. The analysis was performed with a Ga^+ primary ion beam, 25 keV voltage, 3 nA beam current, and 45 ° angle of incidence.

References

[1] NDA, Radioactive Wastes in the UK: A Summary of the 2016 Inventory, 2016.

O36

Chemical durability of titanite ($CaTiSiO_5$) - a host phase of nuclear waste

Yaping Sun, Ming Zhang

Institute of Materials, China Academy of Engineering Physics, Jiangyou, Sichuan province, 621908, China, e-mail: ypsun0717@163.com

Introduction

Ceramic waste forms are regarded as the second generation of candidate materials for immobilizing high level radioactive-waste (HLW), and the chemical stability of the forms is one of the key factors to determine whether the deep geological disposal is feasible for the application. In order to immobilize radionuclides more than 100,000 years, any suitable form is expected to be highly resistant to corrosion of groundwater and fluids. So it is important to gain a better understanding about what happens when groundwater is percolating through geologic disposal repository into waste forms, and to what degrees the radionuclides can be leached out. Considering radioactive nuclides presented in waste forms would result in radiation damage to the crystal structure, and even lead to an amorphous state (metamict state). How may the radiation damage affect the chemical durability or leaching resistance? Limited systematic works have been carried out, however.

As ceramic waste forms commonly consist of mineral phases, study of the damage effect and leach behavior of those natural minerals containing with radioactive nuclides would be useful. Titanite ($CaTiSiO_5$) is one kind of natural minerals which have been proposed as an actinide-bearing host for HLW. The study on reaction between natural titanites whose structure is damaged by self-containing actinides and water is of significant importance. It could provide insights into what happen inside the titanite-based waste forms.

Experimental

The present study was performed to evaluate the leaching resistance of actinide-containing (mainly U and Th) natural titanites ($CaTiSiO_5$) 2974 (from Renfrew, Ontario, Canada), E2312 (Sebastapol Twp., Ontario) and M28173 (Gjerstad, Norway). Synthetic titanite is also investigated for comparison. Leach experiments were conducted mainly according to the product consistency test B (PCT-B), partially according to the Materials Characterization Center (MCC), which have become the DOE's standard leaching tests. The samples were mixed with liquids (e.g., distilled water, simulated groundwater, strongly acidic or alkaline liquids and solutions) at a ratio of 20-50 ml/g, and held at temperature 90°C or 200°C for 7 or 30 days in a stainless-steel vessel. In order to study the hydrothermal reaction of titanites deeply, heavy water (D_2O), heavy-oxygen water ($H_2{}^{18}O$) is used as leaching agent. X-ray Diffraction (XRD), Infrared (IR), Raman, and Scanning Electron Microscope and Energy Dispersive Spectrometer (SEM-EDS) measurements of titanite were carried out to investigate the effect of leach on treated samples.

Results and Discussion

IR results (Fig.1) show that the effect of neutral water, simulated groundwater (not showed in Fig.1) and 1 M Na_2CO_3 solution on the structure of sample 2974 is very weak. Acid solutions (0.05 HCl) result in a certain effect on 2974, and an obvious effect of oxygen or hydrogen isotope was observed. However, in the 0.5M $AlCl_3$ (and 0.05M HCl, pH=1) solution, the peaks of titanite are almost disappeared, replacing by the characteristic peaks of M-O (Ca-O, Ti-O, Si-O) bend, and SiO_2, indicating a dissolution of titanite

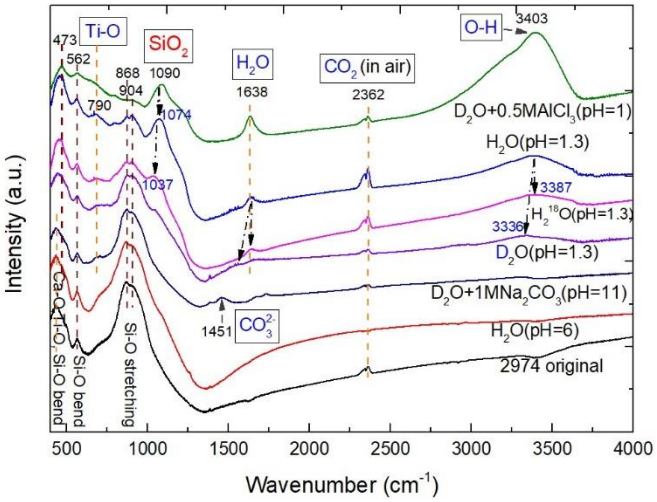

Fig. 1. IR spectrum of natural titanite 2974 under different hydrothermal condition.

Raman results (Figure 2) show the effect of hydrothermal alteration of titanite 2974 in H_2O at temperature 200°C for 30 days, which exhibits an obvious appearance of TiO_2 in 154 cm^{-1}, a loss of Raman spectral details and band weakening indicatig a modification of local crystal structure. There is an obvious difference in leaching resistance between natural titanite and synthetic titanite (not showed in Fig.2).

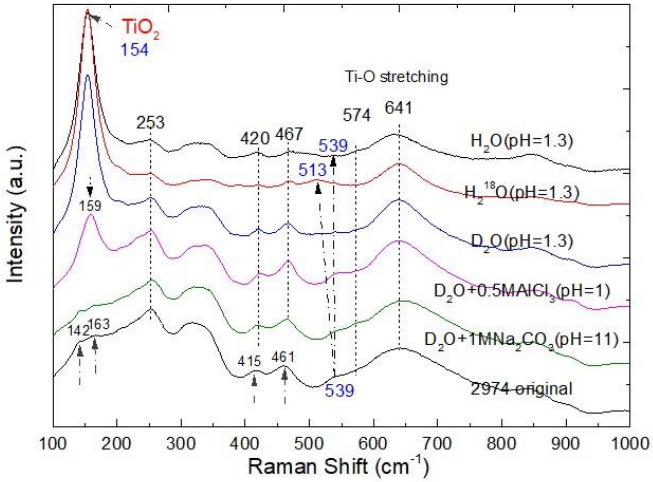

Fig. 2. Raman spectrum of natural titanite 2974 under different hydrothermal condition.

Results of XRD are consistent with IR and Raman. In addition, the natural titanite and synthetic titanite powders leaching in the 1M NaCl-1M HCl and 1M AlCl3-1M HCl solution are both dissolved.

Conclusion

The results indicate in the mild environment which component is close to the groundwater, even at a high temperature of 200°C, titanites are very stable and no phase change is detected by XRD, IR and Raman. But in the strongly acidic, titanites are easily dissolved so it is necessary to avoid the contact for the safe disposal of titanite-base waste forms. Further research is needed to study the effect of radiation damage on the chemical durability of natural titanite.

O37

Multi-scale characterization of UMo/ZrN coated particles used in Al dispersion fuel for research reactors

F. Housaer[1], O. Tougait[1], N. Nuns[1], M. Touzin[2], F. Beclin[2], A. Addad[2], F. Vanni[3], B. Stepnik[3], H. Palancher[4], X. Iltis[4], I. Glagolenko[5], J.L. Schultness[5], M. Hammond[5], D.D. Keiser[5], A. Yacout[6], S. Van den berghe[7], A. Leenaers[7]

[1] UCCS, UMR 8181, Université Lille1, 59655 Villeneuve d'Ascq, e-mail: francois.housaer@univ-lille1.fr
[2] UMET, UMR CNRS 8207, Université Lille1, 59655 Villeneuve d'Ascq, France
[3] FRAMATOME, CERCA, SPL, ZI Les Bérauds, 54 avenue de la déportation, BP 114, F-26104 Romans-sur-Isère, France
[4] CEA, DEN, DEC, Cadarache, F-13108 Saint-Paul-Lez-Durance, France
[5] Nuclear Fuels and Materials Division, Idaho National Laboratory, P. O. Box 1625, Idaho Falls, ID 83415-6188, USA
[6] Nuclear Engineeing Division, Argonne National Laborary, 9700 S. Cass Ave., Lemont, IL 60439, USA
[7] Nuclear Material Science Institute, SCK-CEN, Boeretang 200, 2400 Mol, Belgium

The conversion program of the High Performance Research Reactors (> 100 MW) works for developing low enriched uranium (LEU) fuels to substitute the high enriched uranium (HEU) ones that are still in used in US and Europe mainly [1]. The uranium-molybdenum (U-Mo) fuel system was selected for this aim [2, 3]. For two decades, joint R&D efforts succeed in pushing back the irradiation performances of the UMo fuels [4]. However, at very high burn up, the mechanical integrity of fuel plates is affected by swelling and pillowing effects. Such limits in the used conditions are ascribed to fission gas accumulation at the inter-diffusion layers (IL) [5, 6] at the UMo/Al matrix interface that grow, even at low power. So, coating of the UMo fuel kernel by a thin layer as a diffusion barrier [7, 8] has been recently proposed to prevent IL formation between UMo and Al. Because of its superior thermophysical properties, ZrN is regarded as the best candidate by the European Dispersion Fuel program [9]. Despite beneficial ensues of the diffusion barrier; it has been recently shown that the IL growth is affected by fuel recrystallization [4] rising questions about the microstructure of the fuel powder. The aim of the present work is to deeply characterize the morphology and microstructure at both particle and grain scales of the available commercial products.

Centrifugally atomized U-7wt%Mo spherical particles were produced by KAERI (Korea Atomic Energy Research Institute), which were subsequently coated with about 1-µm-thick ZrN layer using PVD technic at SCK-CEN (Studiecentrum voor Kern Energie, Centre de l'Energie Nucléaire). The coating was carried out on as-atomized powders and annealed ones, haven been heat treated at 1000°C for one hour under Ar. The free powder and details of their coating surface are shown Fig. 1.

The detailed characterization of the UMo/ZrN powder was performed using a multi-scale methodology. As shown in Fig. 2, the powder main features were investigated at the nanoscale, the microscale and the particle scale on both free UMo/ZrN particles and polished cross-sections of powder particles embedded in Al compacts.

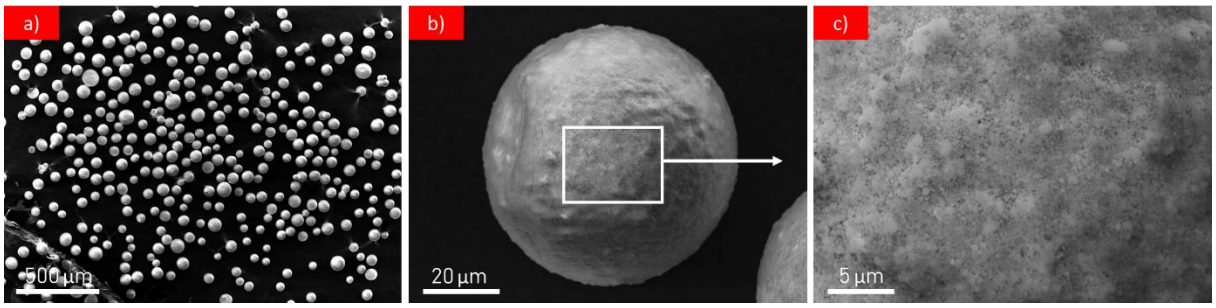

Fig. 1. a) SEM image of the ZrN coated UMo powder, b) SEM image of a selected powder particle, c) SEM image of the ZrN coating surface of the selected powder particle.

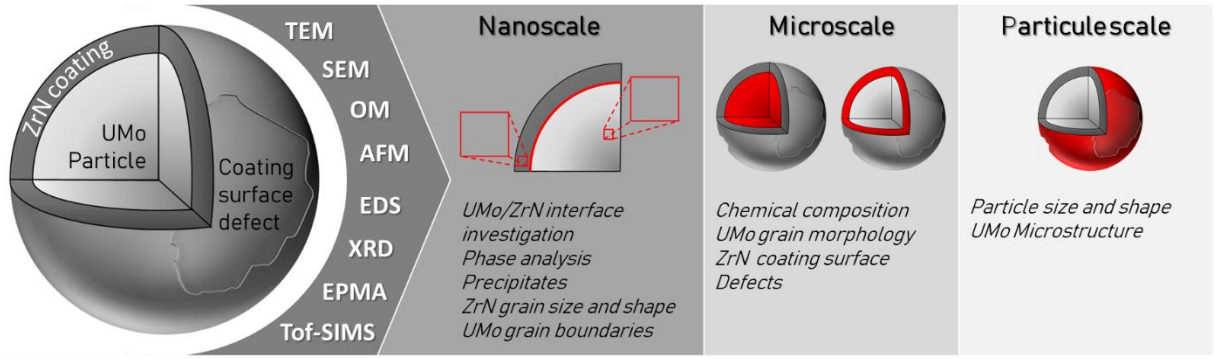

Fig. 2. Experimental multi-scale characterization of ZrN coated UMo Particle.

The UMo/ZrN nanoscale investigations were ensured by transmission electron microscopy (TEM) on focused ion beam (FIB) thin-sections and scratching residues of the ZrN coating, by using HAADF STEM images and SAED diffraction patterns.
The powder microscale examination was conducted by means of powder X-Ray Diffraction (pXRD), Time of Flight Secondary Ion Mass Spectroscopy (Tof-SIMS), Scanning Electron Microscopy, coupled with EDS (Energy Dispersive Spectroscopy) and EPMA (Electron Probe MicroAnalysis), Atomic Force Microscopy and Optical Micoscopy (OM), on both free powder and cross-section samples.
Finaly, a statistical approach using automated SEM and OM images analysis procedure was developed to determine the morphology of the particles in terms of size and shape, with a special care on the deviation from the sphericity (circularity), and proper evaluation of the ZrN width. For this latter, a procedure based on the difference of the apparent diameters, UMo and UMo/ZrN was developed.

In this presentation, the main results of the microstructural features at both elemental grain and particle sizes will be given as a portrait of the centrifugal UMo - ZrN PVD coated powder particles, as well as the selected criteria needed to characterize the powder.

References

[1] J.L. Snelgrove *et al.*, *Nucl. Eng. Des.* **178**, 119-126 (1997).
[2] D.B. Lee *et al.*, *J. Nucl. Mater.* **250**, 79–82 (1997).
[3] B. Ye *et al.*, *J. Nucl. Mater.* **499**, 191-203 (2018).
[4] S. Van den Berghe and P. Lemoine., Nucl. Eng. Tech. **46**, 125-146 (2014)
[5] M.K. Meyer, *et al.*, *J. Nucl. Mater.* **304**, 221-236 (2002).
[6] H. J. Ryu *et al.*, *J. Nucl. Mater.* **321**, 210–220 (2003).
[7] A. Leenaers, *et al.*, *J. Nucl. Mater.* **335**, 39–47 (2004).
[8] J. Rest, Comprehensive Nuclear Materials, (2012).
[9] A. Leenaers *et al.*, *J. Nucl. Mater.* **476**, 218-230 (2016).

O38

Use of Digital Autoradiography to characterize the effect of acidic leaching on mobilisation of ^{238}U series radionuclides in ISR context.

Angileri Axel[1], Sardini Paul[1], Patricia Patrier[1], Daniel Beaufort[1], Guillaume Amiard[3], Descostes Michael[2].

[1] IC2MP – Hydrasa, Poitiers University UMR 7285 CNRS, France, axel.angileriniv-poitiers.fr
[2] AREVA Mines, Paris, France.
[3] PPRIME, Poitiers University, UPR 3346 CNRS, France.

In situ recovery (ISR) is a primary method used to extract U from underground. ISR facilities are used to extract U on low-grade ores where regular mining and milling process may be ~~too~~ expensive. The method consists of injecting acidic solution (lixiviant) through a series of wells into the permeable U-mineralized body to dissolve the uranium-bearing minerals. The lixiviant is pumped through recovery wells to the processing plant where U is extracted from the solution.

This method is based on the geochemical behaviour of uranium which is highly soluble under oxidizing conditions (U^{6+}) and very poorly soluble under reducing conditions (U^{4+}). Natural ^{238}U decay chain includes intermediate radio-isotopes with different geochemical behaviours. The solubilisation of uranium will produce a strong radioactive disequilibrium. As daughter element of ^{238}U series are ultra-traces (in the range of ppq) it will be impossible to locate and quantify them using elementary chemical analysis (EDX, WDS). The most use technic to study the mobility of daughters' isotopes is sequential leaching.

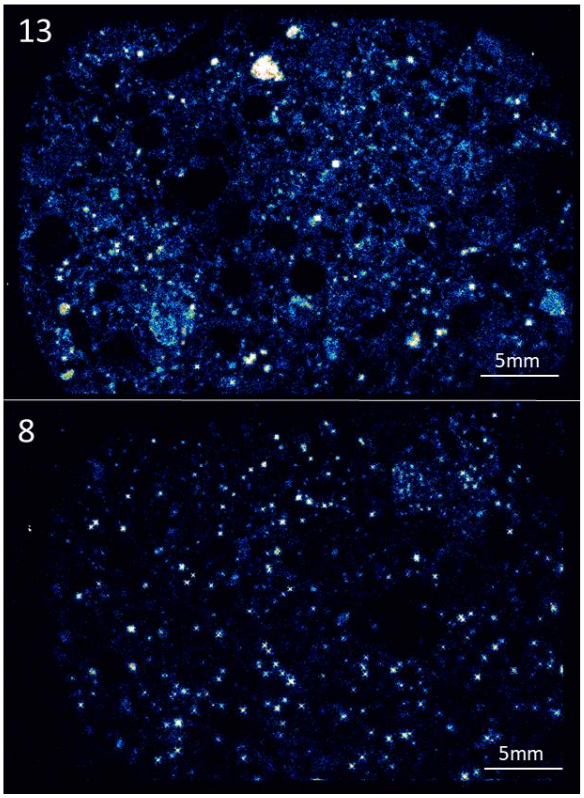

Figure 4 : Alpha autoradiograph on raw ore (top) and leached sample (bottom)

This work is based on a comparative analysis of 2 sand samples from the ISR experimental site of the Dulaan Uul uranium prospect (Mongolia). Both samples were polished thin-sections. The first sample (raw ore) comes from the untreated ore body and the second (leached sand) is from a part of the ore body which was leached during 6 months. The samples consist in coarse to very coarse sand composed of round granitoid type lithic fragments, quartz, alkali feldspar, muscovite, chloritized biotite and subordinate zircon, monazite, and epidote. Previous chemical analysis [1] indicate U-concentration and U-Ra ratio of 400 ppm and near 1 (secular equilibrium) respectively in the untreated ore sample. U-concentration of 6 ppm and U/Ra ratio of 29 were measured in the sample of leached ore.

Three techniques were used in this work: i) the alpha digital autoradiography was used as a mapping tool to locate radioactive regions on the thin-section at micrometric scale, ii) QuemScan chemical mapping was used to obtain a large chemical/mineralogical map of the samples at micrometric scale and iii) a scanning electron microscope coupled with focused ion

beam (SEM-FIB) was used to produce transversal nanometric cross sections directly from the thin sections. Alpha autoradiographs (i) were coupled with the elementary chemical maps (ii) to precisely locate radioactive regions of interest (ROI). The MEB-FIB (iii) was used to study the mineralogy, petrography and chemistry of these ROIs.

Alpha maps of both samples display high active spots (hot spots), diffuse radioactive and inactive zones, cf Fig.1. This heterogeneity illustrates that, for both samples, the alpha activity location is related with the mineralogy and the petrology of the sample even after acidic leaching. Using the autoradiograph/QuemScan maps coupled we observed on the raw ore sample an association between U-rich phases and Fe-Ti minerals, mainly Ilmenite ($FeTiO_3$). Two type of Fe-Ti minerals were identified: the type 1 is composed by strongly altered minerals with dissolution holes sometimes filled by clay minerals. Nanocrystals of uraninite (UO_2) coat the dissolution surfaces of Fe-Ti minerals, cf Fig.2. The type 2 show little trace of alteration and is not associated with clays or uraninite.

The same approach was applied on the leached sample. The remaining U was associated in zircon crystals. Hot spots of alpha activity were located in zones containing Fe-Ti minerals and more rarely barite. The barite shows two specific morphologies. The first is dendritic and often associated with clay minerals. The second one shows overgrowth on a needle-shaped core.

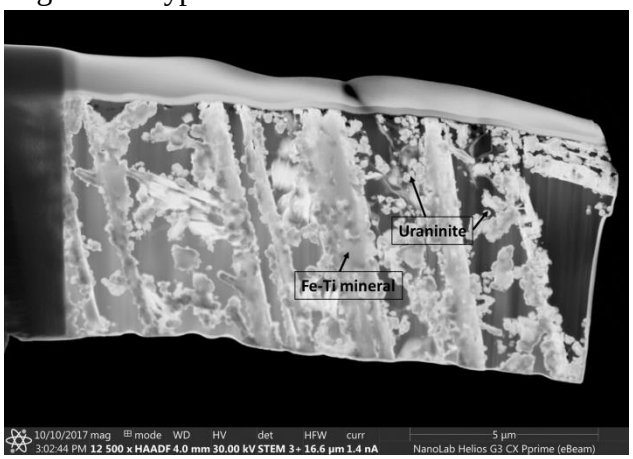

Figure 5: SEM imaging of FIB-cross section showing altered Ilmenite lamellas coated by uraninite nanocrystals

These results bring new information about the fate of intermediate radionuclide in ISR conditions. The relationship between the alpha activity and the mineralogy of the leached samples indicate that daughters' elements appear to be immobile during the leaching process. Intermediate elements seem to be still associated with Fe-Ti minerals. Mineralogical observation may also indicate others process like adsorption on clay phases or co-precipitation with barium sulphates. This work uses digital autoradiography as a rapid and powerful tool to localize and to have an overall understanding of the mobility of the alpha radio-isotopes. Coupling with the uranium content is fundamental to locally deduce the radioactive equilibrium state in the thin-sections.

Reference

[1] M.Reinholdt *et al.* « Réactions minérales et mobilité de l'U et du 226Ra en contexte d'exploitation minière par In Situ Recovery du test expérimental de Dulaan-Uul (Mongolie) », BG Mines AREVA, France, Tech. Report, AMS-DOP-DRD-NT-0094, 16 Sept., 2016.

O39

The oxidation kinetics of nitriding uranium based on ultraviolet-visible reflectance spectroscopy

Haibo Li [a], Huoping Zhong [a], Yuejiao Gu [b], Guangfeng Zhang [a], Gan Li [a], Ping Zhou [a], Yin Hu [a] * and Kezhao Liu [b] **

[a] Science and Technology on Surface Physics and Chemistry Laboratory, P.O. Box No. 718-35, Mianyang, 621907, PR China
[b] Institute of Materials, China Academy of Engineering Physics, P.O. Box 919-71, Mianyang, 621900, PR China

The oxidation kinetics of uranium surface treated by pulsed laser nitriding were studied using reflectance spectroscopy. The growth of the oxide thickness generally follows a parabolic growth model for the nitriding uranium with pure O_2, which is coincided with the diffusion barrier model. The activation energy equaling to 98 kJ/mol was obtained by monitoring the oxide growth in the temperature range of 400-460 K. In comparison, the growth of oxide thickness of untreated uranium was also monitored, indicating that corrosion resistance could be obviously improved after nitriding treatment. It may result from the formation of UNO compound after oxidation, which would resist the diffusion of oxygen ions in the oxide layer.

Keywords. Oxidation kinetics, Pulsed laser nitriding, Reflectance spectroscopy, Activation energy, Corrosion resistance.

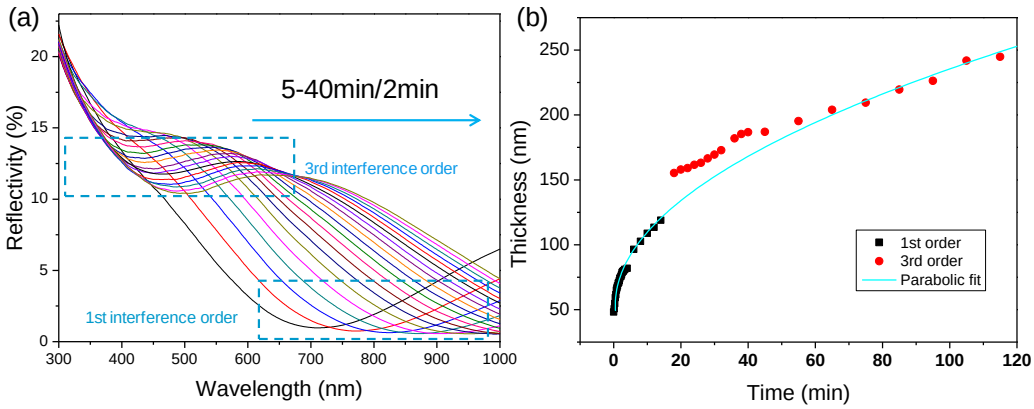

Fig. 1 (a) time-dependent reflectance spectra of nitriding uranium on the oxidizing process at 460 K. (b) growth of oxidation thickness calculated from the reflectance spectra (dots) and the parabolic fitting curve (line).

O40

Heat capacity of $NpPt_3$ and $NpPt_5$ at low temperatures

J.-C. Griveau, E. Colineau, R. Eloirdi, D. Bouëxiere, and R. Caciuffo

European Commission, Joint Research Centre (JRC), Directorate for Nuclear Safety and Security, Postfach 2340, D-76125 Karlsruhe, Germany, e-mail: jean-christophe.griveau@ec.europa.eu

Actinides-platinum intermetallics constitute an interesting binary family due to the variety of crystallographic structures existing through the series. Interacting magnetic features taking place between 5f and 6d electrons are probably at the origin of the stabilization of particular crystallographic structure and competitions between some, for instance hexagonal $P6_3/mmmc$ and cubic F-43m for the $AnPt_5$ phase [1]. While numerous systems have been reported through the An-Pt systems especially for uranium (~ 6 phases) and plutonium (~10 phases), only two have been reported for neptunium, namely NpPt [2] and $NpPt_3$ [3]. Among them, basic properties have been thoroughly examined only for $NpPt_3$, Np counterpart of heavy fermion unconventional superconductor UPt_3 [4], by magnetic, transport, Mössbauer and neutron studies [1,5,6]. It appears that this compound displays a subtle B-T magnetic phase diagram with remaining questions on the nature of the magnetic order below the antiferromagnetic transition temperature T_N= 30 K Here we report on the re-examination of basic properties of $NpPt_3$ and on a new Np-Pt system, namely $NpPt_5$.

Magnetic properties of annealed (1500°C) hexagonal polycrystalline samples $NpPt_3$ have been determined by high sensitivity DC and ac SQUID technique. Using a modified Curie Weiss law to describe its magnetic susceptibility, an effective moment of μ_{eff} =2.87 μ_B and a θ_P ~ -52 K are obtained, very similar to previously reported data [1,6]. DC magnetization measurements vs. temperature in ZFC and FC show different behavior and magnetization vs. magnetic field show an hysteric effect below 19 K probably due to a meta-magnetic transition ~ 3 T, clearly enhanced below 10 K. Heat capacity measurements at B= 0 T from 300 K down to very low temperatures (~ 0.5 K) under high magnetic field (~9 T) show two critical temperatures, T_N ~ 30 K and T_1~ 19 K (Fig 1), both presenting magnetic field dependencies up to 9 T but while T_N decreases with increasing magnetic field, T_1 is increasing, consistently with the possible ferro or ferri magnetic-like structure suggested by neutron diffraction studies [6]. These magnetic features are reminiscent of the $PuPt_3$ behavior, initially reported as a simple antiferromagnet (T_N= 40-60 K) [7] but recently suggested as presenting a ferromagnetic-like transition induced by field at 20 K [8]. Synthesis of single crystals of $NpPt_3$ would definitely clarify the B-T diagram as this system should be highly anisotropic and magnetic field dependent vs. crystallographic direction dependent.

A new Np-Pt system is also reported, namely $NpPt_5$ with a cubic structure (a=0.7445 nm, F-43m). This cubic structure is in continuity with other $AnPt_5$ compounds such as $PaPt_5$ and UPt_5 while $PuPt_5$ would present two allotropic phases (cubic and hexagonal) [9,10]. $NpPt_5$ displays a single magnetic antiferromagnetic transition at T_N~4 K and an enhanced heavy fermion state (γ_e~ 0.450 $J.mol^{-1}.K^{-2}$). A modified Curie Weiss law reproduces well the magnetic susceptibility from 300 down to 50 K leading to an effective moment of 2.80 μ_B (close to Np^{3+}), θ_P~ -46 K and χ_0~520x10^{-6} emu/mol.

Other properties of both systems will be presented and compared to their 4f/5f counterparts.

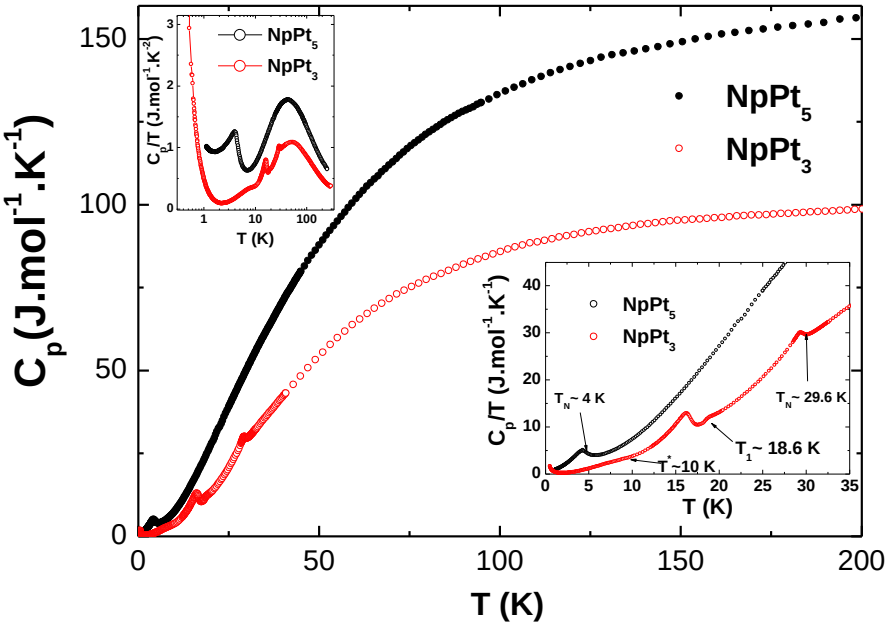

Fig. 1. Heat Capacity curves of polycrystalline $NpPt_3$ and $NpPt_5$ samples at B= 0 T. Several transitions are visible for $NpPt_3$- T_N= 29.6 K - antiferromagnetic state on set-, T_1= 18.6 K flip and possible magnetic domains formations T* 7.8 K as reported by magneto-transport [5]- while only one transition is visible for $NpPt_5$ revealing an antiferromagnetic order at ~ 4 K. At very low temperatures (T<2 K), both systems present a clear up turn probably arising from the nuclear magnetic spin energy contribution.

References

[1] B. Erdmann and C. Keller , Actinide (lanthanide) – Noble metal Alloy Phases, preparation and properties, *J. Sol. State Chem.*, **7**, 40 (1973).
[2] B. Erdman and C. Keller, *Inorg. and Nuc. Chem. Lett.*, **7**, 675, 1971.
[3] A. W. Mitchell and D. J. Lam, *J. of Nuc. Mat.* , **52**, 125, (1974).
[4] G. R. Stewart *et al.*, *Phy.,. Rev. Lett.*, **52** ,679 (1984).
[5] M. Amanowicz *et al.*, "Low-Temperature Magnetotransport of the Intermetallic Actinide Compound $NpPt_3$". In: *Oomi G., Fujii H., Fujita T. (eds) Transport and Thermal Properties of f-Electron Systems. Springer, Boston, MA*, (1993).
[6] N.M. Bouillet *et al.*, *23emes Journées des Actinides*, Schwarzwald, Germany **P 1.13** (1993).
[7] A. R. Harvey *et al.*, *Phys. Rev. B*, **7**, 4137 (1973).
[8] E.D. Bauer *et al.* Pu-futures – The Science 2016, sept. 18-22, Kongresshaus Baden - Baden (Germany), **C-62**, p. 326 (2016).
[9] V.I. Kutaitsev *et al.*, Sov. Atom. Energy, **23** 1279 (1967)
[10] D. E. Peterson *et al. U.S. Ntis, Ad Rep*, **1**, 35 . (1977).

O41

Atomistic Simulations of Self-Irradiation Effects on Dislocation Dynamics in fcc Actinide Alloys

A.V. Karavaev, V.V. Dremov, G.V. Ionov

Russian Federal Nuclear Center – Zababakhin Institute of Technical Physics (RFNC-VNIITF), 13, Vasiliev st., Snezhinsk, Chelyabinsk region, 456770, Russia, e-mail: a.v.karavayev@vniitf.ru

Self-irradiation of fissile materials such as plutonium and its alloys continuously produces radiation defects of crystal structure and decay products, which tend to accumulate, diffusively migrate through the lattice, form clusters, and so on. The microstructure (morphology) of the defects (the characteristic equilibrium size of defect clusters, their shape, clustered and isolated defect fractions) greatly influences the mechanical material properties.
The atomistic simulations approach with the modified embedded atom model (MEAM) for interatomic interaction has been applied to the direct large-scale molecular dynamics simulation of dislocation dynamics in *fcc* δ-phase Pu-Ga alloys. First, parameters of the MEAM potential were fitted to accurately reproduce experimental phonon dispersion curves and density of states at ambient conditions (see Fig. 1) as well as the stacking fault energy and the edge dislocation core structure. With the use of the new MEAM parameterization we demonstrated predictive capabilities of Classical MD in simulations of strength properties of δ-phase Pu-Ga alloys. Indeed, experimental information on static yield stress was not anyhow used in our optimization of the MEAM parameterization. Nevertheless the simulations of dislocation dynamics allowed us to evaluate the yield stress dependence on Ga concentration (see Fig. 2) and its evolution due to aging (see Fig. 3). Both results proved to be in a pretty good agreement with experimental data.

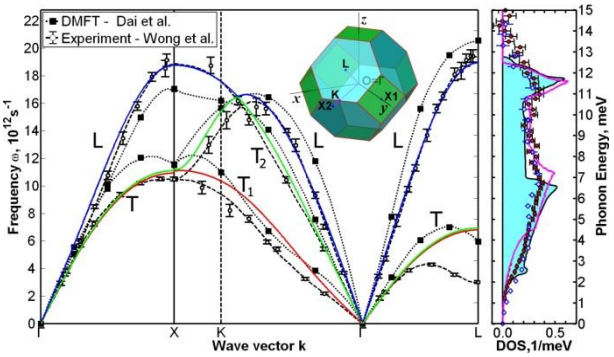

Fig. 1. On the left – phonon dispersion curves in δ-Pu-Ga alloys. The experimental data [1] measured by inelastic X-ray scattering at the ambient conditions for Pu 2 at. % Ga are shown as open circles with the confidence bands (The dashed lines are approximations of the experimental points). The solid red, green, and blue lines show phonon dispersion curves calculated at the ambient conditions for Pu 2 at. % Ga with MEAM interatomic potential. Dotted curves with black squares are calculated dispersion relations for pure δ-Pu based on DMFT [2]. Phonon densities of are plotted in the right panel. Black solid line bounding filled area – DOS derived from the experimental data [1]. Magenta solid lines are DOS for the MEAM. Blue diamonds with the confidence bands are DOS of Pu 2 at. % Ga alloy at T = 300 K experimentally measured by inelastic X-ray scattering [3]. Red circles with the confidence bands are experimental results obtained by inelastic neutron scattering for δ-Pu 5 at. % Al alloy at 300 K [4] shown for comparison.

The results of the MD simulations evidence that the accumulation of radiogenic helium in the form of nanometer-sized bubbles is the main factor affecting strength properties during long-term storage. The developed technique of static yield stress evaluation can be applied to δ-phase Pu-Ga alloys with arbitrary Ga or other alloying addition concentrations. On the other hand, the

results of CMD simulations presented here serve as an independent test for the adequacy of data obtained with the accelerated aging technique to natural aging of δ-phase Pu-Ga alloys at least as of static yield stress evolution.

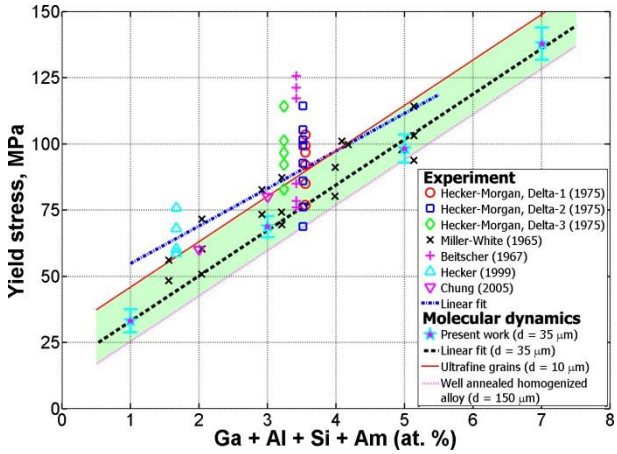

Fig. 2. Yield stress of δ-Pu-Ga alloys as a function of alloying addition amount. Experiment: Hecker-Morgan – [5], Miller-White – [6], Beitscher – [7], Hecker (1999) - private communication, Chung – [8].

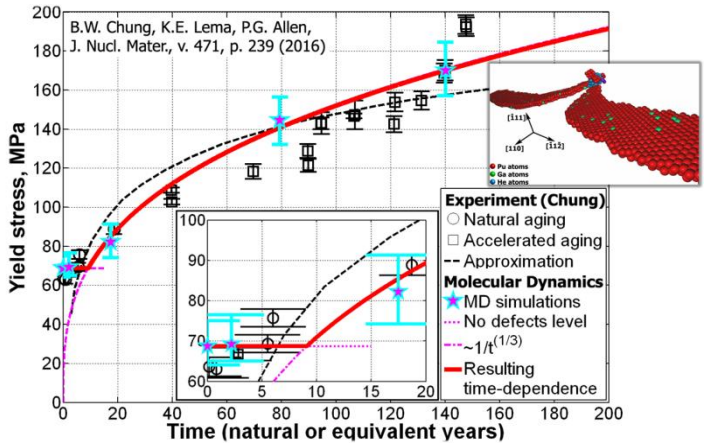

Fig. 3. Dependence of δ-phase Pu-Ga alloy yield stress on sample age. Open symbols with confidence bands – the accelerated aging experiments [8-10] (circles – naturally aged material, squares - spiked alloy samples for accelerated aging). The dashed line represents approximation of the experimental point proposed in [11]. Pentagrams with confidence bands represent results of our CMD simulations [11]. The dotted line is the level of the yield stress in the absence of defects. The dash-dotted line is the hardening due to the increasing concentration of helium bubbles in the material with age. The thick solid line is the resulting time dependence of the yield stress. Radiogenic helium from the Pu-239 α-decay accumulated in the fcc Pu-Ga alloys in the form of nanometer-sized bubbles cause pining of edge dislocations impeding their sliding (inset on the right).

References

[1] J. Wong *et al.*, *Science* **301**, 1078 (2003).
[2] X. Dai *et al.*, *Science* **300**, 953 (2003).
[3] M.E. Manley *et al.*, *Phys. Rev. B* **79**, 052301 (2009).
[4] R.J. McQueeney *et al.*, *Phys. Rev. Lett.* **92**, 146401 (2004).
[5] S.S. Hecker, J.R. Morgan, in: R. Lindner (Ed.), *Plutonium 1975 and Other Actinides*, 1976, North-Holland, Amsterdam, p. 697.
[6] D.C. Miller, J.S. White, *J. Nucl. Mater.* **17**, 54 (1965).
[7] S. Beitscher, *J. Nucl. Mater.* **24**, 113 (1967).
[8] B.W. Chung *et al.*, *J. Nucl. Mater.* **355**, 142 (2006).
[9] B.W. Chung *et al.*, *J. Nucl. Mater*. **385**, 91-94 (2009).
[10] B.W. Chung *et al.*, *J. Nucl. Mater.* **471**, 239-242 (2016).
[11] A.V. Karavaev, V.V. Dremov, G.V. Ionov, **496**, 85-96 (2017).

O42

Theoretical studies of the properties of actinide hydride

Hongzhou Song,[1] Gongmu Zhang[1], Mingfeng Tian[1],Haifeng Song[1]

[1] *Institute of Applied Physics and Computational Mathematics, Beijing 100094, People's Republic of China, e-mail: song_hongzhou@iapcm.ac.cn*

Actinide compounds have been attracting scientific attentions because of their industrial, military, and environmental importances, as well as the vast theoretical prospects around the intriguing 5f electrons. Recently, several researches turn their interests into electronic structures and physical properties of hydrides such as plutonium hydride and uranium hydride.
The electronic structure and thermodynamic properties of plutonium and uranium hydride's(deuteride's) bulk and surface under extreme conditions are investigated using the first principles projector augmented wave (PAW) method. The LDA (GGA)+U schemes has been used to account for the strong on-site coulomb repulsion among the localized Pu 5f electrons. We discuss how the choice of U as well as the choice of exchange-correlation potential affects those properties. Calculation results show that the pure LDA or GGA fails to give the proper electronic structure compared with experiments, while the LDA+U schemes can effectively remedy these failures.Such questions are an instance of the more general topic of correlation sensitivity for other actinide compounds.

Keywords: Actinide hydride, under extreme conditions, PAW method

References

[1] S. Y. Savrasov, G. Kotliar, and E. Abrahams, Nature 410, 793 (2001).
[2] C.D. Taylor *et al.*, Phys. Rev. B 82, 224408(2010) .

O43

The hydriding resistance of plutonium mononitride: A view from AIMD

Bo Sun,[1] Gongmu Zhang[1], Hai-Feng Liu[1],Haifeng Song[1]

[1] *Institute of Applied Physics and Computational Mathematics, Beijing 100094, People's Republic of China, e-mail: zhang_gongmu@iapcm.ac.cn*

Based on the non-local van der Waals density functional (vdW-DF)+U scheme, we carry out the ab initio molecular dynamics (AIMD) study of the interaction dynamics for H2 molecules impingement against Pu-nitride (PuN) surfaces. We show that except for the weak physisorption, PuN surface is so difficult of access that almost all of H2 molecules will bounce back to the vacuum when their initial kinetic energies are not sufficient. PuN is found to be one kind of stable and uniform passivation layer against the hydrogen-corrosion of Pu-metal — specifically, the incorporation of PuN and H-atom is proven to be thermodynamically unstable. Overall, our current study reveals the mechanical and chemical resistances of Pu-nitride to hydrogen corrosion, which have strong implications to the understanding of the surface corrosion and passivation of Pu metal.

Keywords: Pu-nitride; Surface corrosion; AIMD; vdW-DF+U

O44

Disorder effects in the electrical resistivity of γ-($U_{0.78}$-$Mo_{0.22}$) single crystal thin films

Daniel Chaney[1], Joseph Sutcliffe[1], Christopher Bell[1], Ross Springell[1]

[1] *University of Bristol, BS8 1TL, UK, email: dc12791@bristol.ac.uk*

The uranium molybdenum system belongs to a class of highly disordered alloys exhibiting negative temperature coefficients of resistivity, $\alpha = d\rho/dT$ [1]. In 1973 Mooij [2] correlated α with the residual resistivity (RR) of disordered alloys, showing that negative α would be expected in alloys where RR $\geq 150\ \Omega\text{cm}^{-1}$. This correlation can be explained by the approach of the electron mean free path to the interatomic spacing, resulting in weak localisation. Kaveh and Mott [3] first showed that this would lead to negative α, as the constructive interference between scattered waves is reduced by inelastic scattering; a mechanism that increases with temperature. Below the Debye temperature (θ_D), the inelastic diffusion length (L_i) is governed by electron-electron interactions leading to $-\alpha \propto T$. Above θ_D, L_i is dominated by electron-phonon scattering such that $-\alpha \propto T^{1/2}$. At very low temperatures there also exists an important contribution from *long range* Coulomb interactions producing a change in the density of states near the fermi energy ($-\alpha \propto T^{1/2}$) [4]. Such phenomena have been observed in several disordered alloys [5,6], however, a systematic study of the *bcc* uranium molybdenum system has not been conducted. This is of particular interest when considering its use as a potential nuclear fuel [7] due the importance of thermal transport. Molybdenum concentration is expected to be a significant parameter due to its influence on both the level of disorder and interatomic spacing.

Single crystals allow us to isolate the effects of randomly distributed Mo atoms from other sources of disorder: dislocations, grain boundaries etc. normally found in stabilised *bcc* uranium

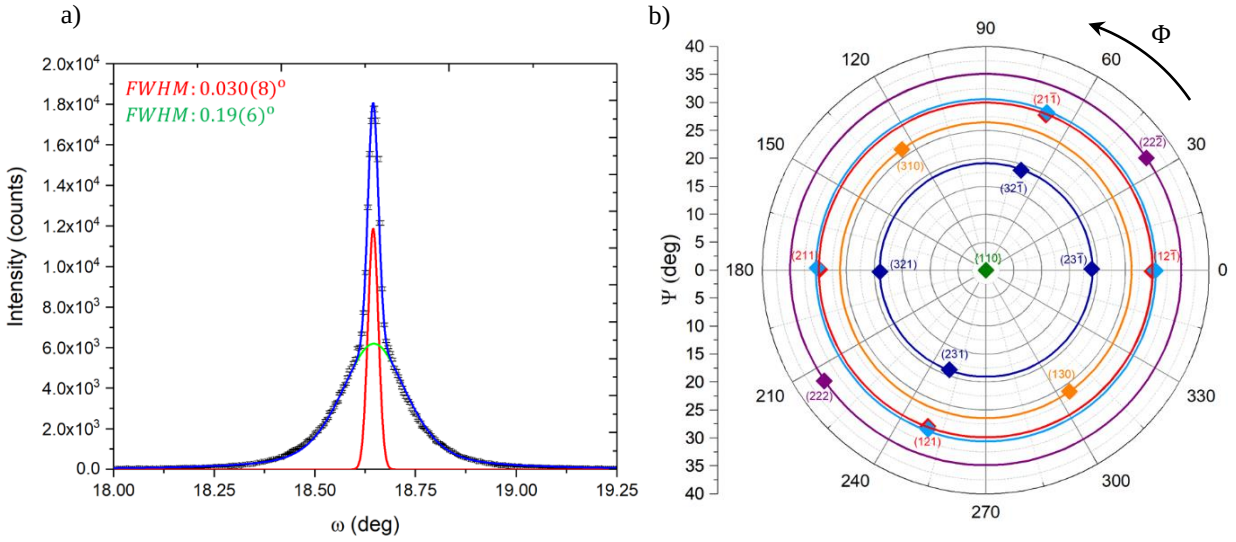

Fig. 1. a) Rocking curve of the (110) (specular) peak showing a clear two component profile indicative of high quality films. b) Polar plot showing positions of U-Mo reflections (curves indicate regions probed), Nb reflections shown in light blue.

alloys. Building on previous work [8] we have grown high quality (mosaic = 0.03deg, fig.1a), [110] oriented, γ-($U_{0.78}$-$Mo_{0.22}$) single crystal thin films. Using a combination of specular and

off specular x ray diffraction we have shown that $a = b = 3.41(3)$ and $c = 3.42(6)$ Å with a single domain, epitaxial relationship: $(110)_{\mathrm{Nb}}||(110)_{\mathrm{U-Mo}}\ [110]_{\mathrm{Nb}}||[110]_{\mathrm{U-Mo}}$, fig. 1b. Synthesis and characterisation combined with initial results from transport studies will be presented.

References

[1] B.S. Chandrasekhar and J.K. Hulm, *J. Phys. Chem. Solids*, **7**, 259, (1958)
[2] J.H. Mooij, *Phys. Stat. Sol. (a)*, **17**, 521 (1973)
[3] M. Kaveh and N.F. Mott, *Phil. Mag.*, **B47**, 69, (1983)
[4] B.L. Altshuler and A.G. Aronov, *Solid State Commun*, **30**, 115, (1979)
[5] M.A. Howson and D. Greig, *J. Phys. F: Metal Phys.*, **13**, L155, (1983)
[6] M.A. Howson, *J. Phys. F: Metal Phys.*, **14**, L25, (1984)
[7] G. Hofman, L. Walters and T. Bauer, *Progress in Nuclear Energy*, **31**, 83-110, (1997)
[8] A.M. Adamska, R. Springell and T.B. Scott, *Thin Solid Films*, **550**, 319-325, (2014)

Poster Session

P1

Structure and electronic properties of Uranium-Vanadium alloys

Oleksandra Koloskova[1], Volodymyr Buturlim[1], Mykhaylo Paukov[1], Ladislav Havela[1]

[1] *Charles University, Faculty of Mathematics and Physics, Ke Karlovu 5, 12116 Prague 2, Czech Republic, koloskova.alexandra@gmail.com*

It is well known that if Uranium is alloyed with certain transition metals (as Mo, Zr, V, Ti, Nb, Re, Ru, Pd, or Pt) it can preserve the *bcc* (γ-U) structure to low temperatures. Such γ-U alloys have a high applicability due to their higher malleability, ductility and stability with respect to irradiation effects compared to α-U. In particular, some of these alloys are used as a low-enriched nuclear fuel with high U density. All such alloys studied so far are Pauli paramagnets with a superconducting ground state [1].
From the alloys mentioned, the alloy uranium–vanadium has not been really explored and the low-temperature properties are unknown. Our aim is to determine phase composition and magnetic and superconducting properties of $U_{0.9}V_{0.1}$ and $U_{0.95}V_{0.05}$ synthesized by splat cooling. The U–V phase diagram contains no intermediate phases. There is a very low V solubility in α- and β-U, while the equilibrium phase diagram indicates a higher solubility in the *bcc* phase, which can reach approx. 14 at.%. [2]. Although the V metal has also the *bcc* structure, its lattice parameter is much smaller than that of *bcc* U.
Splat cooling is one of methods of ultrafast cooling of materials. A drop of a melt is hit by two colliding Cu anvils, producing a thin foil in approx. 1 ms. This gives the cooling rate of 10^6 K/s. It eliminates decomposition processes at solidus-liquidus and facilitates retention of high-temperature phases especially if the α-phase cannot contain solutes (those need to segregate by diffusion, which is impeded by efficient quenching). Therefore we start the U-V study with the concentrations, falling into the high-temperature *bcc* phase stability (5 and 10 at.%). However, equilibrium phase diagrams are not really relevant for ultrafast processes. For example, the U-Pt systems exhibit the quenched bcc phase for Pt concentrations exceeding the upper Pt solubility limit [3]. Hence the study should continue with higher V concentrations.
Basic magnetic, resistivity and specific-heat data on the alloys will be presented, as well as study of hydrogen absorption, which will be compared with other existing hydrides data, indicating quite uniformly ferromagnetism with high Curie temperatures for U-T based hydrides, representing different varieties of UH_3 [4].

This work was supported by the Czech Science Foundation under the grant No. 18-02344S.

References

[1] S. Sowa *et al.*, *Acta Phys.Polonica* A **130**, 521 (2016).
[2] M.R. Staker, *Journal of Alloys and Compounds* **226**, 167 (1998).
[3] N.-T.H. Kim-Ngan *et al.*, *J.Nucl.Mater.* **479**, 287 (2016).
[4] L. Havela *et al.*, *J.Mag.Mag.Mater.* **400**, 130 (2016).

P2

Magnetic Excitation Spectrum and Bulk Modulus Behavior of δ-phase Pu

Vladimir Matvienko, Alexey Mirmelstein

[1]*Russian Federal Nuclear Center-E.I. Zababakhin Institute of Technical Physics, 13 Vasiliev street, 456770 Snezhinsk, Russia, email: mvn1969@mail.ru*

It is well known that metallic plutonium is characterized by a whole number of unique physical properties thanks to which it acquired reputation of the most mysterious element in the periodic system. Despite significant progress, both in the field of experimental research, and in theory, physics of metallic plutonium continues to be widely discussed. In particular, the problem of the elastic properties of plutonium has not been sufficiently developed. It has long been known that the δ-phase of pure (unalloyed) plutonium contracts with increasing temperature. This effect is usually explained in terms of the so-called "Invar" mechanism [1,2]. However, physical nature of the two-level system of the "Invar" model is rather vague. Unusual softening of the bulk modulus with increasing temperature is also challenging since this effect in the δ-phase of Pu-Ga alloys is observed within the same temperature interval where the crystal lattice compresses or has almost zero thermal expansion coefficient [3]. Most likely, the anomalous behavior of bulk modules is related to the peculiarities of the magnetic degrees of freedom, but the interpretation proposed in [4] raises serious questions (see, for example, [5]). Here we suggest another approach based on the results of inelastic scattering experiments [6]. Considering δ-Pu as a Kondo system and using the thermodynamic relations [7] we demonstrate that this approach allows, in principle, to explain the anomalous softening of the δ-Pu bulk modulus. However, to prove this approach additional experimental investigations of the magnetic excitation spectrum of plutonium are required.

References

[1] A.C. Lawson *et al.*, *Philos. Mag*. **86**, 2713 (2006).
[2] T. Lee *et al.*, *Phys. Rev. B* **89**, 174114 (2014).
[3] A.C. Lawson *et al.*, *Philos. Mag*. 82, 1837 (2002)
[4] A. Migliori *et al.*, *Proc. Natl. Acad. Sci. USA* **113**, 11158 (2016).
[5] M. Janoshek *et al.*, *Proc. Natl. Acad. Sci. USA* **114**, E268 (2017).
[6] M. Janoshek *et al.*, *Sci. Adv.* **1:e1500188** (2015).
[7] J.W. Allen and L.Z. Liu, *Phys. Rev. B* **46**, 5047(1992).
[8] M.E. Manley *et al.*, *Phys. Rev. B* **67**, 014103(2003).

P3

Ground State of Pu Metal: What We Know and What Have Not Yet

Alexey Mirmelstein[1], Yuri Zuev[1], Stanislav Verkhovskii[2], Vasily Ogloblichev[2], Vladimir Matvienko[1]

[1]Russian Federal Nuclear Center-E.I. Zababakhin Institute of Technical Physics, 13 Vasiliev street, 456770 Snezhinsk, Russia, email: mirmelstein@mail.ru
[2] M.N. Mikheev Institute for Metal Physics, Russian Academy of Sciences, Ural Branch, 18 S. Kovalevskaya street, 620108 Ekaterinburg, Russia

In recent years, a remarkable progress has been achieved in understanding physics of plutonium metal owing to the efforts of both experimentalists [1,2,3] and theoreticians [4,5]. It was understood that Pu metal is a multi-configurational system, whose ground state (at least of fcc δ-Pu) is a multi-particle Kondo singlet, and $Pu5f^4$ (Pu^{4+}), $Pu5f^5$ (Pu^{3+}), and $Pu5f^6$ (Pu^{2+}) electronic configurations are involved into spin/charge fluctuations. According to the results of inelastic neutron scattering experiment for δ-Pu [2] the characteristic energy of magnetic fluctuations $E_0 = k_B T_K$ is about 84 meV (where $T_K \approx 975$ K is the Kondo temperature). This value as well as DMFT estimate of $T_K \approx 800$ K [4] seems to lead to a somewhat underestimated value of the electronic specific heat coefficient, γ. Note that electronic structure calculation of δ-Pu by combination of the local-density approximation with an exact diagonalization of the Anderson impurity model gives theoretical estimate of $\gamma \approx 44$ mJ/K^{-2}mol^{-1} [5], in good agreement with experimental data. The monoclinic α-phase of Pu was not studied by inelastic neutron scattering technique, and it remains unknown whether the 5f electrons in dense α-phase are itinerant or partially localized with enhanced f-spd hybridization, and hence with higher Kondo temperature, as compared to δ-Pu.

According to [1] the fractional occupations of $5f^4$, $5f^5$, and $5f^6$ states as well as the average 5f count N_f are practically very close for δ- and α-Pu. In this connection, a few questions arise. First, what is the difference between δ- and α-Pu in terms of quantum mechanical description? Secondly, what is the temperature dependence of N_f and fractional $5f^4$, $5f^5$, and $5f^6$ states? Remind that in the intermediate-valence system the regime of localized magnetic moments reestablishes at $T > T_K$, and the magnetic susceptibility follows the Curie-Weiss law, while the effective f element valence tends to an integer value. Such a behavior is observed in the 4f-based intermediate-valence compound, e.g. in $CePd_3$ and CeNi. The above questions arise when analyzing, e.g., thermal expansion of δ- and α-Pu.

A number of anomalous thermodynamic properties of the fcc δ-phase Pu-Ga alloys is described by the atomistic modeling in terms of Invar mechanism [6,7]. This phenomenological model considers material as a two-level system the state of which is described by mixture of two states. These states have different ionic sizes and their concentration depends on temperature and Ga content [6,7]. In quantum mechanical picture the ions with integer valence involved into fluctuations also have different sizes, however it is not clear what is the physical nature of two-level system and what is the relationship between the static Invar model and fluctuating multi-configuration quantum mechanical picture [see ref. 7 and discussion in ref. 8 and 9]. It is very important, however, that the Invar model suggested for atomistic modeling of fcc Pu-Ga alloy directly accounts for presence of the stabilizing element in the crystal lattice while quantum mechanical electronic structure calculations of δ-Pu purposefully neglect partial Pu substitution by Ga. In this connection, it is of interest to investigate local electronic structure of the Pu-Ga alloys with different Ga concentration using the NMR technique.

Here, we would like to emphasize three results obtained in our NMR experiments. First, ^{71}Ga-^{69}Ga SEDOR (spin echo double resonance) experiment reveals almost isolated Ga distribution, so that the nearest neighborhood of Ga ions in the *fcc* crystal lattice is formed by the Pu ions only. Therefore, in δ-phase Pu-Ga alloy a short-range order is formed, which excludes formation of the Ga atom pairs. Similar result was obtained by EXAFC experiments [9].
Secondly, even within the temperature intervals corresponding to existence of the low-symmetrical α-, β-, γ- structural states of the composition with low Ga concentration $Pu_{0.995}Ga_{0.005}$ (monoclinic at low temperature) the local charge surrounding of the Ga atoms is found to be quite similar to that observed in the Ga-stabilized fcc Pu alloys. This behavior looks like a preformation of electronic structure of the fcc Pu alloy induced by an individual Ga ion embedded into α-Pu structure.
Thirdly, measurements of Knight shift of ^{69,71}Ga NMR line in the Pu-Ga alloys with different Ga concentration reveal monotonic Curie-Weiss behavior of the spin susceptibility as a function of temperature within a wide temperature interval from the existence range of the ε-phase down to 300 K (α-phase range) crossing domains of δ-, γ-, and β-phases. At T ~ 300 K the spin susceptibility reaches its maximum and then decreases. Note, the energy scale of ~ 300 K (~ 25 meV) is consistent with the experimental value of the electronic specific heat coefficient of the *fcc* δ-Pu alloy.
In conclusion, we believe that the results of NMR investigations of the Pu-Ga alloys with different Ga concentration will be useful for better understanding of the electronic structure of the Pu alloys, particularly for elucidating the mechanisms of the fcc phase stabilization by alloying (mainly trivalent) elements.

References

[1] C.H. Booth *et al.*, *Proc. Natl. Acad. Sci. USA* **109**, 10205 (2012).
[2] M. Janoschek *et al.*, *Sci. Adv.* **1:e1500188** (2015).
[3] A.V. Mirmelstein *et al.*, *JETP Letters* **90**, 485 (2009).
[4] J.H. Shim *et al.*, *Nature (London)* **446**, 513 (2007).
[5] A.B. Shick *et al.*, *Phys. Rev. B* **87**, 020505(R) (2013).
[6] A.C. Lawson et a., *Philos. Mag.* **86**, 2713 (2006).
[7] T. Lee *et al.*, *Phys. Rev.* B **89**, 174114 (2014).
[8] A. Migliori *et al.*, *Proc. Natl. Acad. Sci. USA* **113**, 11158 (2016).
[9] M. Janoshek *et al.*, *Proc. Natl. Acad. Sci. USA* **114**, E268 (2017).
[10] S.D. Conradson *et al.*, *Phys. Rev. B* **89**, 224102 (2014).

P4

Application of electrospinning technique to nanostructured intermetallic, borates and chalcogenides

Ana C. Ferreira, António P. Gonçalves, Joaquim B. Branco

Centro de Ciências e Tecnologias Nucleares, Instituto Superior Técnico, Universidade de Lisboa, Campus Tecnológico e Nuclear, Estrada Nacional 10, ao km 139.7 2695- 066 Bobadela, Portugal. e-mail: jbranco@ctn.tecnico.ulisboa.pt

Electrospinning is a technique that has been originally developed to produce high-tech ultra-fine polymer fibers [1]. This route enables low cost production of nanometer scale fibers with tunable surface properties. Such fibers have extremely high surface area, very high porosity, high permeability, low basic weight, the ability to retain electrostatic charges, among others properties [2].

The purpose of this work was to apply electrospinning for the preparation of compounds containing *f*-block elements with nanofibers shape. Moreover, the expected high surface area and low dimensionality can bring benefits to the catalytic, thermoelectric or magnetic properties of these materials, which will be the aim of future studies. Preliminary results showed that nanofibers of some compounds as $DyFe_3$, CuS, and LaB_6, can be successfully produced by this technique, which, to our knowledge, happens for the first time. Examples of SEM images of nanofibers prepared in this work are presented in Figure 1.

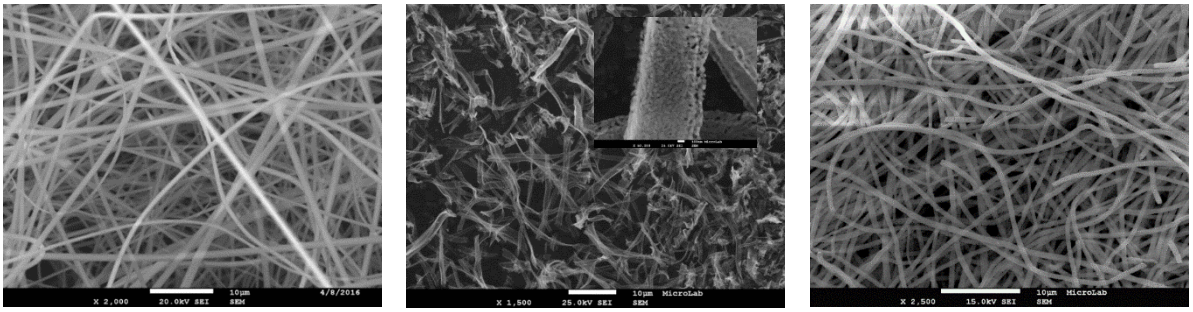

(a) (b) (c)

Fig. 1. SEM images of nanofibers (a) $DyFe_3$-PVP as spun; (b) $DyFe_3$-PVP 800 ºC under air; (c) CuS-PVP as spun.

Acknowledgements: The authors gratefully acknowledge also the FCT support through the UID/Multi/04349/2013 project.

References:

[1] D.H. Reneker, I. Chun, *Nanotechnology* 7 (1996) 216 34.; b) H. Fong, W. Liu, C.S. Wang, R.A. Vaia, *Polymer* 43 (2002) 775.

[2] I.S. Chronakis, *Micro-/Nano-Fibers by Electrospinning Technology: Processing, Properties and Applications,* in Y. Quin (Ed.), *Micro-manufacturing Engineering and Technology*, Elsevier, Oxford, 2010, pp. 264.

P5

Thermal expansivity and thermal conductivity of UC – a density functional theory study

Dominik Legut,[1] and Urszula D. Wdowik [2]

[1] *IT4 Innovations Center, VSB-Technical University of Ostrava, 17. listopadu 15, CZ 708 33, Czech Republic, e-mail: dominik.legut@vsb.cz*
[2] *Institute of Technology, Pedagogical University, ul. Podchorazych 2, 30-084 Cracow, Poland*

Recent density functional theory (DFT) studies carried out for UC allowed to establish a significant role of the spin-orbit and strong electron correlations in predicting fundamental properties of uranium monocarbide (UC) [1]. Results of these DFT studies triggered additional theoretical investigations on uranium carbide aimed at determining its thermal expansivity and thermal conductivity. This research takes into account anharmonic effects via the quasi-harmonic theory as well as phonon-phonon interactions [2,3]. Results of the calculations are confronted with earlier and most recent experiments [4, 5].

Acknowledgement
This work was supported by the European Regional Development Fund in the IT4Innovations national supercomputing center - Path to Exascale project, No. CZ.02.1.01/0.0/0.0/16_013 /0001791 within the Operational Programme Research, Development and Education and by the Ministry of Education, Youth and Sports from the National Programme of Sustainability (NPU II) project "IT4Innovations Excellence in Science - LQ1602".

References

[1] U. D. Wdowik, P. Piekarz, D. Legut, and G. Jagło, *Phys. Rev. B* **94**, 054303 (2016).
[2] A. Togo and I. Tanaka, *Scr. Mater*. **108**, 1-5 (2015).
[3] A. Togo, L. Chaput, and I. Tanaka, *Phys. Rev. B* **91**, 094306 (2015).
[4] J. F. Andrew and T. W. Latimer, *Report LA-6037MS*, Los Alamos (1975).
[5] L. Havela *et al.* (measurement 2017)

P6

Cerium Behavior in Various Media as Compared with Plutonium

T.Kazakovskaya, Yu. Belova, G.Baranov

Russian Federal Nuclear Center RFNC-VNIIEF

Introduction. It is widely known that cerium and plutonium (very unusual metals with special properties) attract more and more investigators all over world. The most characteristic chemical features of these metals are: a) the high chemical activity of their metallic states and b) the stable 3+ oxidation state in solids and solutions [1] It seems very interesting to the authors to compare chemical behavior of Ce and Pu in various media and to consider the probability to use some kinds of protective coatings to reduce corrosion.

Peculiarities of Pu and Ce chemistry. The Pu element occupies a unique place in the history of chemistry being one of the most complex elements in the periodic table. The metal exhibits six solid allotropes at ambient pressure and its phases are notoriously unstable with temperature, pressure, etc. [2]. With little provocation, the metal can change its density by as much as 25%. It is highly reactive in air, has five chemical oxidation states (six if the metal is included), and can form numerous compounds and complexes in the environment [3]. Cerium is a rare-earth metal with unique properties, in some cases Ce is successfully used as a plutonium imitator [2].

Behavior in air media. The essence of Pu oxidation and corrosion processes is very important for safe and efficient use and storage of this metal. The overall rate of oxidation is less for alloyed plutonium than it is for unalloyed plutonium. Haschke (1999) has also speculated that Pu–Ga alloys oxidize at a lower rate than unalloyed plutonium at all temperatures in moist air. At elevated temperatures, Pu exhibits an autothermic reaction, igniting spontaneously in air when the temperature reaches 500˚C. The dioxide is the main corrosion product when Pu metal is exposed to oxygen or air, but there is always a layer of the cubic sesquioxide present at the metal-oxide interface. However, at room temperature, its thickness is small compared to that of the dioxide.

Ce (even compact metal) starts oxidizing at room temperature. When temperature rises up to 300ºC the process in air is so fast that all metal mass could ignite, generating a considerable amount of heat enough for melting cerium dioxide (CeO_2) formed during the oxidation process. When Ce reacts with O_2 at the first stage Ce_2O_3 is formed, then Ce_2O_3 during further oxidation transforms into CeO_2. The finish corrosion products are hydrated carbonates.

Protective coatings. The authors investigate the stability of Ce samples covered with varnish (2 types) and electroplated by copper. The corrosion tests in air media under room temperature and relative humidity equal to 75 % were done. The experiments demonstrate that the protective coatings raise the stability of cerium samples 4-12 times.

As for Pu at the present all attempts to coat plutonium metal with varnish or galvanic coating were not a success.

Behavior in water solutions. Because of its electropositive nature plutonium atom in water solution easily loses from 3 to 7 outer electrons [1]. The chemical behavior of plutonium depends on its oxidation state. If this parameter equals to 4 Pu is strongly hydrolyzed forming hydrogels or solid colloids. These colloids are aging, and, solubility decreases.

Cerium is also easily hydrolyzed in water solutions, and cerium hydroxide is formed. The prevailing oxidation state in water solutions is 4 (the same as Pu has).

Electrochemical behavior. In the literature it is difficult to find information about polarization of Pu and Ce in water solutions. The authors tried to get polarization curves of Pu and Ce in fresh water and in an imitator of sea water (3.5% Na Cl solution). Polarization of Pu in water

electrolytes were studied earlier by specialists of VNIINM, Russia. The authors repeated this investigation and provided the identical experiments with Ce. The experiments demonstrated that polarization curves for Pu and Ce in water solutions are similar. This fact corresponds to high electrochemical activity of these elements. Both for Pu and Ce there is no passivation area. The experimental results demonstrate that the electrochemical activity of Ce in sea water imitator is significantly lower than of Pu, while in fresh water the activity of both metals are practically the same.

Conclusion The experiments confirmed that Ce is a metal with extremely high chemical and electrochemical activity. The possibility of Ce protection with varnish or galvanic coatings is investigated. The protective coatings reduce the oxidation rate 4-12 times. The electrochemical investigation demonstrates the necessity of further experiments to define the mechanism of Pu and Ce with water media.

References

[1] The Chemistry of the Actinide and Transactinide Elements. Vol. 1–6, Springer.
[2] Challenges in Plutonium Science, vol.1. Los Alamos National Laboratory.
[3] Khimicheskaya encyclopediya, vol.5, BSE, 1998.

P7

The Development of Ceramic Matrices on the Phosphate Basis with $NaZr_2(PO_4)_3$ Structure for Immobilization of Actinides

Albina Orlova,[1] Anton Kanunov[2]

[1] Lobachevsky State University of Nizhni Novgorod,
Gagarina Ave, 23, Nizhni Novgorod, 603950, Russia, e-mail: albina.orlova@inbox.ru
[2] Russian Federal Nuclear Center – All-Russia Research Institute of Experimental Physics,
Mira ave, 37, Sarov, 607188, Russia

The radiation- and corrosion-resistant crystalline forms of immobilization for the most dangerous radioactive wastes are the solid compositions on the basis of natural mineral analogues. Single-phase crystalline ceramics may be used for immobilization both separate radioactive nuclides (e.g., ^{239}Pu) and for radioactive wastes of a complex composition. In the last case an atomic structure of the ceramic matrix should have several cation and anion positions where various radionuclides presenting in the wastes may be disposed in. The materials with similar matrix are a good form for immobilization of long-living actinides such as Pu, Np and Am. Among materials for actinides' immobilization the phosphates of $NaZr_2(PO_4)_3$ family or NZP (natural analogue is kosnarite mineral $KZr_2(PO_4)_3$) and the engineering ceramics on their basis deserve a special attention [1–5]. The interest to its is caused both by an wide isomorphism and by its high stability in the respect of destructive factors of natural; and technogenical character [5].

There are crystallographic positions with different forms and sizes of coordination polyhedrons in $NaZr_2(PO_4)_3$ structure. Crystallochemical formula of compounds with such a structure has this appearance: $(M1)^{[6]}(M2)^{[8]}{}_3\{[L^{[6]}{}_2(X^{[4]}O_4)]^{n-}\}_\infty$, where $\{[L_2(XO_4)]^{n-}\}_\infty$ – structure framework (a topological domain); L – framework position; $(XO_4)^{n-}$ – tetrahedral anion; M1 and M2 – types of external to framework cation positions; $^{[4]}$, $^{[6]}$, $^{[8]}$ – coordination number (c.n.).

Uranium, neptunium and plutonium (M^{4+}) phosphates with $AM_2(PO_4)_3$ composition, where A – alkaline metal cation, have been studied by us in a wide temperature range (up to 1200ºC). Among the determined polymorphous structures the structure of NZP is also present [6, 7]. In the development of these activities for more detailed study of phase formation, peculiarities of structure and also for development of ceramics production method based upon actinide NZP-phosphates with 3+ and 4+ oxidation levels of Np, Pu, Am and Cm, the investigation have been carried out with the use of surrogates. Ce, Sm and Eu have been selected as such ones. It is well know that cerium is one of the most widely distributed fission product in spent nuclear fuel and in the course of matrices study (that are used for immobilization of radioactive wastes) cerium is usually introduced as the surrogate of neptunium and plutonium [8], which have similar values ion radii: $r(Ce^{4+})$ = 0.87Å, $r(Pu^{4+})$ = 0.86Å, $r(Np^{4+})$ = 0.87Å, c.n. 6. The next cations: Ce^{3+} (r = 1.01Å, c.n. 6), Sm^{3+} (r = 0.96Å, c.n. 6) and Eu^{3+} (r = 0.95Å, c.n. 6) have been selected as surrogates of Pu^{3+} (r = 1.00Å, c.n. 6), Am^{3+} (r = 0.98Å, c.n. 6) and Cm^{3+} (r = 0.97Å, c.n. 6) accordingly.

The subjects of this investigation have been the next complex phosphates: $Ce^{IV}_{0.25}[Zr_2(PO_4)_3]$, $Na[Ce^{IV}_2(PO_4)_3]$, $Ln^{III}_{0.33}[Zr_2(PO_4)_3]$, where Ln^{III} = Ce, Sm and Eu. The synthesis of $Ce^{IV}_{0.25}[Zr_2(PO_4)_3]$ and $Na[Ce^{IV}_2(PO_4)_3]$ was carried out by solid state method, and synthesis of $Ln^{III}_{0.33}[Zr_2(PO_4)_3]$ – by sol-gel method.

The kinetics of phase formation has been illustrated by specific examples of such phosphates as $Ce_{0.33}[Zr_2(PO_4)_3]$ and $Na[Ce_2(PO_4)_3]$, which have been studied with then use of X-ray diffraction analysis. During isothermal annealing at 700ºC in the course of first 0.5–2 hours the formation of a phase with NZP-like structure was observed in the case of $Ce_{0.33}[Zr_2(PO_4)_3]$ and formation of a phase with the indices that met the values for structural analogue – $NaTh_2(PO_4)_3$ (space group C2/c) in the case of $Na[Ce_2(PO_4)_3]$. There was an additional phase ZrP_2O_7 which was registered in X-ray patterns. Other intermediate compounds were in an amorphous state and its reflex were absent in the X-ray pattern of the sample. After 12 hours mass fraction of the aim phases amounted 0.9 and 0.92 for $Ce_{0.33}[Zr_2(PO_4)_3]$ and $Na[Ce_2(PO_4)_3]$ accordingly. At increasing temperature to 800ºC its mass fraction reached 0.98 after isothermal annealing for two hours of both phosphates samples. The value of weighted profile factor R_{wp} for each experiment didn't exceed 5%.

It was found the formation of the crystalline single-phase reaction products $Ce_{0.25}[Zr_2(PO_4)_3]$ and $Ln_{0.33}[Zr_2(PO_4)_3]$, where Ln = Ce, Sm and Eu in structure type of $NaZr_2(PO_4)_3$ in space group $P\,\bar{3}\,c$ (primitive trigonal cell). In X-ray pattern of $Na[Ce_2(PO_4)_3]$, heated to 800ºC, the reflexes which were characteristic for the structure of $NaTh_2(PO_4)_3$ (monocline structure, space group C2/c) were present. At increasing temperature to 1000ºC the polymorphous transition took place with formation of corresponding phase of trigonal structure, space group $P\,\bar{3}\,c$ with $NaZr_2(PO_4)_3$ structural type. After annealing at 1200ºC the reflex were observed which were typical only for NZP phase. During bringing into comparasion these data for cerium phosphate $Na[Ce_2(PO_4)_3]$ and isoformular neptunium phosphate $Na[Np_2(PO_4)_3]$ and plutonium phosphate $Na[Pu_2(PO_4)_3]$ it was noted its analogous behavior during heating – exactly the presense of phase transitions with formation of high-temperature phases with NZP structure at the temperatures 1000, 1100 and 1300ºC for Ce-, Np- and Pu-containing phases accordindly. On the refinement base of crystal structure for Ce-Zr-phosphate $Ce_{0.33}[Zr_2(PO_4)_3]$ and for high-temperature Na-Ce-phosphate phase $Na[Ce_2(PO_4)_3]$ it follows that the structure framework is formed with the help of topological domains such as $\{Zr_2(PO_4)_3\}$ and $\{Ce_2(PO_4)_3\}$, which in its turn consist of ZrO_6 and CeO_6 octahedrons and of PO_4 tetrahedrons that are connected one with other by Zr—O—P and Ce—O—P structural bridges.

With the use of phosphate composition the ceramics powders specimens was prepared by compaction with following annealing. The values of specimens' relative density were 90–95%. The ceramics specimens were subjected to hydrolytic leaching tests in a stationary regime at room temperature. The values of rare earth leaching rates from phosphates of $Ln_{0.33}[Zr_2(PO_4)_3]$-types were less than $(2.5–3.0)\times10^{-8}$ g/(cm^2·day), and these values evidence a high stability level of similar compounds. According to X-ray diffraction analysis, the phase composition of the specimens in course of leaching experiments kept the same one.

On the example of extreme member of solid state solution row – $Ca_xPu_{(1-2x)0.25}[Zr_2(PO_4)_3]$ (it was studied earlier in [9]) for a specimen wit x = 0.5 the Spark Plasma Sintering electro pulse technology was used for synthesis of engineering ceramics. The achieved characteristics at sintering time τ = 12 min: experimental density $\rho_{exp.}$ = 3.17(1) g/cm^3, relative density $\rho_{rel.}$ = 99.1%, Vickers micro hardness HV = 540 kg/mm^2, fracture toughness K_{1c} = 1.2 MPa·m^{½}, grain size (r-radius) $0.5 \le r \le 2.5$ μm [10]. The use of indicated above technology is an effective technique and it might be useful in future activities on actinide immobilization.

References

[1] R. Roy *et al.*, *Mater. Res. Soc. Proc.*, **15**, 15 (1983).
[2] R.C. Ewing. Radioactive Waste Forms for the Future / Eds. W.Lutze and R.C.Ewing. – Elsevier, Amsterdam, 1988. P. 589.
[3] A.I. Orlova *et al.*, *Radiochemistry*, **36**, 322 (1994).
[4] R.C. Ewing *et al.*, *Reviews in Mineralogy and Geochemistry*, 48, 673 (2002).

[5] A.I. Orlova. Structural Chemistry of Inorganic Actinide Compounds / Eds. S.V. Krivovichev, P.C. Burns and I.G. Tananaev. – Elsevier, 2007. P. 315.
[6] Yu.F. Volkov *et al.*, *Radiochemistry*, **45**, 319 (2003).
[7] A.I. Orlova *et al.*, *Proceedings of the 3-rd Annual Meeting for Coordination and Review of LLNL Contract Works Excess Weapons Plutonium Immobiliyation in Russia*. St-Petersburg, 2002. P. 407.
[8] S.V. Yudintsev *et al.*, *Doklady Chemistry*, **460**, 21 (2015).
[9] D.M.Bykov *et al.*, *Proceedings of the XVIII Mendeleev Congress on General and Applied Chemistry*. Moscow, 2007. P. 2476.
[10] A.I. Orlova *et al.*, *Inorganic Materials*, **48**, 313 (2012).

P8

Thermal Expansion Anisotropy in the Uranium-Niobium Alloy

A.E. Shestakov, I.V. Artamonov

Russian Federal Nuclear Center – VNIITF, Vasilyeva str. 13, Snezhinsk, Russia,
a.e.shestakov@vniitf.ru

The uranium-6.3 wt.% niobium alloy was supplied in the form of a cylindrical blank 20 cm in diameter to be further used in our investigation. In the final treatment, it was quenched from 720°C to fix the metastable α"-phase. The test sample (a 10×5×0,5-mm plate) was cut from a solid material blank, the bearing surface was ground and polished. The X-ray investigation revealed no other phases apart from α"-phase.

X-ray powder Bragg-Brentano diffractometer with a vertical goniometer was used for measurements at elevated temperatures. The copper anode tube was also used. Oxidation was reduced by means of the vacuum cell with a beryllium window.

The measurements were made at 25, 60, 80, 100, 120, and 150°C. The sample material exhibited phase transformation at the temperature above 150°C, and the diffraction pattern showed a strong line of the high-temperature phase.

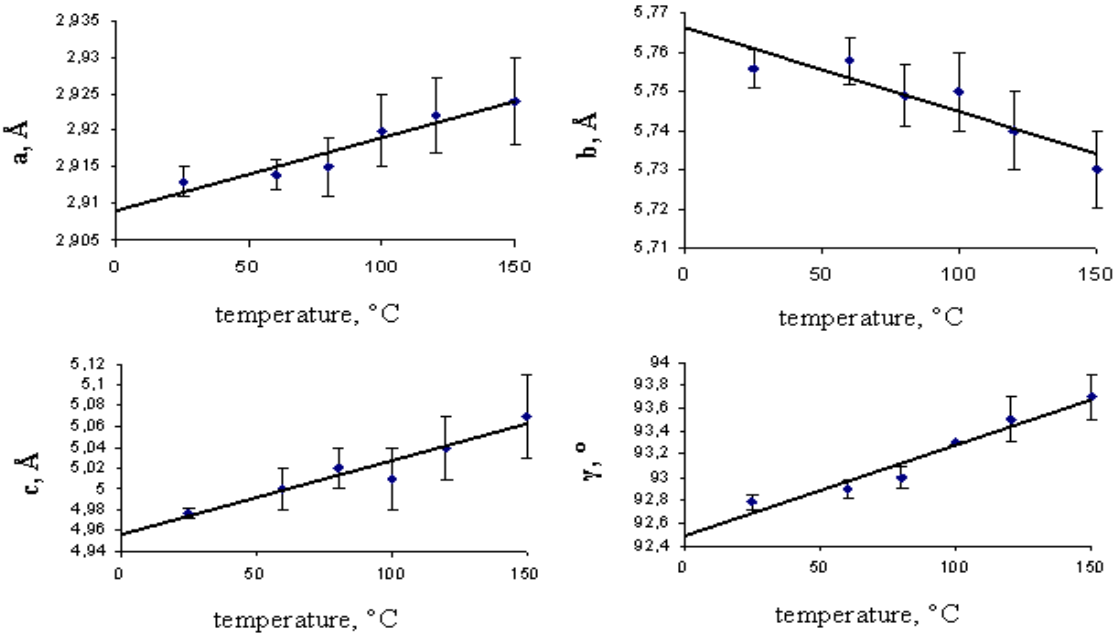

Parameters of the monoclinic crystal lattice of the uranium-6.3 wt.% niobium α"-phase alloy versus temperature

Assuming the α"-phase lattice parameters ramp, the dependence for the temperatures within 25-150°C can be written as:

$a = 2{,}909 \cdot (1 + 3{,}4 \cdot 10^{-5} \cdot T)$, $b = 5{,}767 \cdot (1 - 3{,}8 \cdot 10^{-5} \cdot T)$, $c = 4{,}957 \cdot (1 + 14 \cdot 10^{-5} \cdot T)$

$\gamma = 92{,}48(1 + 8{,}6 \cdot 10^{-5} \cdot T)$,

where: *T*- centigrade temperature; multiplier preceding the bracket — lattice parameter at 0°C; multiplier preceding the temperature — thermal coefficient.

The dependence of the elementary cell volume on the temperature was used to obtain the volumetric coefficient of thermal expansion. It is $\beta = 120 \cdot 10^{-6}\,\mathrm{K}^{-1}$.

P9

Metallographic study of U-Zr-Mo alloy shell after explosive loading

D.A. Belyaev, A.S. Aleksandrov, Yu.N. Zuyev, E.A. Kozlov, I.L. Svyatov, E.A. Levi

Russian Federal Nuclear Center – Zababakhin All-Russia Research Institute of Technical Physics (RFNC-VNIITF), 456770, Snezhinsk, Chelyabinsk region, Russia, e-mail: bad1331@gmail.com

This presentation describes investigation of a thick-wall spherical shell from the alloy of uranium with molybdenum and zirconium, which survived after high-intensity explosive loading. Investigation was performed in the meridional section of the shell (figure 1) to obtain qualitative data on hardness and microhardness, metallurgical inclusions, damage, and also material microstructure.

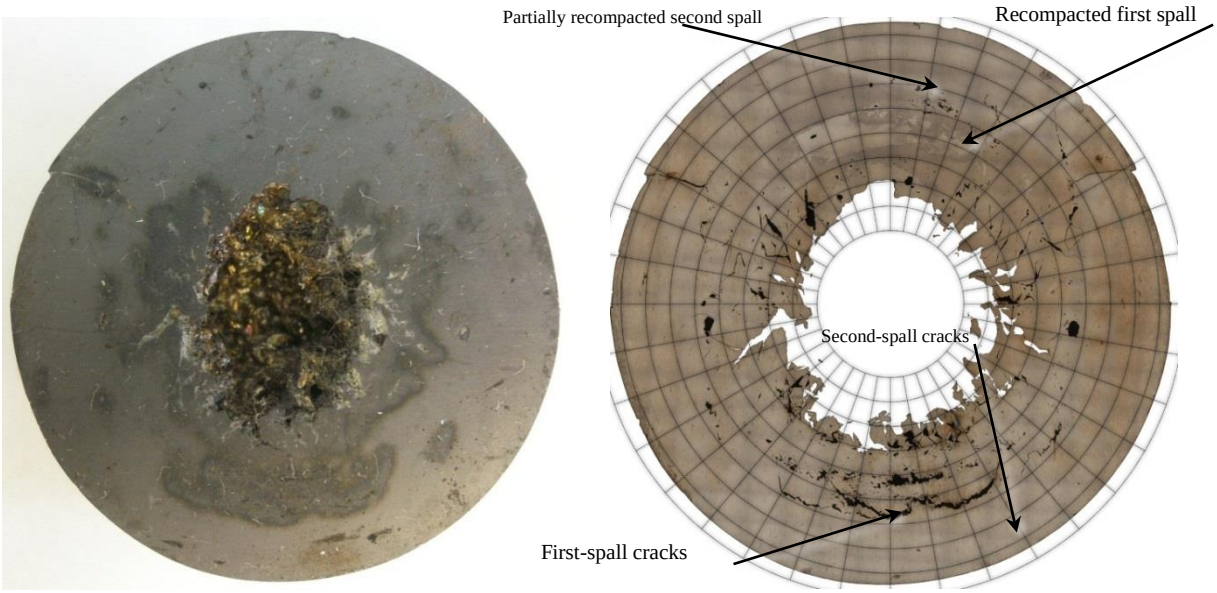

Fig. 1. Meridional section of the shell after cutting and prolonged oxidation. Surface condition prior to the study (left). Panoramic picture of the polished section surface used to study the dam-aged state (right)

Structural changes are observed to widely present in the shell material (figure 2).
The localized damage observed both at R ≈ 12…14 mm and R ≈ 16…18 mm are the first and second converged spalls, respectively. What is more, in the southern sector the first spall was recompacted with the remelting of a large region of the material in the adjacent layers (region with the enhanced hardness for the first spall). Cracks of the second spall in the northern sector were also recompacted almost completely.

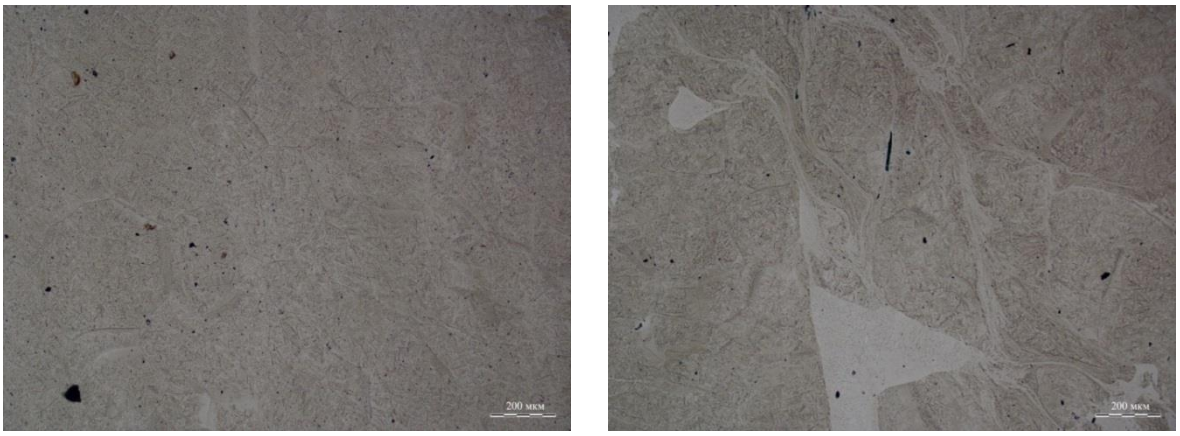

Fig. 2. Shell material structure that is similar to that in the as-received state. Outer layers of the shell (left). Recompaction of cracks with melting traces along edges (right).

In the southern sector, only partial recompaction of the first spall is observed in inner layers. Outer layers of the first spall involve different-size cracks. The second spall in the southern sector failed to recompact.

The shell material bears marks of plastic deformation throughout the test meridional section.

At the microstructural level, changes involve plastic deformation and local remelting when edges of shock-induced discontinuities are welded.

P10

Thermal and elastic properties of (Th,Ce)O_2 mixed oxides: a self-consistent thermodynamic approach

Filanovich A.N., Povzner A.A.

Ural Federal University, Ekaterinburg, Mira st. 19, 620002, Russia, e-mail: a.n.filanovich@urfu.ru

Nuclear fuel based on mixture of thorium dioxide ThO_2 with uranium or plutonium dioxides (MOX-fuel) is perspective for many types of breeder reactors. Effective and safe usage of these fuels requires information on its thermal and mechanical properties. However, in the case of $Pu_xTh_{1-x}O_2$ the available experimental data on these properties is very scarce due to high specific activity and radiotoxicity of plutonium. Therefore, in place of PuO_2, its surrogate CeO_2 is often used since the physicochemical properties of these two compounds are similar. It has been shown in [1,2] that different fabrication processes as well as sintering atmosphere (Ar–H2 and air) lead to different porosity and inhomogeneity of $Th_{0.95}Ce_{0.05}O_2$ samples, which can affect functional characteristics of the fuel pellets. In the present study we implement a self-consistent thermodynamic approach to study thermal and elastic properties of ThO_2 and $Th_{0.95}Ce_{0.05}O_2$ MOX obtained under different conditions of fabrication.

We start from considering thorium dioxide in order to make an initial estimation of thermodynamic parameters, in particular, the ones affecting anharmonicity of the acoustic and optical phonons. Fig. 1 shows results of calculations of the lattice heat capacity of ThO_2, where one can see that our model enables to describe available experimental data. Then a thermodynamic model for $Th_{0.95}Ce_{0.05}O_2$ with different porosity was developed based on the model for ThO_2 and some specific parameters taken from experimental data [1,2]. Fig. 2 demonstrates temperature dependencies of heat capacities of $Th_{0.95}Ce_{0.05}O_2$ samples obtained by powder processing and pelletization (POP) and coated agglomerate pelletisation (CAP) and in different sintering atmospheres. It is evident that despite the same atomic composition, the heat capacities are different, which is captured by our model.

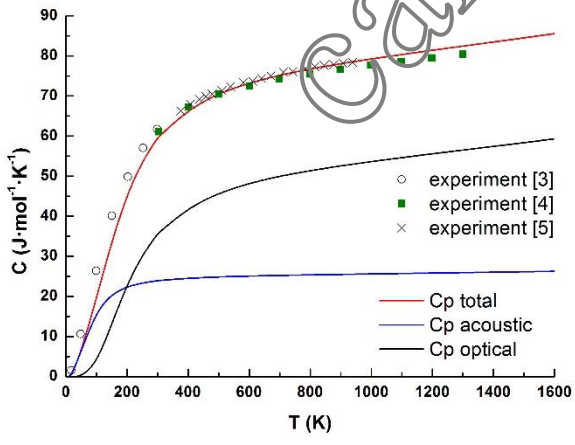

Fig. 1. Temperature dependence of molar heat capacity of ThO_2

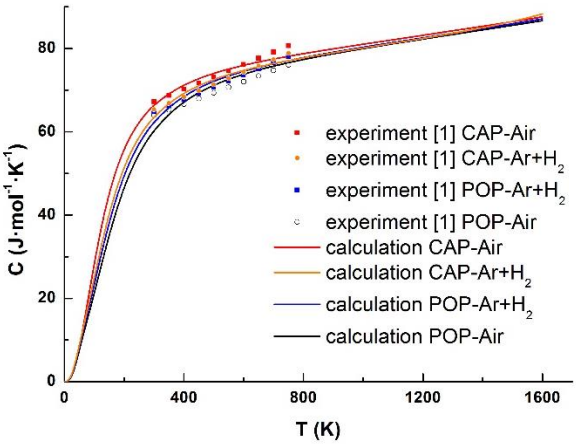

Fig. 2. Temperature dependence of molar heat capacity of $Th_{0.95}Ce_{0.05}O_2$ MOX obtained under different conditions of fabrication

Further, we have calculated temperature dependencies of coefficient of thermal expansion, bulk modulus and thermal conductivity of the considered systems and analyze the effect of porosity on the properties under consideration.

References

[1] P.S. Somayajulu *et al.*, *J. Nucl. Mater.* **Vol. 467**, 644-659 (2015).
[2] P.S. Ghosh *et al.*, *J. All. Compd*. **Vol. 638**, 172–181 (2015)
[3] D.W. Osborne *et al.*, *J. Chem. Phys.* **Vol. 21**, 1884 (1953).
[4] S. Dash *et al.*, *J. Nucl. Mat.* **Vol. 393**, 267 (2009).
[5] R. Agarwal *et al.*, *J. Nucl. Mater.* **Vol. 322**, 98 (2003).

P11

Preliminary study of $U_{1-x}M_xC$ systems (M = Ta, Nb) for ISOLDE targets

Gonçalo Domingos, Tiago K. C. Alves, Frederico Malacho, António Pereira Gonçalves

Centro de Ciências e Tecnologias Nucleares (C^2TN), Instituto Superior Técnico, Universidade de Lisboa, Estrada Nacional 10,2695-066 Bobadela LRS, Portugal,
e-mail: goncalo.almeida.domingos@gmail.com

Introduction

At ISOLDE a large variety of radioactive ion beams are produced by the bombardment of a stationary target with a high energy proton beam. The isotopes formed by nuclear reactions must then diffuse and release from the target, before being ionized, extracted and separated, both online and offline. Uranium carbide based materials (UC_x) constitute the majority of ISOLDE targets, due to the large variety of radioisotopes produced by its bombardment. However, a limitative pass of the ISOLDE process is the release time, in particular for radioisotopes with small lifetime. Therefore, it would be useful to decrease the release time of the daughter nuclei, which would result in an increase of the production yield. Several methods can be envisaged to achieve this objective [1]. One possibility is the increase of the target temperature, which is expected to allow higher diffusion rates inside the target and effusion to ionizer channel of the produced nuclei. This work aims to study the structure and morphology of materials from the $U_{1-x}M_xC$ (M = Ta, Nb) system, which are expected to have higher melting points than UC_x if stable solid solutions are obtained.

Samples with $U_{1-x}M_xC$ (M = Ta, Nb; $0.05 \leq x \leq 0.20$) compositions were prepared by arc melting the stoichiometric quantities of pre-prepared corresponding carbides (also produced by arc) under argon atmosphere. The materials were characterized by X-ray diffraction (XRD). Simulated powder patterns of possible phases were calculated using the PowderCell package [2]. SEM observations and EDS analysis were performed on selected samples.

Results and Conclusions

Figure 1 shows selected X-ray diffractograms of as-cast samples. Their approximate phase composition is given in table 1.

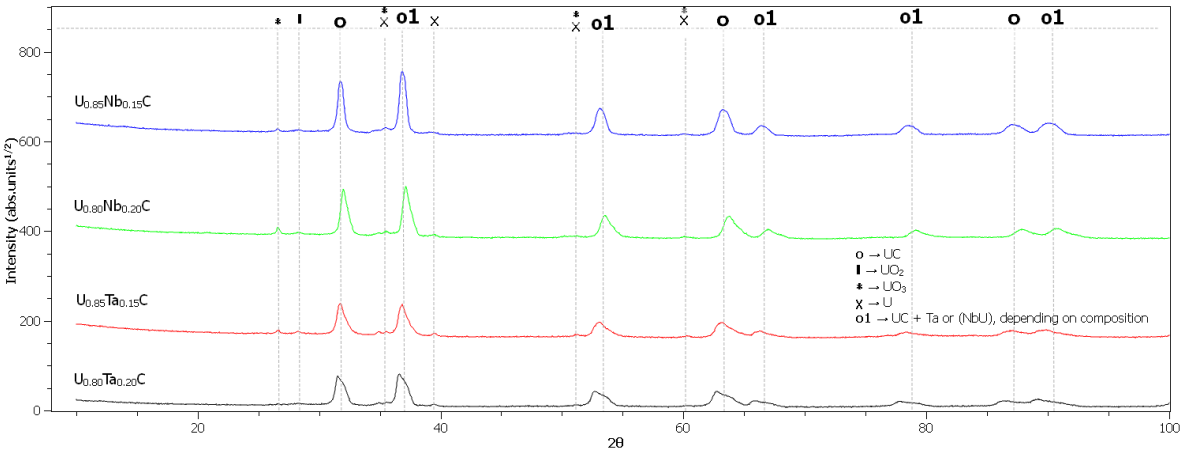

Fig. 6: X-ray diffractograms of selected samples. Phases legend at left.

Table 1. Approximate compositions obtained from XRD analysis

	$U_{0.80}Ta_{0.20}C$	$U_{0.85}Ta_{0.15}C$	$U_{0.80}Nb_{0.20}C$	$U_{0.85}Nb_{0.15}C$
UC	78	74	71	73
U	4	4	2	5
UO_2	4	4	5	5
UO_3	6	7	15	11
Ta	8	11	---	---
NbU	---	---	7	6

All samples are predominantly composed by the UC-based phase (> 70%). The broadening of this phase peaks may be in part related to the solidification of a range of UC_x phases during cooling, since UC can exist either in hypostoichiometic or hyperstoichiometric forms [3]. The presence of metallic Ta and NbU also broadens peaks identified as "o1" in figure 1. The lack of TaC and NbC phase peaks in the diffractograms supports the idea that TaC and NbC form solid solutions with UC. Still, the presence of small quantities of metallic U, Ta and uranium oxides indicates that higher carbon concentrations and more time under arc are needed to reach more homogeneous samples.

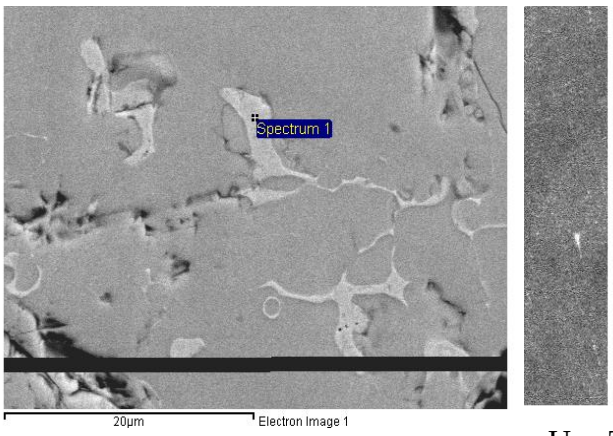

Figure 2. SEM micrograph of $U_{0.80}Ta_{0.20}C$.
Figure 7. SEM micrograph of $U_{0.80}Nb_{0.20}C$.

SEM images of the $U_{0.80}Ta_{0.20}C$ and $U_{0.80}Nb_{0.20}C$ compositions are present in Figures 2 and 3. All samples show good homogeneity, with darker areas (with slight nuances) corresponding to a solid solution of UC and TaC or NbC, and the bright ones to isolated UC islands. The sample with $U_{0.80}Ta_{0.20}C$ composition has also a small region composed of TaC, while the one with $U_{0.85}Ta_{0.15}C$ composition has not. However, in all niobium compositions, no such equivalent regions of NbC were observed. Therefore, the solubility limit of NbC in UC needs to be further studied for other compositions. The solidification of UC appears to be the last, since during cooling TaC and NbC would form a solid solution with UC until eventually are totally consumed, leaving only this composition behind. This meets the expectation that the solid solutions should have higher melting points when compared to pure UC.

Acknowledgements: this work was partially supported by FCT, Portugal, under the projects UID/Multi/04349/2013 and CERN-FIS-PAR-0005-2017.

References

[1] Panteleev, V., Alyakrinskiy, O., Andrighetto, A. *et al. Eur. Phys. J. Spec. Top*. **150**, 297-300 (2007).
[2] Werner, K., Nolze, G., Powder Cell 2.4 for Windows [Computer Software], (2000).
[3] Mague, J.; *Organometallics* **Suplement Volume C12** , 2-3 (1984).

P12

Nano-UCx target for CERN-MEDICIS facility

S. Chowdhury[1], M.S. Henriques[2], L. Maria[1], A. Cruz[1], T. Stora[3], A.P. Gonçalves [1]

[1] *Centro de Ciências e Tecnologias Nucleares (C²TN), Instituto Superior Técnico, Universidade de Lisboa, Estrada Nacional 10, 2695-066 Bobadela LRS, Portugal*
[2] *Institute of Physics, ASCR, Na Slovance 2, 182 21 Prague, Czech Republic*
[3] *CERN – European Organization for Nuclear Research, CH-1211 Genève 23, Switzerland*

The Isotope Separator On Line Device (ISOLDE), is a CERN facility that has been deeply involved in the production of isotopes for research in Particle Physics, Solid State Physics and Materials Science. At ISOLDE a high-energy proton beam hits a target made, by e.g., UC_x, producing isotopes through fragmentation, fission and spallation. The MEDICIS is a new CERN facility that is being under construction [1], which resulted from a spin off idea involving ISOLDE. This facility will use a new generation of target materials and mass separators for the production and collection of the isotopes, which will be after shipped to hospitals for pre-clinical and clinical usage in cancer research. Uranium carbide is one of the best target materials known up to now due to its stability at high temperatures and thermal conducting properties. Our aim is to drop it`s grain size to submicron-scale, achieving a porous nano-grain target material, in order to increase the release of exotic nuclei. Electrospinning is a well-known and easy-to-handle technique to achieve fibers. Here we present our studies on the production and characterization of new nano-UC_x targets prepared using electrospinning.

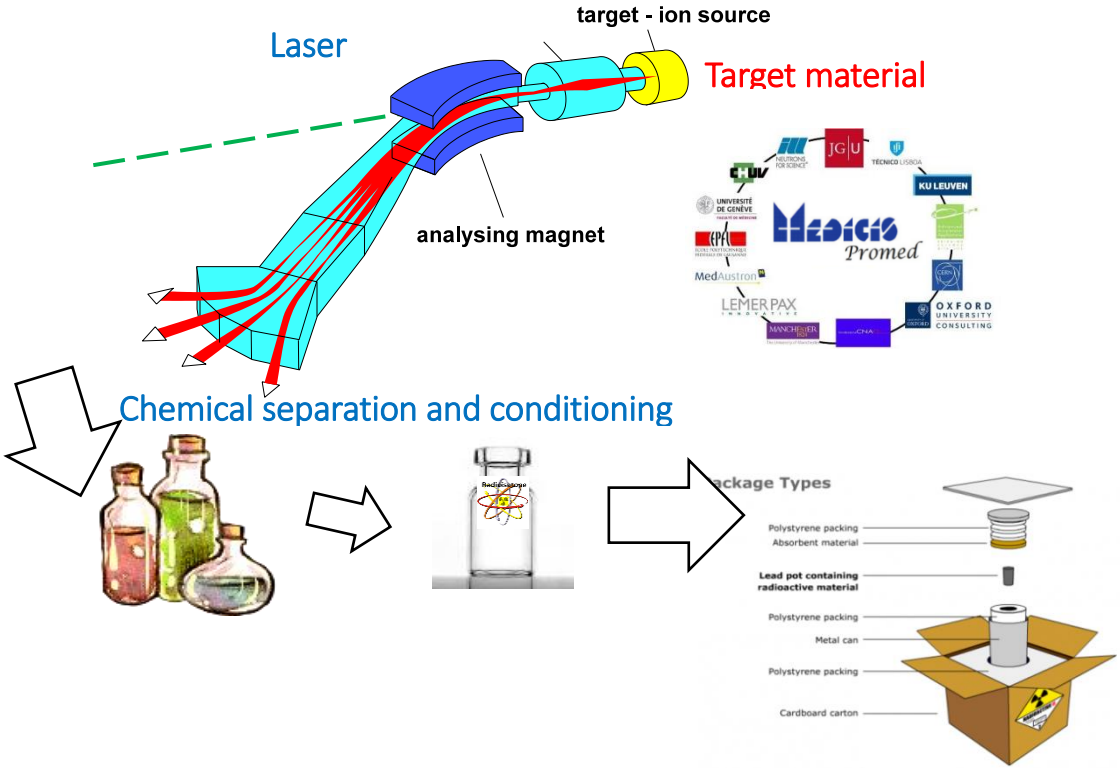

References:

[1] **T Stora *et al.*,** *Appl. Sci.*, *4*(2), 265-281 (2014).

P13

Evaluation of the thermal stability of uranyl peroxide clusters under different atmospheres (inert, reductive and oxidative)

PH. Imbert[1], O. Tougait[1], F. Abraham[1], J. Nos[2]

[1] Univ Lille, UCCS - UMR CNRS 8181, ENSCL-USTL, BP 90108, 59652 Villeneuve d'Ascq Cedex, France, e-mail:imbert.paulhenri@gmail.com
[2] Orano, 1 Place Jean Millier, 92084 Paris La Défense, France

Mixed U^{6+}/Pu^{4+} solid compounds precipitated from aqueous solutions are regarded as possible precursors for MOX nuclear fuel, consisting of a mixed $(U,Pu)O_2$ solid solution with fluorine type of structure [1]. To this respect, the recent advances on the synthesis by cationic exchange of uranyl peroxide nanoclusters containing trivalent rare-earth (Nd^{3+}) or tetravalent thorium (Th^{4+}) ions [2], used as transuranium surrogates, afford the opportunity of an innovative fabrication process [2]. The uranyl peroxide nanoclusters constitute an interesting family of structural compounds that are built from uranyl polyhedra bridged through peroxide or hydroxide ligands [3]. Their high morphological and chemical flexibilities, in terms of (i) number of building-blocks with assemblies containing up to 120 monomers (ii) shape, such as spheres, crown, (iii) coordination chemistry, with inclusion of ligands such as pyrophosphate or oxalate, (iv) nature of the internal and external countercations, such as ammonium, alkaline or alkaline-earth cations, yielded about 40 arrangements reported in the literature, up to now [4].

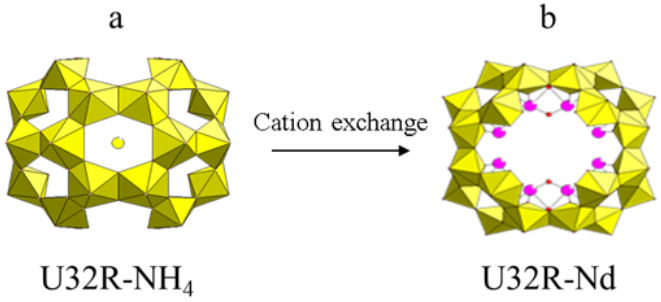

Fig 8. Crown cluster U32R-NH_4 (a) U32R-Nd obtain after cation exchange (b)

The uranyl peroxide, $(NH_4)_{40}[(UO_2)_{32}(O_2)_{40}(OH)_{24}]\cdot nH_2O$ (Fig 1), denoted in the following as U32R-NH_4, precipitates at room temperature within 15 min. with a sharp selectivity [5]. Its high anionic moiety associated to its crown shape make it rather promising for exchange chemistry. The recent successful substitution of the NH^{4+} by Nd^{3+} cations, leads to the preparation of the rare-earth containing uranyl peroxide materials with the highest exchange rate [6]. In the following this substituted nanocluster phase is denoted as U32R-Nd.

The whole objective study is to evaluate the ability of the U32R-Nd material as a suitable precursor to make simulated pellets of nuclear fuel, after calcination. To this aim the thermal decomposition pathways of U32R based nanoclusters, with NH^{4+} and Nd^{3+} cations yielding an oxide phase with the fluorine structure, have to be studied. Knowing the strong influence of the heat-treatment atmosphere, inert, oxidative or reductive, on the stability of the intermediate phases and the transition temperatures, a comparative investigation was carried out by *in-situ* powder XRD.

This communication will present the detailed results in terms of phase identification and refinement of the lattice parameters for each intermediate product of the thermal decomposition,

carried out for the three different atmospheres and up to 1100°C for inert and oxidative ones and up to 800°C for reductive one.

The ammonium uranyl peroxide nanocluster U32R-NH_4 was obtained by mixing uranyl nitrate with hydrogen peroxide and a NH_3 aqueous solution [3] [7]. U32R-Nd was obtained by cationic exchange as previously described [6], powder of U32R-NH_4 was put in contact with a solution of neodymium nitrate, for one hour. Finally, the solid was recovered by filtration.

The *in-situ* XRD experiments were carried out with a D8 Advance Brücker diffractometer (Θ-Θ mode, CuKα radiation) equipped with an Anton Paar HTK 1200N chamber. The heating ramp was selected at 5°C / minute, the data collections were carried out every 25°C with experimental conditions: 2 Θ range = 10-60°, step = 0.05°, time per step =0.2s.

X-ray diffraction analyzes as the function of the temperature and for the three atmospheres are summarized in Table 1. The results show that both phases U32R-NH_4 and U32R-Nd remain amorphous up to intermediary temperatures at about 550°C. The first phase to crystallize is mostly α-UO_3. The identified structural types are rather limited, with only four forms, α-UO_3 (orthorhombic, *C*2*mm*), α'-U_3O_8 (orthorhombic, *C*2*mm*), U_2O_5 (orthorhombic, *Pmna*) and fluorine-type (cubic, $Fm\bar{3}m$). This later is adopted by $UO_{2\pm x}$ with x = 0.21 at 1100°C and for PO_2 = 1 atm [8].

The results confirm the influence of the atmosphere on the decomposition scheme of both precursors U32R-NH_4 and U32R-Nd and the stability domain of the intermediate products. For a given atmosphere, the effects of the Nd addition are also outlined with the formation of a fluorine-type phase at lower temperatures than for the U-O binary system, as the main example. The stability domain of the other structure-types are also strongly affected by this ternary alloying. The direct comparison of the refined parameters of the various phases allows to readily ascribe the Nd influence.

Table 1. Stability domains and identified structure-types of the various phases formed during the thermal decomposition of U32R based peroxides under air, inert and reductive atmospheres.

U32R-NH_4						**U32R-Nd**					
Air		N_2		N_2/ H_2(3%)		Air		N_2		N_2/ H_2(3%)	
Temperature range (°C)	Structural type	Temperature range (°C)	Structural type	Temperature range (°C)	Structural type	Temperature range (°C)	Structural type	Temperature range (°C)	Structural type	Temperature range (°C)	Structural type
RT-525	Amorphous	RT-525	Amorphous	RT-350	Amorphous	RT-525	Amorphous	RT-525	Amorphous	RT-525	Amorphous
550-575	α-UO_3	550-575	α-UO_3	375-450	α-UO_3	550-875	α-UO_3	550-725	α-UO_3	550-800	Fluorine type
600-825	α'-U_3O_8	600-800	α'-U_3O_8	475	α-UO_3 + F*	900-925	α'-U_3O_8	750-1050	α'-U_3O_8 + F*		
850-1100	U_2O_5	825-900	U_2O_5	500-800	Fluorine type $UO_{2\pm x}$	950-1000	α'-U_3O_8 + F*	1075-1100	Fluorine type		
		925-1075	U_2O_5 + F*			1025-1100	U_2O_5 + F*				
* F = fluorine type		1100	Fluorine type $UO_{2\pm x}$								

References

[1] Abraham, F.; Arab-Chapelet, B.; Rivenet, M.; Tamain, C.; Grandjean, S.; Coord. Chem. Rev., 266-267, 28-68 (2014)

[2] Blanchard, F.; Abraham, F.; Rivenet, M.; Grandjean, S.; Vigier, N.; Hablot, I. Patent FR3015453, WO2015091753, (2015)

[3] Burns, P. C.; Kubatko, K.-A.; Sigmon, G.; Fryer, B. J.; Gagnon, J. E.; Antonio, M. R.; Soderholm, L.; Angew. Chem. *Int. Ed.*, **44**, 2135–2139 (2005)

[4] Qiu, J.; Burns, P.C.; Chem Rev., **113**, 1097-1120 (2013)

[5] Sigmon, G.E.; Burns, P.C.; J. Am. Chem. Soc., **133**, 9137-9139 (2011)

[6] Blanchard, F.; Ellart, M.; Rivenet, M.; Vigier, N.; Hablot, I.; Morel, B.; Grandjean, S.; Abraham, F.; Chem. Com., **52**, 3947-3950 (2016)

[7] Blanchard, F.; Ellart, M.; Rivenet, M.; Vigier, N., Hablot, I.; Morel, B.; Grandjean, S.; Abraham F.; Cryst. Growth Des., **16(1)**, 200-209 (2016)

[8] Guéneau, C.; Baichi, M.; Labroche, D.; Chatillon, C.; Sundman, B.; J. Nucl. Mater., **304**, 161-175 (2002).

P14

The probability of actinide protection with metal coatings

T.Kazakovskaya, E.Goryachev, S.Bezrukov

Russian Federal Nuclear Center RFNC-VNIIEF

Introduction

It is widely known that the chemical reactivity of actinides is very high. In air atmosphere they easily become scattered with corrosion products. The first works devoted to corrosion of such actinide as uranium were performed in the framework of the USA Manhattan Project in the early forties of the last century, later these technologies were patented. To emphasize the peculiarities of actinide (uranium, thorium etc.) protection with metal coatings one ought to know that the standard electrode potentials of these metals have very high negative value, so it is impossible to find an ordinary metal which could serve as anode towards an actinide. That is why the effective protection with metal coatings could be reached only when coating is non-porous. There are various methods to apply the protective metal coating onto actinides.

Galvanic method. The galvanic method in detail was investigated mainly in the USA. □1,2□. The most distinctive feature of actinides is their high inhibitive properties. This opposes generation of high-cohesive coatings. Galvanic coating of small thickness (3-6 □m) is porous, this reduces its protective characteristics. Besides, a lot of ecological problems connected with utilization of harmful solutions arises.

Ion-plasmous method. One could use this method to obtain such metal coatings as Cu, Ni, Ti, Al and some other. Before metal applying, a proper surface preparation is needed. The doubtless advantage of this method is good adhesion of coating to actinides. However, the coating is porous and to ensure reliable protection one must increase coating thickness.The equipment to be used is rather expensive.

Both methods have a significant drawbacks: the coating is not uniform, especially if detail has complex configuration with narrow grooves and closed holes. Besides, to obtain non-porous coating one must increase the coating thickness This reason drops significantly methods advantages.

Ultra-thin diffusion zinc plating coating - is an environmentally-friendly process, new method of applying antirust coating united several new conceptions in one technology. This method embodies the plating process, when the diffuse metal (Zn) transfers into a surface layer at heating the details within he zinc powder medium at the temperatures of 320 –450^{0}C. The forming coating consists not of pure Zn, but of Zn-metal alloys, which appear to be solid solutions of variable composition. The diffusion zinc plating process has a considerable advantages : coatings on the base of diffusion zinc *at any thickness are pore-free*, uniform even in through and closed holes ; that is impossible for galvanic and ion- plasmous technology, the process is environmentally clean. A nonporous ultrathin precision zinc coating provides effective protection against atmospheric and sea-water corrosion and resistance to high temperature. The coating is nonmagnetic and explosion safe.

According to the theory of diffusion layer formation there is a theoretical possibility to form diffusion zinc coating onto actinides: the atomic diameter of Zn atom is about 1.3 times smaller than the average atomic diameter of actinides. Besides there is data about Zn solubility in some actinides (thorium and uranium). The first experiments demonstrated the principal ability to form the diffusion zinc coating onto uranium. But it is necessary to polish up the existing technology of ultrathin diffusion zinc coating to use it for actinides. In particular, the optimal temperature-time parameters eliminating intermetallide formation must be chosen. The experiments are to be continued. .

Conclusion

The advantages and drawbacks of existing methods to apply the protective metal coating onto actinides were analyzed. .
2 The principal ability to form the diffusion zinc coating onto actinides was demonstrated. .

References

[1] J.H.Buddery *et al.* The Development and Properties of an Oxidation- Resistant Coating for Uranium, J. Nucl. Mater, 13 No2, 1964, pp.169-181.
[2] US Patent №3,668,084

P15

Upgrading of a U/Th laboratory for regulatory compliance in France

Stéphanie Fryars[1], Louise-Anne Cariou[1], Mathieu Pasturel[1]

[1] Univ Rennes, CNRS, Institut des Sciences Chimiques de Rennes -UMR6226, F-35000 Rennes, France, e-mail: stephanie.fryars@univ-rennes1.fr

Following a statutory inspection[1] in 2014, the working practices of our U / Th research laboratory have been revised to bring them into compliance with the latest French/European regulations[2-4].
The main goal was to drastically reduce our stocks of nuclear materials accumulated over several years of research activity, reaching close to 18kg of natural and depleted uranium (U-nat and U-dep) and natural thorium (Th-nat).
A full inventory of these materials (raw materials and over 1000 research samples) was carried out. We disposed of most of our non-incinerable solid waste via ANDRA[5], amounting to just below 2kg of nuclear materials. Our stock will soon be less than 1kg of each radionuclide, with removal of most of our non-incinerable (soluble) salt waste, also via ANDRA. In doing so, our annual declaration for the IRSN[6] will be exempted and subsequently the regulatory reporting requirements will be reduced significantly.
Enhanced physical protection of our nuclear materials has been put in place, including traceability procedures. Radioprotection protocols and procedures have been revised and documented to help maintain best-practice in laboratory safety. These procedures greatly facilitate the management of these materials, while also improving laboratory safety (exposure of personnel, risk of loss of material through theft, etc).
We share our experience of this 18-month effort, in the hope that it may benefit our European colleagues in saving time and effort while also improving safety.

References

[1] Ministry of Ecology, Sustainable Development and Energy: Department of Nuclear Safety
[2] Articles L.133-1 et seq. of the Defence Code
[3] Order of 31 May 2011 relative to measures taken for tracking, for accountancy and for physical protection applicable to nuclear materials being declared
[4] Council Directive 2013/59/Euratom of 5 December 2013 laying down basic safety standards for protection against the dangers arising from exposure to ionising radiation
[5] French National Radioactive Waste Management Agency
[6] Institute for Radiological Protection and Nuclear Safety

P16

Methanation of CO_2 over nickel – actinide bimetallic oxides

Joaquim B. Branco, Ana C. Ferreira

Centro de Ciências e Tecnologias Nucleares(C^2TN), Instituto Superior Técnico, Universidade de Lisboa, Campus Tecnológico e Nuclear, Estrada Nacional 10, ao km 139.7 2695-066 Bobadela, Portugal, e-mail:jbranco@ctn.tecnico.ulisboa.pt

Due to the emission of greenhouse gases (GHG), namely CO_2, many studies continue to be dedicated to its use as reagents in different processes aiming the production of value-added chemicals such as hydrocarbons or alcohols [1]. In this work, we have studied the methanation of carbon dioxide over nickel-*5f* block bimetallic oxides. The compounds were prepared by two methods: i) controlled oxidation under dry air of binary intermetallic compounds of the type $AnNi_2$ (An=Th, U) [2]; ii) using the sol gel method [3]. The best results were those obtained over the thorium-based catalyst that present an activity and selectivity equivalent to that of a commercial supported rhodium catalyst on alumina (5wt. % Rh/Al_2O_3). The catalysts present also an unusual long stability in the gaseous stream and they were characterized by different techniques (XRD, SEM/EDS, H_2-TPR). To our knowledge, this is the first time that nickel-actinide bimetallic oxides were tested for the methanation of carbon dioxide.

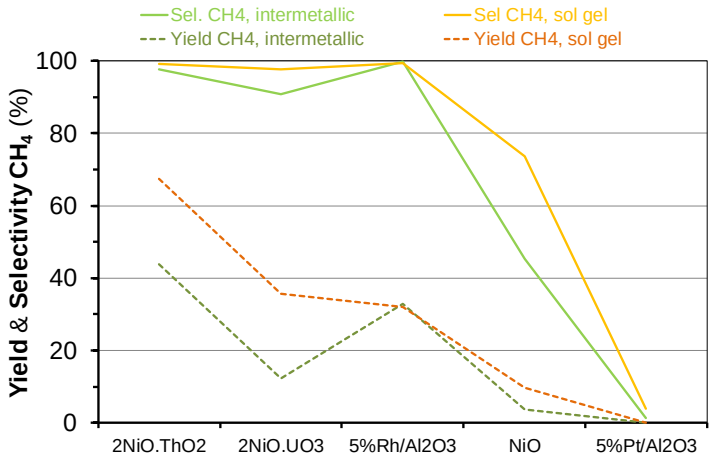

Fig. 1. Methanation of CO2 over nickel-*5f* block bimetallic oxides at atmospheric pressure and 350 ºC (H_2/CO_2=4; GHSV=15000 mL/g.h).

Acknowledgements

C^2TN/IST authors gratefully acknowledge also the FCT support through the UID/Multi/04349/2013 project.

References

[1] a) L. Shi,; G. Yang, K. Tao, Y. Yoshiharu, Y. Tan, N. Tsybaki, *Accounts of Chemical Research* **46**, 1838 (2013); b) A. Bansode, A. Urakawa, *J. Catal.* **309**, 66 (2014).

[2] a) A. C. Ferreira, A. P. Gonçalves, T. A. Gasche, A. M. Ferraria, A. M.B. do Rego, M. R. Correia, A. M. Bola, J. B. Branco, *J. Alloys Compd*. **497** (1-2) 249 (2010). b) J. B. Branco, A. C. Ferreira, A. M. Ferraria; A. M .B do Rego, T. A. Gasche *ACS Catal.* **2**, 2482 (2012).

[3] J. B. Branco, A. C. Ferreira, T. A Gasche, J. P Leal. *Adv. Synt. Catal.* 356 (2014) 3048-3058.

P17

"MEDICIS-Promed", a EU project to produce radioisotope beams for medicine: an actinide perspective

A.P. Gonçalves,[1] S. Chowdhury[1], M. Nazarova[2], K.S. Novoselov[2] and T. Stora[3]

[1] C²TN, Instituto Superior Técnico, Universidade de Lisboa, Estrada Nacional 10, 2695-066 Bobadela LRS, Portugal
e-mail: apg@ctn.tecnico.ulisboa.pt
[2] National Graphene Institute, University of Manchester, Booth St. E, Manchester, M13 9PL, UK
[3] ISOLDE, CERN, CH-1211 Genève 23, Switzerland

The use of radioisotopes for medical applications is an actual hot topic. Personalized medicine, in particular for cancer, uses such type of isotopes for imaging and targeted radionuclide therapy. However, their availability, (isotopic) purity and quality are critical issues. The ISOL method is a technique to produce radioactive ion beams that can strongly contribute to overpass such problems. In this method, high-energy ions (usually protons) hit a suitable target to generate the radionuclides through nuclear reactions (spallation, fission and fragmentation). Heat is also generated in this process and the radioisotopes produced diffuse to the surface of the target and effuse into an ion source where they are ionized. The ions are then magnetically separated, resulting in high-purity radioactive ion beams, and collected to be used for medical purposes. Uranium carbide is the reference target material at most ISOL facilities in the world due to its suitability for the production of many of the isotopes wanted, high melting temperature and high thermal conductivity. This communication presents a European project related to the production of radioisotopes for medical applications, emphasizing its connection to the Actinide Sciences.

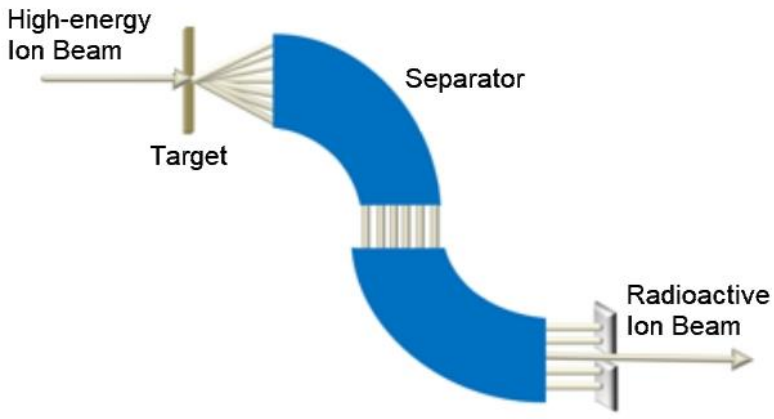

Fig. 1. Scheme of the ISOL method.

"MEDICIS-produced radioisotope beams for medicine" (MEDICIS-Promed) [1] is a Marie Sklodowska-Curie Innovative Training Network of the Horizon 2020 EU program, which integrates a network of fundamental research institutions, private companies and medical schools. It is led by CERN (and profits from CERN facilities like ISOLDE and MEDICIS) and intends to train a new generation of entrepreneurial scientists who will be able to develop and test innovative radiopharmaceuticals and imaging agents for personalized treatments. MEDICIS-Promed has been organized into 3 different scientific work packages that

complement each other in addressing isotope production by mass separation for new personalized treatments in medicine: WP1) Mass separation of new medical isotopes, WP2) PET-aided ^{11}Carbon hadron therapy and WP3) New theranostic pharmaceuticals/surgery tools for personalized treatments of ovarian cancer. WP1 is directly related to actinides, namely to the development of original uranium-based targets for more efficient production of medical isotopes.

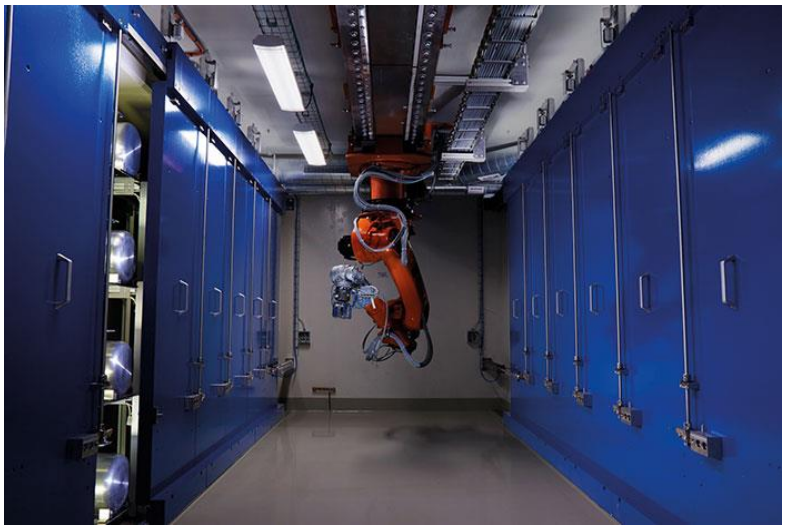

Fig. 2. Robot used in the production of radioisotopes for medicine at CERN.

WP1 activities comprise the investigation of uranium carbide nanofibers targets for increased stability and extraction yield of alpha-emitting radioisotopes. This activity has as main objective to improve the release properties, hence the yield efficiency, of uranium carbide targets, by changing the method of production and the final microstructure. Details can be obtained from the oral and poster presentations entitled "Recent developments in UC_x target at C^2TN" and "Nano-UC_x target for CERN-MEDICIS facility", respectively. A second WP1 activity related to new uranium-based targets consists of the development of metallic foil targets with protective graphene layers to produce innovative isotopes. It has as objective to study the possibility and mechanisms of graphene growth on uranium, thorium and other metals to form a protective layer against corrosion. Preliminary results of the graphene growth on transition metals and its protective properties are presented on the poster entitled "CVD growth of graphene on proton irradiation targets: the case of tantalum".

References

[1] https://medicis-promed.web.cern.ch/.

P18

The Platform of Instituto Superior Técnico for Nanotechnology and Materials (IST-NM)

A.P. Gonçalves,[1] A. Almeida[2], J.P.S. Farinha[3], M.E. Rosa[4] and N. Silvestre[5]

[1] C²TN, Instituto Superior Técnico, Universidade de Lisboa, Estrada Nacional 10, 2695-066 Bobadela LRS, Portugal
e-mail: apg@ctn.tecnico.ulisboa.pt
[2] CeFEMA, Instituto Superior Tecnico, Universidade de Lisboa, Av. Rovisco Pais 1, 1049-001 Lisboa, Portugal
[3] CQFM and IN, Instituto Superior Técnico, Universidade de Lisboa, Av. Rovisco Pais 1, 1049-001 Lisboa, Portugal
[4] IDMEC, Instituto Superior Técnico, Universidade de Lisboa, Av. Rovisco Pais 1, 1049-001 Lisboa, Portugal
[5] IDMEC and LAETA, Instituto Superior Técnico, Universidade de Lisboa, Av. Rovisco Pais 1, 1049-001 Lisboa, Portugal

The Platform of Instituto Superior Técnico for Nanotechnology and Materials (IST-NM) is a transversal, interdepartmental structure of Instituto Superior Técnico (IST [1]), in which teachers and researchers from different IST units participate. IST-NM was created to promote the development of Nanosciences, Nanotechnologies and Materials Engineering field, at the level of research and education. Taking advantage of its transversal structure and multidisciplinary perspective, IST-NM allows a fluid discussion, promotion and coordination of initiatives and opportunities among the various departments, research units and coordinators of educational programs in the areas of Nanotechnologies and Materials Engineering. The IST-NM aims, in conjunction with the various departments and research units of IST, to promote a leading edge research, the transfer of technology to Portuguese and foreign industries, and an advanced training offer in its areas of competence.

Fig. 1. INESC-MN deposition facility.

IST-NM congregates human resources and laboratory facilities to achieve its objectives. It has ~80 members with different expertise and scientific background, ranging from Materials, Biology, Medicine and Chemistry to Computing, Electronic and Physics, and assembles diverse laboratory facilities for nanotechnologies and the preparation and characterization of materials. Some of the most important facilities for nanotechnologies are at INESC Microsistemas e Nanotecnologias (INESC-MN) [2]. INESC-MN operates a 250 m^2 cleanroom (class 100 and class 10 areas) and adjoining 250 m^2 grey area (nominally class 10,000) for magnetic recording head and MR sensor fabrication, thin film semiconductor device, biosensor and lab-on-chip fabrication including microfluidics, and MEMS processing. It comprises skills and equipment

for the materials optimization and thin film deposition, device fabrication and device and thin film characterizations.

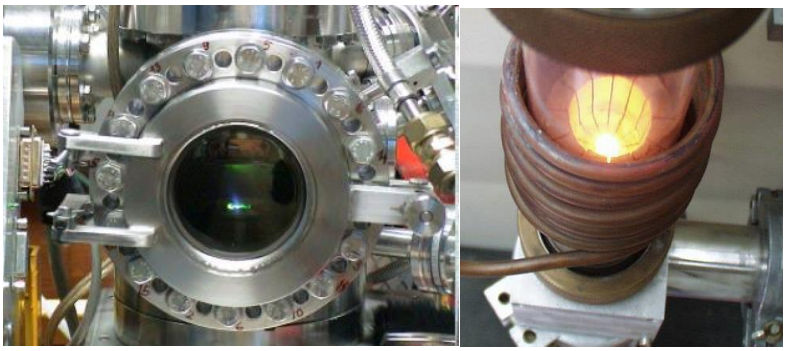

Fig. 2. a) Magnetron sputtering system and b) radioinduction furnace.

Innumerable materials preparation facilities, from the most simple to the very sophisticated, are available at the various research centers of IST. They include ultrafast laser processing (femtosecond laser texturing), laser cladding and 3D manufacturing, thin film deposition systems, high-temperature techniques (arc melting, induction melting, resistive melting, etc.), melt spinning and splat cooling techniques, ion beam deposition and milling systems, magnetron sputtering systems, hybrid PLD/CVD reactors, CVD systems, planetary ball mills, research spinners, electrodeposition and electrospinning systems, microwave reactors, etc.

Fig. 3. a) FEG-SEM, b) single crystal X-ray diffractometer, c) electrical magneto-transport characterization facility.

Several materials characterization facilities are accessible. The electron microscopy laboratory of IST (MicroLab [3]) is available as a service facility to the scientific and industrial community in Portugal. It is equipped with TEM, SEM and FEG-SEM, with EDS and EBSD analysis. Confocal and probe microscoies, (atomic force microscopes) are also available as well as, nanoindentation, and nanowear testing equipment. X-ray diffraction (powder and single crystal) and tomography, spectroscopies (NMR, Raman, infrared, UV, AUGER, XPS, HREELS, Mössbauer, XRF, PIXE, RBS, etc.), magnetic (AC susceptibility, DC magnetization, heat capacity) and electrical magneto-transport (resistivity, thermopower, magnetoresistance, Hall effect, thermal conductivity) characterization systems, etc. are available. Some of the preparation and characterization equipments can be used with actinides (mostly uranium and thorium), in particular those facilities located at the IST Nuclear and Technological Campus [4].

References

[1] https://tecnico.ulisboa.pt/en/
[2] https://sites.google.com/site/inescmn/
[3] http://microlab.tecnico.ulisboa.pt/
[4] http://www.ctn.tecnico.ulisboa.pt/uk/uk_main.htm

P19

Novel Aminopolycarboxylate-Based Metal Complexants for Improved Differentiation of Trivalent 4*f* and 5*f*-Elements

Colt R. Heathman[1], Travis S. Grimes[1], Vyacheslav S. Bryantsev[2], Santa Jansone-Popova[2], Peter R. Zalupski[1]

[1]Aqueous Separations and Radiochemistry, Idaho National Laboratory
[2]Chemical Sciences Division, Oak Ridge National Laboratory

Novel complexing agents, which effectively differentiate trivalent actinides from lanthanides are key for developing advanced separation schemes capable of closing the nuclear fuel cycle. One class of complexants considered for the application in the nuclear fuel cycle industry are aminopolycarboxylates (APCs). The combination of the ethylenediamine or diethylenetriamine backbone paired with acetate moieties effectively sequesters trivalent *f*-elements amongst many other metal ions. The very stable and relatively inert nature of the metal complexes hinders the ion transport across the liquid-liquid interface. A variety of structural modifications of the aminopolycarboxylate framework may be implemented to improve the metal exchange dynamics. This study addressed the influence of structural modifications on the coordination environment and thermodynamic properties of substituted APCs. Thermodynamic and coordination characteristics of the new series of complexants reveals insight into the tunability of aminopolycarboxylate complexants and their role in developing improved *f*-element separations schemes. This contribution evaluates modified APCs as holdback complexants to demonstrate improved differentiation of trivalent actinides from trivalent lanthanides.

P20

Comparison of Conventional and Advanced Nuclear Fuel Performance

Lottie Harding,[1] Sophie Rennie[1], Eleanor Lawrence Bright[1], Dave Goddard[2], Robert Burrows[3] Ross Springell[1]

[1] *University of Bristol, BS8 1TL, UK, e-mail: lottie.harding@bristol.ac.uk*
[2] *National Nuclear Laboratory, Springfields, Preston, Lancs. PR4 0XJ, UK*
[3] *National Nuclear Laboratory, Stonehouse, Gloucestershire, GL10 3UT, UK*

Accident Tolerant Fuels (ATF) are a key concept in the drive to improve safety in the nuclear industry [1]. The 2011 Fukushima Daiichi accident highlighted the thermal limitations of the current UO_2-Zr system and as such, significant effort is being invested in researching accident tolerant alternatives with better thermal conductivities. In order to be widely adopted and offset any R&D costs, ATFs should ideally offer some economic benefit in the form of increased uranium density, allowing for either higher burn-up or lower fuel enrichment. The 2016 UK Nuclear Innovation and Research Advisory Board prioritised the development of ATF research, aiming to benefit the future of commercial nuclear power with more efficient and safer fuels for both current and next-generation reactors [2].

In particular, UN and U_3Si_2 have been identified as potential ATFs due to their high thermal conductivity, high melting point, and high uranium density [3]. This project looks at the performance of these proposed ATFs, with a specific focus on comparing the thermal behaviour of UN and U_3Si_2 against conventional UO_2 material. Here, we present a preliminary investigation into the thermal conductivity of actinide thin films of poly- and single-crystal UO_2 and UN using the 3-ω technique.

We will focus on the effect of irradiation, for which thin films are ideal samples. The limited sample thickness enables homogeneous damage profiles to be induced using ion-irradiation. Fig. 1 shows initial SRIM [4] calculations that demonstrate a near constant damage profile with film depth. Such studies can shed new light on our understanding of how the thermal conductivity changes as a function of irradiation.

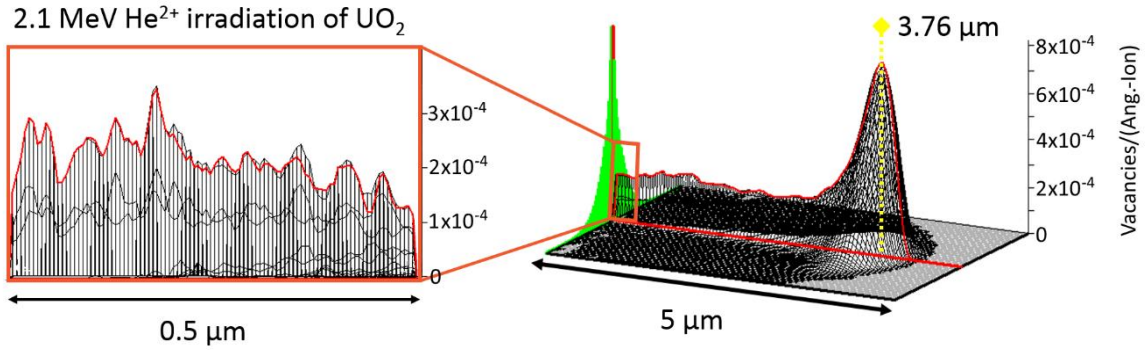

Fig. 1. The irradiation damage profile calculated using the monolayer method in SRIM for the irradiation of a 0.5 µm UO2 layer and bulk UO2 sample with 2.1 MeV He^{2+} ions. The dashed yellow line represents the peak of the damage, located at 3.76 µm.

References

[1] K. Gofryk *et al.*, *Nature Communications*, **5(4551)**, (2014).
[2] Nuclear Innovation and Research Advisory Board., *NIRAB-117-3*, (2017).
[3] K.A Terrani *et al.*, *Journal of Nuclear Materials*, **512-519**, 448 (2014).
[4] J,F, Ziegler *et al.*, Nucl. Instruments and Methods in Phys. Research Sec, B., **268(11)**, (2010).

P21

Contribution to the understanding of uranium natural geochemical cycles in granitic rock

Marja Siitari-Kauppi[1] and Karl-Heinz Hellmuth[1]

[1] *Department of Chemistry, University of Helsinki, P.O.Box 55, Finland,*
e-mail: marja.siitari-kauppi@helsinki.fi

Uranium is a mobile element in environmental systems and it changes easily oxidation state depending on the surrounding water-rock conditions; it is in fact a suitable indicator of past and prevailing geochemical conditions. To understand the processes of uranium mobilization and immobilization in geologic media, investigations were focused on primary U(IV) phases (mostly uraninite UO_2), the alteration of these minerals and subsequent re-deposition of secondary U(VI) phases. The accessible open porosity of granitic rock adjacent to water conducting fractures is also one of the key parameters to evaluate the mobility of uranium and other elements in granitic rocks. Oxidizing meteoric waters percolate through the rock along the rock fracture system and diffuse into the rock matrix, thereby dissolving U from the primary U minerals. As the water is moving downward it is evolving by interaction with the rock minerals. With greater depth the water composition is changing in a way that different U phases may be precipitated depending on water chemistry. At the Palmottu U enrichment in SW-Finland precipitation of uranophane ($Ca(UO_2)_2(SiO_3OH)_2 \cdot 5H_2O$) was observed on fracture surfaces and in micro fissures in the rock matrix. Deeper in the rock system (below about 60 m) no U(VI) minerals were found. The advantage of U is its radioactive decay which allows the dating of these processes. Dating of pure crystals of uranophane in fractures gave evidence that U deposition has been active during various periods in the geological past and is going on presently. Dating of U(VI) phases within microfissures is also needed, but could not be conducted yet [1]. Understanding the mechanisms of U mobility is essential for understanding the geochemical conditions in fractured granitic rock, the chemical buffering capacity of the rock system under changing external conditions and the nature of radionuclide transport in fractures and rock matrix. By chemical analogy conclusions can be drawn on the behavior of transuranium element species in water-rock systems which are not existing in nature. Such knowledge is relevant for the assessment of the safety of geological nuclear waste repositories.

In this work the natural uranium geochemistry and mineralogy at the Palmottu site is discussed based on findings with SEM/EDS and SEM/EPMA on U minerals. On the other hand, the rock matrix is studied with C-14- PMMA autoradiography to characterize the accessible pore network of rock matrix.

Fig. 1 presents an example of the Eastern Granite on the Palmottu hill [2]. Halos on the C-14-PMMA autoradiographs of the sample indicate the presence of natural radioactivity. The darkened areas are very frequent in this sample. The network of migration pathways confers moderately high permeability and has allowed transport of uranium on a scale of several centimetres. Natural radioactivity is interfering locally with the C-14-PMMA autoradiography, but it is evident that grain boundary porosity dominates in most of this quartz-rich rock.

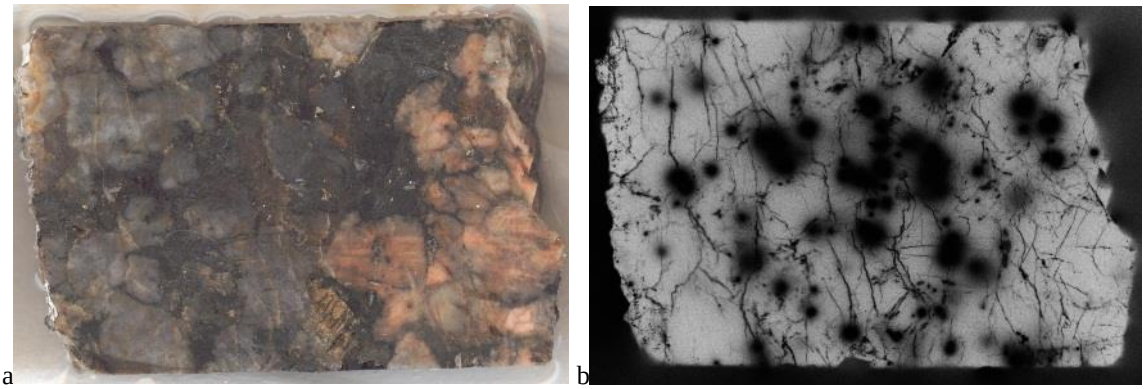

Fig. 1. Drill core from rock outcrop (exposed surface: left). a) Photoimage of the polished rock surface and b) corresponding autoradiograph. Abundant hot spots on autoradiographs to a depth of 6 cm from the surface, indicating U-rich phases. C-14-PMMA shows well developed network of migration pathways indicating high permeability and easy mobility of uranium. [2]

Fig. 2 presents the BSE image of one of the darkened areas on the autoradiograph. The determination of the mineralogy was done using an electron microprobe (W.D.S. analysis) in order to differentiate chemically the primary mineral and their alteration products. The thin sections are carbon-coated for SEM examination using a JEOL JSM 5600- LV scanning electron microscope in backscattered electron mode. The uraninite grains are moderately altered in the hill samples. They often display poorer crystal form and contain less uranium and lead than the unaltered grains from deep borehole cores. A poorly crystalline alteration rim; coffinite phase, containing uranium and silica often surrounds the uraninite grains. One typical combination, where the secondary uranium was found, was calcite filled fractures. The precipitated uranium was found together with calcite in several microfractures transsecting potassium feldspar and quartz grains.

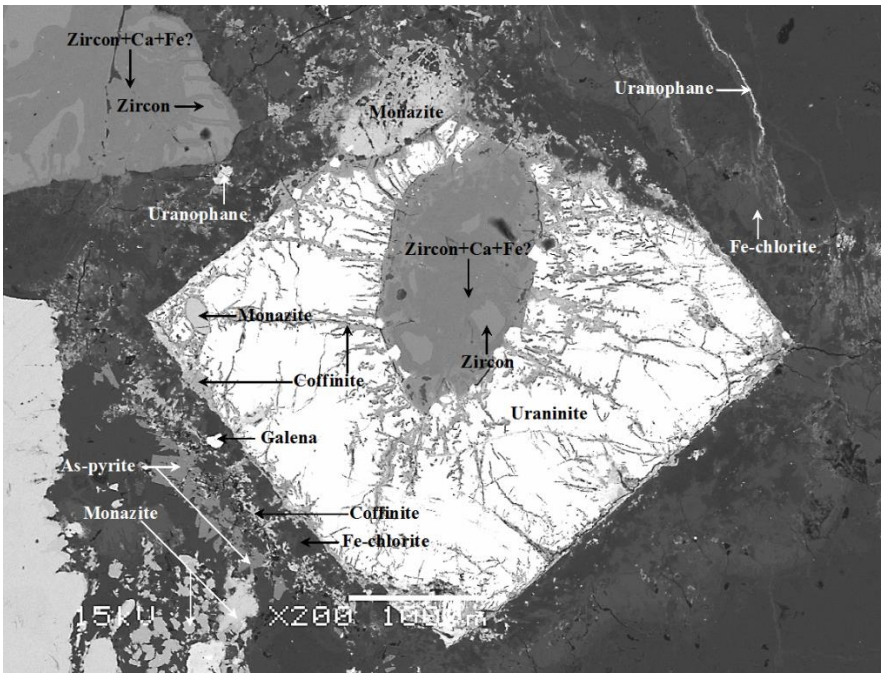

Fig. 2. BSE image of uraninite grain with zircon inclusion from outcrop drill core. (analysed by D Proust, University of Poitiers)

References

[1] D. Read *et al.*, *Global and Planetary Change* **Vol. 60**, page 235-249 (2008).
[2] D. Read *et al.*, *Report, TKK-KAL-A-34* (2004)

P22

Morphological characterization of UMo/ZrN fresh powders for the EMPIrE irradiation experiment by a statistical approach

F. Housaer[1], O. Tougait[1], N. Nuns[1], M. Touzin[2], F. Beclin[2], A. Addad[2], F. Vanni[3], B. Stepnik[3], H. Palancher[4], X. Iltis[4], I. Glagolenko[5], J.L. Schultness[5], M. Hammond[5], D.D. Keiser[5], A. Yacout[6], S. Van den berghe[7], A. Leenaers[7]

[1] *UCCS, UMR 8181, Université Lille1,* 59655 Villeneuve d'Ascq,
e-mail: francois.housaer@univ-lille1.fr
[2] *UMET, UMR CNRS 8207, Université Lille1, 59655 Villeneuve d'Ascq, France*
[3] *FRAMATOME, CERCA, SPL, ZI Les Bérauds, 54 avenue de la déportation, BP 114, F-26104 Romans-sur-Isère, France*
[4] *CEA, DEN, DEC, Cadarache, F-13108 Saint-Paul-Lez-Durance, France*
[5] *Nuclear Fuels and Materials Division, Idaho National Laboratory, P. O. Box 1625, Idaho Falls, ID 83415-6188, USA*
[6] *Nuclear Engineeing Division, Argonne National Laborary, 9700 S. Cass Ave., Lemont, IL 60439, USA*
[7] *Nuclear Material Science Institute, SCK-CEN, Boeretang 200, 2400 Mol, Belgium*

Substantial efforts are conducted to develop low ^{235}U enriched fuels for the high power research reactors that are still in use in US and Europe. The uranium-molybdenum (U-Mo) fuel system was selected for this aim. The conversion project focusses on two fuel-designs, monolithic fuels (Al cladded UMo foils) and dispersed fuels (UMo particles) [1, 2]. In this second case, the UMo powder particles are dispersed in an Al matrix constituting a green body, which is subsequently embedded in an Al frame. The final product, which is a thin plate, is produced by hot-rolling. Various post-irradiation examinations [3-5] have revealed that the growth of an interaction layer (IL) between the dispersed UMo fuel particles and the surrounding matrix strongly impacts the fuel plate's integrity. The IL growth mechanism is suspected to be driven by diffusion process at low burn up [6] and fuel recrystallization at high burn up [7]. So, coating of the UMo fuel kernel by a ZrN thin layer as a diffusion barrier [6, 8] and homogenization of the UMo core have been recently proposed to prevent IL formation and plate swelling. In parallel to the R&D on the fissile materials, several fabrication processes at the prototype scale are explored. These envisaged technological routes concern both the UMo powder production and the coating methods. The aim of the EMPIrE experiment is to test the impact of these technological options on the fuel features by means of detailed post-irradiation examinations. However, general correlations about the influence of the fabrication processes have to include stepwise investigations of the life products at both powder and plate fabrication stages. The aim of the present study comprises a detailed examination of the selected UMo powder batches at the UMo/ZrN powder fabrication step, i.e. before plate fabrication and irradiation experiment. The present work aims to finely characterize each batch in terms of the morphology and microstructure for both ZrN coating and UMo particles.

The starting U-7%wt.Mo powder particles were produced by either centrifugal or rotating electrode atomization processes by KAERI (Korean Atomic Energy Research Institute) or CERCA (Compagnie pour l'Etude et la Realisation de Combustibles Atomiques) respectively. The particle coating, about 1µm-thick-ZrN layer, was performed by means of PVD (SCK-CEN: Studiecentrum voor Kern Energie, Centre de l'Energie Nucléaire) or ALD (Argonne National Laboratory) technics. The coating was carried out on as-atomized or heat-treated powders. Finally, some batches were classified by particle size distribution, by sieving the

powder in the range 40-120 µm. The main properties were investigated at the particle scale: shape and size distribution, and evaluation of the quality and width of the diffusion barrier coating. The detailed characterizations were performed using a statistical approach based on an automated SEM images analysis procedure using ImageJ [9,10] (Fig. 1).

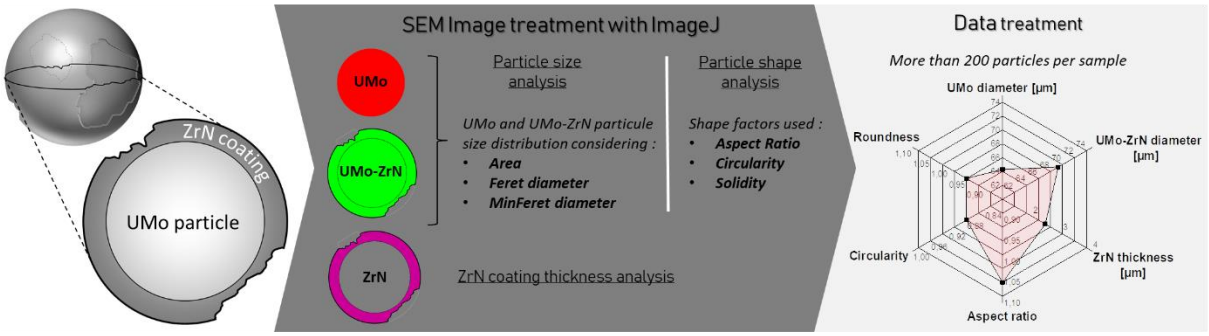

Fig. 1. Statistical approach to characterize ZrN coated UMo particle.

The investigation of the powder main features requires SEM images of finely dispersed powders of both free UMo/ZrN particles and polished cross-sections. For the sample preparation, the powder was deposited on a graphite tape and embedded in Al compacts, respectively. The magnification was adjusted to record images with more than 200 particles per sample and high resolution with good definition of particle contour, surface and UMo core.
The size of each particle were defined by the diameter of a circle of equal projection area (*i.e. the diameter of a circle that has the same area as the projection area*), the Feret's diameter (*i.e. the longest distance between any two points along the selection boundary*) and the minimal Feret's diameter *(i.e. the minimal Feret's diameter calculated after considerations of all possible orientations*).
The ZrN layer thickness were determined by difference between the core and the whole particle diameters. However, this deduced ZrN thickness using the particle cross-section needs to be corrected from the underestimated particle diameter and the overestimated ZrN length resulting from the cutting.
Several shape parameters were used to qualify the aspect ratio *(i.e. the ratio of length of major axis to minor axis*), the solidity (*i.e. the extent to which the shape is convex or concave*) and the circularity *(i.e. the ratio of the area to the square of the perimeter).*

The communication will present the methodology of characterization and the main features of the powder batches selected for the EMPIrE irradiation tests.

References

[1] D.B. Lee *et al., J. Nucl. Mater.* **250**, 79–82 (1997).
[2] B. Ye *et al., J. Nucl. Mater.* **499**, 191-203 (2018).
[3] A. Leenaers *et al., J. Nucl. Mater.* **476**, 218-230 (2016).
[4] D.M. Wachs *et al., J. Nucl. Mater.* **476**, 270-292 (2016).
[5] W.J. Kim *et al., J. Alloys. Compd.* **589**, 94-100 (2014).
[6] A. Leenaers, *et al., J. Nucl. Mater.* **335**, 39–47 (2004).
[7] S. Van den Berghe and P. Lemoine., Nucl. Eng. Tech. **46**, 125-146 (2014)
[8] J. Rest, Comprehensive Nuclear Materials, (2012).
[9] C. Igathinathane *et al., Comput. Electron. Agric.* ***63****, 168-182 (2008).*
[10] E.C. Crawford *et al., Comput. Geosci.* ***35****, 347-359 (2009).*

P23

Influence of chemical pressure on the ferromagnetism in UBeGe

Roman Gumeniuk,[1,2] Walter Schnelle,[2] Franz Weitzer,[2] Andreas Leithe-Jasper[2], Yuri Grin[2]

[1] *Institut für experimentelle Physik, TU Bergakademie Freiberg, Leipziger Str. 23, 09596 Freiberg, Germany e-mail: roman.gumeniuk@physik.tu-freiberg.de*
[2] *Max-Planck-Institut für Chemische Physik fester Stoffe, Nöthnitzer Str. 42, 01187 Dresden, Germany*

UBeGe is a strongly anisotropic ferromagnet with T_C =157 K and with a large coercive field of 0.55 T [1]. It crystallizes with the hexagonal ZrBeSi type of structure, which is a distorted variant of a simple AlB_2 prototype. In the current work, we tried to reduce the U-U distances in the mentioned structure by applying chemical pressure (*i.e.* substituting Ge by smaller Si-atoms).

A series of $UBeGe_{1-x}Si_x$ samples was prepared by arc-melting of the elements in a purified argon atmosphere with the further annealing at 950 °C for 1 week. All samples preparations and manipulations were performed within the Laboratory of high-safety Standards at MPI. The preliminary indexing of the XRD powder patterns revealed an orthorhombic distortion of the initial hexagonal structure for the compounds with Si-content $x > 0.5$. In agreement with this finding, we observe also an enhancement of the Curie temperature T_C for $UBeGe_{0.5}Si_{0.5}$ (Fig. 1). Interestingly, $UBeGe_{0.8}Si_{0.2}$ shows a huge coercive field H_{ci} = 1.4 T despite the lower T_C in comparison with pure UBeGe (Fig. 1).

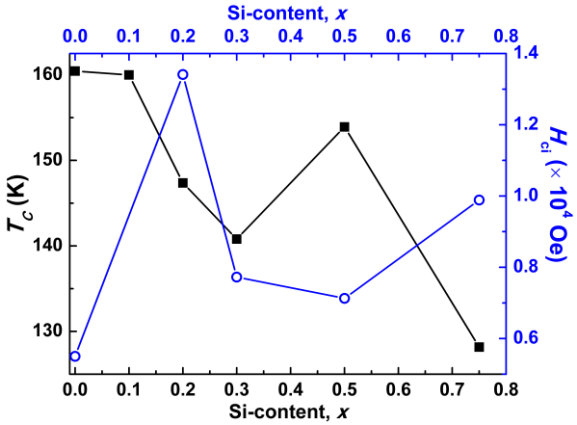

Fig. 1 The dependence of the Curie temperature T_C and coercive filed H_{ci} *vs* Si-content x in the $UBeGe_{1-x}Si_x$ series.

References

[1] R. Gumeniuk, *et al.*, submitted to Phys. Rev. B
[2] A. Leithe-Jasper, *et al.*, Scientific report of MPI-CPfS 2003–2005, Dresden, Germany. p. 25.

P24

CVD growth of graphene on proton irradiation targets: the case of tantalum

M. Nazarova[1,2], K.S. Novoselov [1,2]

[1]*School of Physics and Astronomy, University of Manchester, Oxford Rd, Manchester, M13 9PL, UK*
E-mail: marina.nazarova@manchester ac.uk
[2]*National Graphene Institute, University of Manchester, Oxford Road, Manchester, M13 9PL, UK*

Radioisotopes are indispensable in modern medicine, especially for diagnostic imaging, radiotherapy and radiopharmacology (*1*). Pure radioactive isotopes are often produced by proton irradiation of various targets including, among other, uranium, thorium and tantalum. During the store and transportation target materials are subjected to harsh conditions, and their surface has to be protected against corrosion. As graphene is chemically inert and completely impermeable, it can be used as a corrosion protection for metal targets. It was already proven that graphene protects transition metal surface against corrosion or reduces the corrosion rate (*2, 3*).

Here we will present conformal grown graphene on tantalum using CVD technique and the results of its corrosion resistance. The various growth conditions for deposition of graphene on tantalum foil were applied in present work. Obtained results showed that thin layers of tantalum carbide were produced with the islands of graphene on the top of the surface. It will be shown the role of variable growth parameters, thermodynamic and kinetic conditions on the formation of carbide - graphene layers. Briefly, the role of gas precursors, its ratio, pre-treatment of tantalum surface was found to greatly affect the results. Further, the highest growth temperature did not exceed 1150 °C, which is relatively low for the formation of tantalum carbide. Then, we will present the optimal parameters for large-scale deposition of carbide, and graphene-related materials with tantalum surface coverage up to 90%. We will also present the properties of fabricated layers such as surface morphology, element analysis, and optical characteristics. Finally, we will show that the corrosion tests have revealed the resistance of deposited materials.

References

[1] R. d. S. Augusto *et al.*, CERN-MEDICIS (Medical Isotopes Collected from ISOLDE): A New Facility. Applied Sciences 4, 265-281 (2014).
[2] N. T. Kirkland, T. Schiller, N. Medhekar, N. Birbilis, Exploring graphene as a corrosion protection barrier. Corros Sci 56, 1–4 (2012).
[3] D. Prasai, J. C. Tuberquia, R. R. Harl, G. K. Jennings, K. I. Bolotin, Graphene: Corrosion-Inhibiting Coating. ACS Nano 6, 1102-1108 (2012).

List of Participants

Jean-Charles Alexandre
CEA DIF
France
jean-charles.alexandre@cea.fr

Manuel Almeida
Instituto Superior Técnico
Portugal
malmeida@ctn.tecnico.ulisboa.pt

Alfred Amon
Max-Planck-Institute for Chemical Physics of Solids
Germany
alfred.amon@cpfs.mpg.de

Axel Angileri
Poitiers University - IC2MP
France
axel.angileri@univ-poitiers.fr

Miguel Gerónimo Avila
independiente Consultorio Privado de Medicina Nuclear y Medicina de Alta Complejidada
Rep.Argentina Sud América
miguelavila_arg@yahoo.com.ar

Antonios Banos
University of Bristol
United Kingdom
ab13306@bristol.ac.uk

Dmitry Belyaev
Russian Federal Nuclear Center – Zababakhin All-Russia Research Institute of Technical Physics (RFNC-VNIITF)
Russia
bad1331@gmail.com

Joaquim Branco
DECN-CTN/IST
Portugal
jbranco@ctn.tecnico.ulisboa.pt

Volodymyr Buturlim
Charles University, Faculty of Mathematics and Physics
Czech Republic
vovabuturlim@gmail.com

Roberto Caciuffo
European Cpommission, Joint Research Centre
Germany
roberto.caciuffo@ec.europa.eu

Daniel Chaney
University of Bristol
United Kingdom
daniel.chaney@bristol.ac.uk

Sanjib Chowdhury
Instituto Superior Técnico
Portugal
sanjibbua@gmail.com

Eric Colineau
European Commission
Germany
eric.colineau@ec.europa.eu

Gonçalo Domingos
Instituto Superior Técnico
Portugal
goncalo.almeida.domingos@gmail.com

Boris Dorado
CEA
France
boris.dorado@cea.fr

Vladimir Dremov
Russian Federal Nuclear Centre - Institute of Technical Physics
Russia
V.V.Dryomov1968@gmail.com

Maciej Fidrysiak
Jagiellonian University
Poland
maciej.fidrysiak@uj.edu.pl

Stéphanie Fryars
Institut des Sciences Chimiques de Rennes
France
stephanie.fryars@univ-rennes1.fr

David Geeson
AWE plc
United Kingdom
David.Geeson@awe.co.uk

Evgeny Gerber
Rossendorf Beamline at ESRF
France
evgeny.gerber@esrf.fr

John Gibson
Lawrence Berkeley National Laboratory
USA
jkgibson@lbl.gov

Danuta Goc-Jaglo
Institute of Physics, Jagiellonian University
Poland
danuta.goc-jaglo@uj.edu.pl

Nir Goldman
Lawrence Livermore National Laboratory
USA
goldman14@llnl.gov

Jean-Christophe Griveau
European Commission, Joint Research Centre (KA-JRC)
Germany
jean-christophe.griveau@ec.europa.eu

Roman Gumeniuk
TU Bergakademie Freiberg, Institut für Experimentelle Physik
Germany
roman.gumeniuk@physik.tu-freiberg.de

Itzhak Halevy
NRCN
ISRAEL
halevy.itzhak.dr@gmail.com

Lottie Harding
University of Bristol
United Kingdom
lottie.harding@bristol.ac.uk

Ladislav Havela
Charles University,
Faculty of Mathematics and Physics,
Department of Condensed Matter Physics
Czech Republic
havela@mag.mff.cuni.cz

Colt Heathman
Idaho National Laboratory
Unites States
colt.heathman@inl.gov

Amir Hen
European Synchrotron Radiation Facility (ESRF)
France
amir.hen@mail.huji.ac.il

François Housaer
Lille1 University
France
francois.housaer@univ-lille1.fr

Paul-Henri Imbert
Université Lille1
france
imbert.paulhenri@gmail.com

Igor Izosimov
Joint Institute for Nuclear Research
Russia
izig@mail.ru

Stepan Kalmykov
Lomonosov Moscow State University
Russia
stepan@radio.chem.msu.ru

Anton Kanunov
Russian Federal Nuclear Center- All-Russia Scientific Research Institute of Experimental Physics
Russia
a.kanunov@mail.ru

Alexey Karavaev
Russian Federal Nuclear Center – Zababakhin Institute of Technical Physics (RFNC-VNIITF)
Russia
a.v.karavaev@gmail.com

Tatiana Kazakovskaya
Russian Federal Nuclear Center - All- Russia Scientific Research Institute of Experimental Physics
Russia
knttvk@yandex.ru

Oleksandra Koloskova
Charles University, Faculty of Mathematics and Physics
Czech Republic
koloskova.alexandra@gmail.com

Kristina Kvashnina
Rossendorf Beamline at ESRF
France
kvashnin@esrf.fr

João Leal
Instituto Superior Técnico
Portugal
jpleal@ctn.tecnico.ulisboa.pt

Dominik Legut
IT4Innovatins, VSB - Technical University of Ostrava
Czech Republic
dominik.legut@vsb.cz

Andreas Leithe-Jasper
MPI CPfS
Germany
jasper@cpfs.mpg.de

Haibo Li
Institute of Materials, China Academy of Engineering Physics
China
lihaibo635@163.com

Gan Li
Institute of Materials, China Academy of Engineering Physics
China
lgzf1980@163.com

Silvie Maskova
Charles University
The Czech Republic
maskova@mag.mff.cuni.cz

Vladimir Matvienko
Russian Federal Nuclear Center- E. I. Zababakhin Institute of Technical Physics
Russia
mvn1969@mail.ru

Alexey Mirmelstein
Russian Federal Nuclear Center - E.I. Zababakhin Institute of Technical Physics
Russia
mirmelstein@mail.ru

Marina Nazarova
The University of Manchester
United Kingdom
marina.nazarova@manchester.ac.uk

Isabel Paiva
Instituto Superior Técnico
Portugal
ipaiva@ctn.tecnico.ulisboa.pt

José António Paixão
University of Coimbra
Portugal
jap@fis.uc.pt

Mathieu Pasturel
Institut des Sciences Chimiques de Rennes
France
mathieu.pasturel@univ-rennes1.fr

Laura Pereira
Instituto Superior Técnico, Universidade de Lisboa
Portugal
lpereira@ctn.tecnico.ulisboa.pt

António Pereira Gonçalves
Instituto Superior Técnico
Portugal
apg@ctn.tecnico.ulisboa.pt

Adam Pikul
Institute of Low Temperature and Structure Research, Polish Academy of Sciences
Poland
A.Pikul@int.pan.wroc.pl

Ruizhi Qiu
Institute of Materials, China Academy of Engineering Physics
China
qiuruizhi@itp.ac.cn

Peter Franz Rogl
Universität Wien
Austria
peter.franz.rogl@univie.ac.at

Gerda Rogl
University of Vienna, Institute of Materials Chemistry and Research
Austria
gerda.rogl@univie.ac.at

Anne-Laure Ronzani
CEA DIF
France
anne-laure.ronzani@wanadoo.fr

Leonid Sandratskii
Max Planck Institute of Microstructure Physics
Germany
lsandr@mpi-halle.de

Paul Sardini
UNIVERSITY OF POITIERS
France
paul.sardini@univ-poitiers.fr

Alexander Shestakov
Russian Federal Nuclear Center – VNIITF
Russia
alexander.e.shestakov@gmail.com

Peng Shi
Institute of Materials, China Academy of Engineering Physics
China
shipeng@caep.cn

Marja Siitari-Kauppi
University of Helsinki
Finland
marja.siitari-kauppi@helsinki.fi

Hongzhou Song
Institute of Applied Physics and Computational Mathematics
China
song_hongzhou@iapcm.ac.cn

Jozef Spalek
Marian Smoluchowski Institute of Physics, Jagiellonian University
Poland
jozef.spalek@uj.edu.pl

Yaping Sun
Institute of Materials, China Academy of Engineering Physics
China
ypsun0717@163.com

Eteri Svanidze
MPI CPfS
Germany
svanidze@cpfs.mpg.de

Aleksandr Tcepilov
RFNC-VNIITF
Russia
tierno2000@gmail.com

Mingfeng Tian
Institute of Applied Physics and Computational Mathematics
China
mftian@iapcm.ac.cn

James Tobin
University of Wisconsin-Oshkosh
USA
tobinj@uwosh.edu

Olivier Tougait
Université de Lille
France
olivier.tougait@univ-lille1.fr

Huilong Yu
Institute of Materials, China Academy of Engineering Physics
China
yuhuilong2002@126.com

Gongmu Zhang
Institute of Applied Physics and Computational Mathematics
China
zhang_gongmu@iapcm.ac.cn

Yanzhi Zhang
Institute of Materials, China Academy of Engineering Physics
China
zhangyanzhi@caep.cn